Sensorless Field Oriented Control in Modular Design Six Phase Permanent Magnet Synchronous Machine

Chetan Kumar

Master of Science Thesis

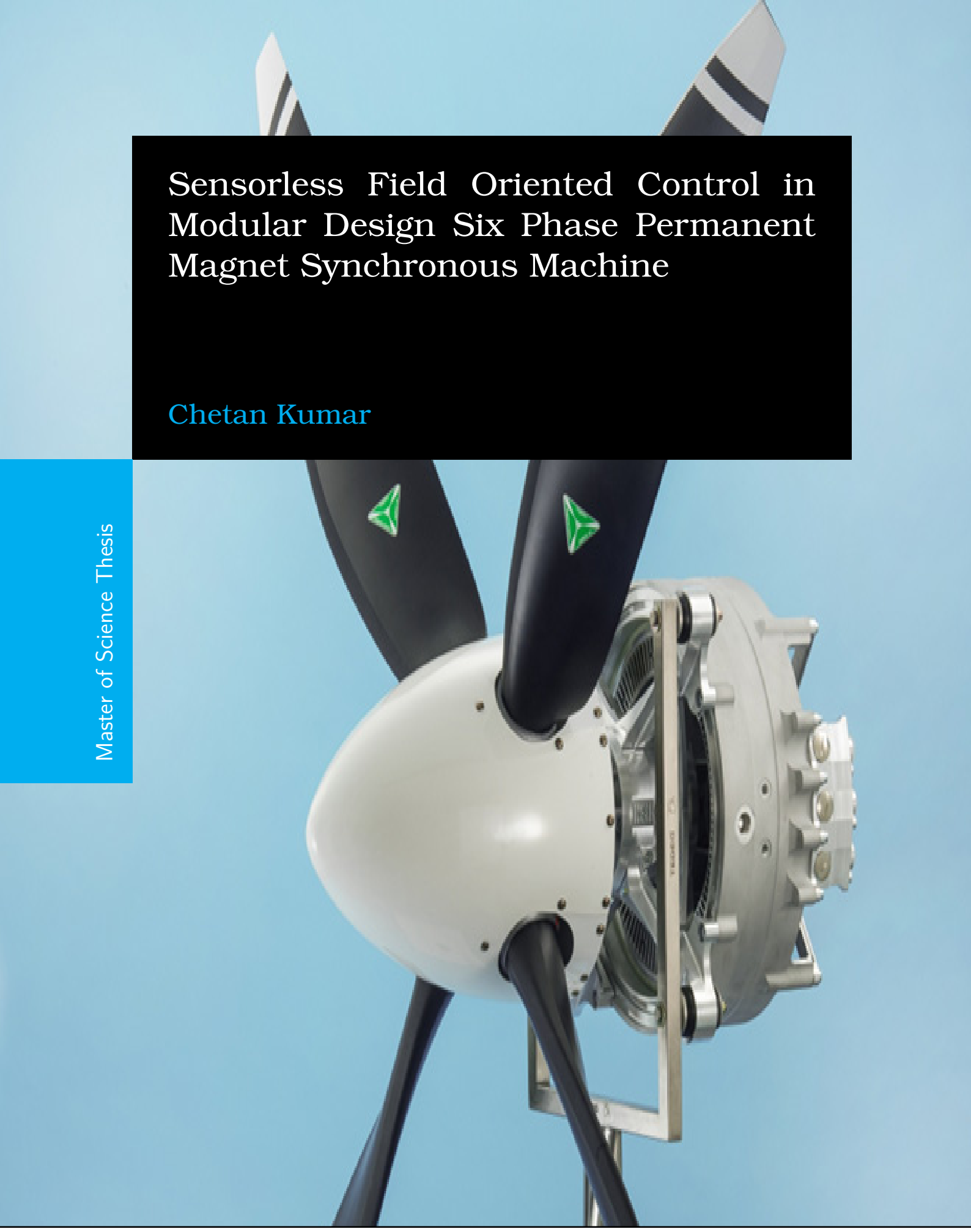

TU Delft Delft University of Technology

Electrical Sustainable Energy

Sensorless Field Oriented Control in Modular Design Six Phase Permanent Magnet Synchronous Machine

by

Chetan Kumar Byatarayanapura Jagadeesha

in partial fulfillment of the requirements for the degrees of

MSc in Electrical Engineering at Delft University of Technology
To be defended publicly

on Thursday November 17, 2016 at TU Delft.

Supervisors:	Dr. ir. Henk Polinder,	TU Delft
	Ir. Udai Shipurkar,	TU Delft
Thesis committee:	Dr. ir. P. Bauer,	TU Delft
	Dr. ir. H. Polinder,	TU Delft
	Dr. ir. M. Cvetkovic,	TU Delft
	Dr. ir. J. Dong,	TU Delft
	Ir. U. Shipurkar	TU Delft

TU Delft Delft University of Technology

An electronic version of this thesis is available at http://repository.tudelft.nl/.
Cover page image : Siemens (http://victoriaevclub.com/siemens-260-kw-electric-aircraft-motor-makes-first-public-flight/)

Abstract

An ever increasing emphasis on climate change and limiting carbon emission into the atmosphere, has led to lot research and innovation towards the greener mode of transport in the areas such as More Electric Aircraft (MEA), electric ship propulsion, electric and hybrid vehicles. Electric machines are largely used as the mean of a propulsion system for all the transportation related application, except for the aircraft where it is used controlling subsystems.

For improving the efficiency, reliability, and maintainability in an aircraft, the technological advances in the aerospace industry is moving towards the electrification of onboard services by reducing or removing the presence of the hydraulic, mechanical and air/pneumatic systems. The modular design multiphase machine offers a number of advantages compared to the traditional three-phase machine, in terms of the fault tolerance and reliability in aerospace applications. Modular systems refer to the system which can be decomposed into a number of independent modules or components. This system can have their faulted modules bypassed and continue operation after fault, increasing system availability. Modular design permanent magnet drives are widely selected for aerospace application in the high-performance drive systems, due to their fault tolerant capability, power density, reliability and high efficiency associated with the control possibilities.

At first, the modular design of the Permanent Magnet Synchornous Machin and power converter under consideration is explained using literature. Further, application of the modularity to the whole electrical drive system including the control circuit is presented. Subsequently, sensorless field oriented control (FOC) was implemented in the three phases of the machine using the inbuilt InstaSPIN FOC algorithm in microcontroller device. The control technique is later extended from three phase to six phase machine.

Acknowledgements

Firstly, I would like to thank Dr. Henk Polinder, for providing me the opportunity to work in this research and for his guidance throughout the duration of this thesis. Feedback from the discussion, I received from him helped me to clear many doubts that I had during the learning process.

I would like to thank my daily supervisor, Udai Shipurkar for his assistance technically and morally at every step with constant guidance, encouragement and mentoring. I would also like to acknowledge for all the time and effort he devoted for me during the implementation part of the prototype in the Laboratory. And he has been very helpful when I was writing this document.

I thank Dr. Jianning Dong, for his assistance at the end of my thesis, for providing valuable suggestion on the report and helping to sort some issues in which turned out be very important for completion of my thesis. I also extend my gratitude to Bart Roodenburg, Harry Olsthoorn for all their help in the laboratory.

Many thanks to my fellow master students Faisal, Adedotun, Digvijay, Palo, Albert, George, Ashwathi, Nishanth, Siddharth, Meng, Aarvindh and Aimilia who have made this hectic month bearable and fun-filled. I would also like to thank my friends in Delft and back home Balu, Jaggu, Selvam, Vinod, Chidu, PS, Nave and Loke for their support, encouragement and most importantly making this last two years memorable.

I can't thank my family enough for their faith in me. Thanks, Mom-Dad always being there for me and three sister's constant encouragement and support.

Delft, University of Technology — Chetan Kumar
November 11, 2016

List of Acronyms

Acronyms - Motor and Power Converter

- **MEA** - More Electric Aircraft.
- **PMSM** - Permanent Magnet Synchronous Machine.
- **BLDC** - Brushless DC Motor.
- **IM** - Induction Machine.
- **SRM** - Switched Reluctance Machine.
- **DTC** - Direct Torque Control.
- **FOC** - Field Oriented Control.
- **PM** - Permanent Magnet.
- **MMF** - Magneto Motive Force.
- **EMF** - Electromotive Force.
- **CFRP** - Carbon Fibre Reinforced Plastic.
- **PWM** - Pulse Width Modulation.
- **IGBT** - Insulated Gate Bipolar Transistor.
- **EMI** - Electromagnetic Interference.
- **VSI1** - Voltage Source Inverter 1.
- **VSI2** - Voltage Source Inverter 2.
- **CRO** - Cathode Ray Oscilloscope.

Acronyms - Microcontroller

- **DSP** - Digital Signal Processor.
- **MC** - Microcontroller.
- **TI** - Texas Instruments.
- **FAST** - Flux,Angle,Speed,Torque.
- **SPI** - Serial Peripheral Interface.

- **CPU** - Central Processing Unit.
- **SYSCLK** - System Clock.
- **TBCTR** - Time Base Counter.
- **TBPRD** - Time Base Period.
- **FED** - Falling Edge Delay.
- **RED** - Rising Edge Delay.
- **ePWM** - Enhanced Pulse Width Modulator.
- **USB** - Universal Serial Bus.
- **ADC** - Analog to Digital Converter.
- **BOB** - Bipolar Offset Binary.
- **LSB** - Least Significant Bit.
- **ADC** - Analog Digital Converter.
- **ROM** - Read Only Memory.
- **SVPWM** - Space Vector Pulse Width Modulation.
- **SPISOMI** - Serial Peripheral Interface Slave Output Master Input.
- **SPIMOSI** - Serial Peripheral Interface Master Output Slave Input.
- **SPISTE** - Serial Peripheral Interface Slave Transmit Enable.
- **GND** - Ground.
- **LSPCLK** - Low Speed Peripheral Clock Prescale.
- **SPIBRR** - Serial Peripheral Interface Baud Rate Register.
- **SPISTE** - Serial Peripheral Interface Slave Transmit Enable.
- **GPIO** - General Purpose Input Output

Table of Contents

List of Figures

List of Tables

Chapter 1

Introduction

Chapter summary : *This chapter provides a background to the field of research.Then the need for current research is justified. Finally, the chapter concludes with methodology, outline of the thesis and contribution.*

1-1 Background

Air transport is increasing continuously over the decades, as a result, it accounts for 2% of all man-made CO_2 emission and it's expected to increase to 3% by 2050 [6]. In order to reduce the environment impact and make air transport more sustainable, aircraft manufacturers are moving towards building future aircraft based on the More Electric Aircraft (MEA) concept. In this concept, the main idea is to remove or minimize hydraulic, pneumatics, and mechanical systems present in the aircraft and replace them with the optimized electrical system.

The electric motors with advanced control drive system are the possible electric system replacement for the mechanical system in aircraft. These systems with the electrical power is used to drive actuators, pumps, compressor and other subsystems at variable speeds [7]. Addition of electrical drive into aircraft will improve the overall efficiency, reduce the weight of the system [7]. Electric machines designed for the MEA concept should satisfy following criteria [6][7] :

1. High torque/weight ratio.
2. High efficiency throughout the full speed range.
3. Fault tolerant requirements.
    - Electrical, mechanical, magnetic and thermal isolation.
    - High value of phase inductance.

- Fail safe.

From aforementioned criteria, it can be said that electrical machines designed for safety critical applications should include the fault-tolerant capabilities (point 4).
The operating speed of machines used in aircraft will be in the range of 10K to 200K rpm [8]. Feasible high-speed electrical machines satisfying MEA's application reported in the literature are [6] [7] :

- Switched Reluctance machine [9][10].
- Induction machine [11][12].
- Permanent Magnet machine [13][14].

Permanent magnet motor refers to both the permanent magnet synchronous motor (PMSM) and Brushless motor (BLDC). Switched reluctance motor (SRM) was initially researched for aerospace application, for its natural fault tolerance capability. Squirrel cage induction machine (IM) is considered for simplicity, ruggedness, and cheapness. The power density of the IM and SRM is also quite low compared to PMSM machine [6]. Permanent magnet machine can be designed for the fault tolerant operation would offer higher torque density compared to that of SRM [15][7]. An in-depth, comparative analysis of aforesaid machines for aerospace application is beyond the scope of this thesis, but can be found in following literature [6][7][16]. Thesis focuses on PMSM machine, because of its high power density, efficiency, reliability, high torque/inertia and torque/volume ratios [7]. With these characteristics and fault tolerant design included with the higher number of machine phases (more than three) modular design multiphase PMSM is a good choice for the aerospace application. From this design, it will allow the machine to continue operation, in the case of a fault in the machine [17].

1-2 Motivation

Electrical drive system designed for the safety critical application use the modular design for both the machine and supply system [18]. Modularity refers to the concept of designing systems that can be decomposed into a number of modules or components [19]. Application of the modularity to whole drive system including the control circuitry will improve its fault tolerant capabilities in the system as will be shown in the next chapter. The modular design multiphase machine has concentrated winding, hence torque enhancement can be achieved with the lower order stator current harmonics injection [20].

The principle of the speed control of the multiphase machine is similar to that of the conventional three phase machines [18]. Scalar control technique is less significant compared to vector control methods because of its reduced performance during the transient condition. Two of the most commonly used vector control techniques are Direct torque control (DTC) and Field oriented control (FOC). In vector control, magnitude and angle of space vector are controlled, so it offers superior performance control compared to scalar control. FOC is chosen for its simplicity in implementation over DTC.

Field oriented control (Vector control) concept was first proposed in early 1970 by Blaschke

[21]. The controller (Digital signal processor or Microcontroller) used for FOC nowadays includes sophisticated control algorithm for building the control. Implementation cost for controller is affordable [22] as made FOC the common choice for servo drive application. The main difference in FOC of the multiphase machine compared to three phase machine is the coordinate transformation used in the FOC [18]. In the multiphase machine, the current controller has to produce voltage reference to control the machine equal to a number of phases for implementing the FOC. In order to control the PMSM machine using FOC require accurate measurement of the rotor position. The position of the rotor is determined using the position encoder or transducer. However, using the encoder for rotor position measurement will not only result in the reliability problems, but it also increases the cost of the system [23]. To avoid these problems with rotor position sensor and improve the reliability of the system, sensorless control technique is employed. Sensorless control in FOC means the process of estimating the rotor position, using machine measured voltage and current through sensors instead of using the conventional rotor position sensor. There has been little research on sensorless FOC using the distributed controller architecture (Modular design), this gap in the research seems to be a intersteing starting point for the master thesis. If the results from this thesis are satistfying, this will lead to further research in the field fault tolerant systems with distributed controllers.

1-3 Thesis Objective

This thesis entirely focuses on implementing the FOC in permanent magnet synchronous machines for aerospace applications. Out of many types of the PM synchronous machine, this research work deals with surface mounted Halbach array rotor permanent magnet synchronous machine. Sensorless control of the modular design multiphase machine is complex, due to its design and higher number of the phases compared to conventional three phase machine. In this thesis, a technique is formulated which extends conventional three phase control to all the six phases of machine.

As described above primary objective of the thesis is *Implementing sensorless field oriented control (FOC) in modular design multiphase PMSM machine using distributed controllers.* In order to achieve the above-described objective, the project work is split into following parts.

1. To build and test single phase H-bridge inverter modules for machine phases. Inverter modules are used as the power converter for machine.

2. To implement the sensorless control in modular design multiphase machine two microcontrollers are used. Here, two controllers are used to control all the six phases of the machine, each microcontroller will control three phases of the machine. From the reliability and fault tolerant application point of view for the aerospace application, it would be advantageous to follow this motor control architecture, in this way redundancy is introduced in the control circuitary.

3. Sensorless FOC for the three phases of the machine is built using rotor position information estimated from microcontroller based FAST observer.

4. Extending sensorless FOC for six phases of PMSM machine, using Serial Peripheral Interface (SPI) communication built between two TMS320F28069x[1] microcontrollers.

1-4 Methodology and Thesis Layout

This part of the section describes the approach followed, to reach the objectives of the thesis work and it is shown through flowchart in Fig. 1-1. Further, the layout of the thesis is described below :

Figure 1-1: Methodology of the thesis.

[1] x = F/M

- Chapter 2 explains application of modularity to the machine and its drive system design for safety critical application in an aerospace application. Experiments followed to measure machine parameters with the results are presented.
- Chapter 3 describes steps followed to build and test the H-bridge inverter modules for machine phases.
- Chapter 4 is intended to give detail working principle of the field oriented control. Algorithm used for building the microcontroller based sensorless control in a three phase machine is explained. Modules involved implementing the FOC is presented. Experiments carried out to check the sensorless control in three phase machine is presented.
- Chapter 5 describes the method used to communicate between the two microcontrollers. Algorithm involved extending the sensorless control in the six phase machine is explained.
- Chapter 6 is an attempt to explain the hardware issues faced while building the system and also hardware improvements which can be done in the design.
- Chapter 7 summarizes the results obtained in thesis and recommends possible scientific work for the future.

1-5 Contribution

Thesis focuses on the sensorless control of the modular design six phase PMSM for the normal and fault tolerant application specifically designed for the aircraft applications.

This thesis develops the field oriented control system based on distributed microcontrollers. It also implements, and tests the system on a hardware setup of the six phase permanent magnet synchronous machine. The performance of the machine is presented with the experiment results and possible improvement.

Chapter 2

Modularity in Multiphase PMSM System

Chapter summary *The chapter begins with conventional drive setup. Application of modularity in the electrical drive system for the safety critical application is presented. Finally, the chapter ends with the measurement of machine parameters, required for implementing the sensorless field oriented control.*

2-1 Electrical Drive System Architecture

Fig. 2-1 shows typical drive control architecture, common for all the machines. The controller

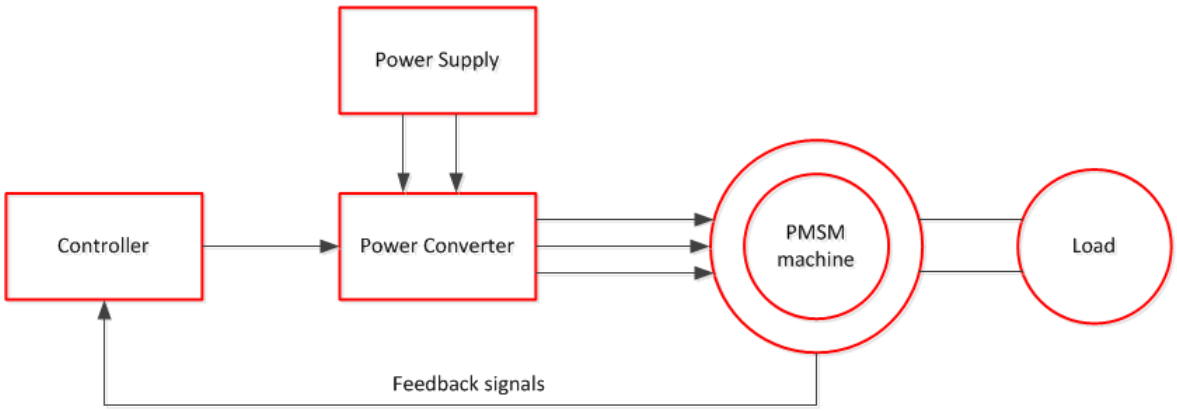

Figure 2-1: Typical drive setup.

in the Fig. 2-1 are used to control the whole drive system. These devices are specifically designed for the motor control applications. Controllers are usually interfaced with the drivers

of switching devices and the feedback signals from electrical machines. Using these interfaces with built-in function in the controller, the drive system is used to control the mechanical load using the electrical machine through the power converter. Controller used in the system nowadays are usually in form of digital signal processor (DSP) or micro-controller (μC or MC)

2-2 Application of Modularity to Electrical Drive system

Electrical drive system designed for the safety critical application (Aerospace application) use the modular[1] design for both the machine and drive system [18]. Previous research has indicated using the modular design in machine and drive system with an appropriate control strategy, will make system fault tolerant. The term fault tolerance in this system is defined as "no single electrical fault may cause the system as a whole to stop functioning"[1]. Incorporating the fault tolerant design would increase its availability, which is one of the primary requirement for the electrical system to be used in aircraft.

Principle faults which occur in the electrical drive system are [24]:

1. Faults in PM machine.
    - Machine winding open circuit.
    - Machine winding short circuit.
        (a) From phase to ground.
        (b) From phase to phase.
        (c) From turn to turn.
    - Short circuit at the machine terminals.
2. Faults in power electronics.
    - Semiconductor open circuit.
    - Semiconductor short circuit.
    - DC bus capacitor failure.
3. Faults in control circuitary.
    - Microcontroller control failure.
    - Drive circuit failure.

The PMSM machine doesn't have inherent fault tolerance capabilities, it's design has to be changed to integrate it. The following subsections will describe application of modularity in the PMSM, power converter and controller to attain the fault tolerant capabilities.

[1] Modularity refers to the concept of designing systems that can be decomposed into a number of modules or components[19].

2-2-1 Design of PMSM Stator

The design modification required in the PM machine for the fault tolerant application are as follows :

- Electrical, mechanical, magnetic and thermal isolation.
- High value of phase inductance.

In the following subsections, the changes in the machine design required for the fault tolerant application is explained in detail as follows [25][24] :

Electrical isolation between phases

In order to achieve this in machine design each phase has to be supplied from the single phase full bridge converter. Using full bridge converter would double the number of semiconductor switches compared to star connected stator winding system.

Limiting the fault current

If the short circuit fault occurs in the machine winding terminal or semiconductor, both scenarios would result in a very large current. To limit fault current, machine stator phase inductance has to be designed to 1 per unit inductance so that fault current is limited to rated value of the machine. The key to achieve such a high inductance in PMSM, which generally has low per unit inductance is by designing a machine with a large leakage inductance, by controlling the depth and width of slot opening [24].

Magnetic isolation between phases

If a fault occurs in the machine, fault current will induce a voltage in the neighboring phases, because of the presence of mutual inductance between phases. Further, current through unfaulted phases will induce MMF, which increases the EMF induced in the faulted phase and also increasing current through it. This would prevent the machine from its adequate control. To reduce the effect of one phase on another phase of the machine, mutual inductance has to be very little or no between the phases. The design of the machine should be such that, phase inductance should be limited only to self-inductance of the phase, the mutual inductance between the phases should be negligible [1].

Physical Isolation between phases

Phase-phase fault is a crucial fault since it will disable two phases if the fault occurs. This fault can be avoided by having each phase wound around single stator tooth, including the end windings. By designing the machine in this way phase to phase fault can be avoided.

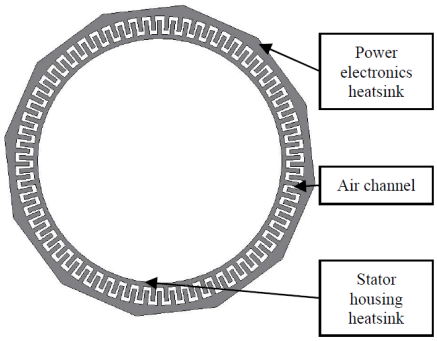

Figure 2-2: Heatsink used to cool the outer stator surface and switches of inverter modules [1].

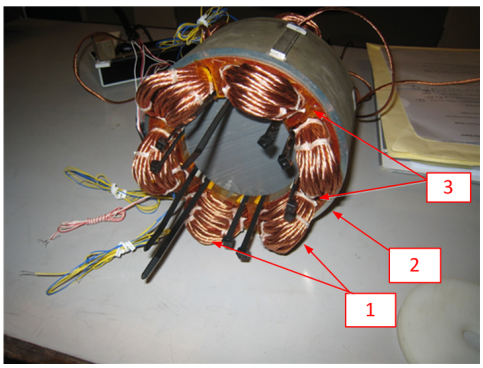

Figure 2-3: Stator of modular design machine.

Thermal isolation between phases

As suggested above, using one winding per slot also have the advantage of reduced thermal interaction and isolation between the phases. To avoid the rise in temperature within the slot, stator outer surface is cooled using the heatsink. Fig. 2-2 shows heatsink used in the prototype machine to cool stator outer surface and also power electronic module switches of the machine.

Number of Phases

The basic requirement for the machine to be used for the fault tolerant application, system should resume its operation in the event of a fault in any one of the machine phases. This can be achieved by increasing the output of remaining healthy phases, however, this is done by overrated design. The factor of the overrated design of the healthy phase for faulted phase is calculated by using the equation 2-1 [25].

$$F = \frac{n}{n-1} \tag{2-1}$$

where F is the overrating factor. n is the number of phases.

If three phases are used than overrating factor would be 50%. If the four, five, and six phases are used than overrating factor would be less than three phases, it will be 33%, 25%, and 20% respectively. The number of phases selected has a direct impact on the system losses and performance of the machine. Number of phases selected is six for the machine under consideration, the approach followed to arrive at six phases can be found in the literature [17].

Conclusion

The following conclusion can be reached with regard to the machine stator design from above discussion:

- Self-inductance of armature winding is one per-unit.
- Only one stator phase winding per slot.
- Each winding wound around a single tooth.
- Six phases on stator.

From last two conclusions, it is suitable to have each of the stator winding wound around the single tooth and each slot contain individual phase. This configuration results in the concentrated stator winding. With this winding arrangement discussed, direct contact between the windings is avoided. Spacer tooth is used between the two stator tooth and coil is wound only around the stator tooth. Spacer tooth is used to provides the return path for the flux [1]. Fig. 2-3 shows the stator structure of the prototype machine under consideration.

The number indicated in the Fig. 2-3 are as follows :

1. Concentrated winding wound around the stator tooth.
2. Outer surface of the stator, heatsink is placed here.
3. Spacer tooth between the two stator phases.

Cross section view of modular design multi-phase machine is shown in Fig. 2-4, here each color of the stator winding on stator tooth indicates in-dependency of the adjacent phases.

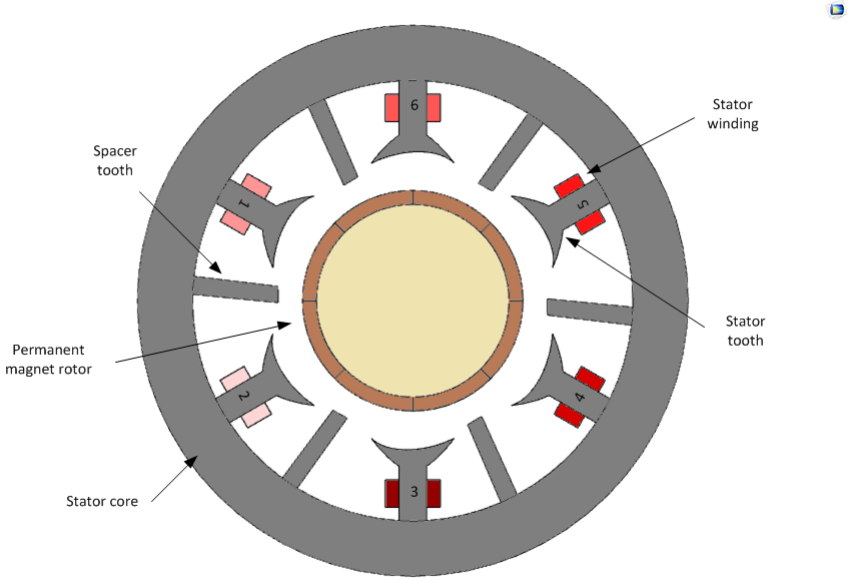

Figure 2-4: Cross-section view of modular design six phase machine.

2-2-2 Design of Power Converter

The modular design approach of having each phase as the single module, should be extended to the power converter (inverter) of the machine too. Significant design requirement for the fault tolerant drive system has been presented by J.A. Haylock [26], described below:

Partitioning

Partitioning divides the system into a number of the independent self-contained systems, ensuring fault at one place doesn't result in the complete failure of the system. Partitioning is introduced, by having six single independent full H-bridge inverter drive machine phase, this also introduces the electrical isolation between the phases.

Isolation between the units

Each phase of the system is designed in such a way that, a fault in one phase doesn't affect the performance of the contiguous phases. However, the continuous operation can be achieved in the faulted system condition only if there is physical, thermal, electrical and magnetic isolation between the phases. This is attained more or less with the machine design, as described in the 2-2-1 subsection and also with the partitioning.

Fault detection and reporting

Rapid action has to be taken in the event of any fault in the system. Such that, it prevents the faulted phase affecting the output (Net shaft torque) and input (Common DC link) of the system. It is achieved through designing the fault detection and diagnostic control algorithm, which would enable correct post-fault tolerant control [26].

Continued operation until next service opportunity

With the post-fault tolerant control algorithm implemented when a fault is detected in the system, it will ensure that system operates until faulted unit is replaced.

Keeping aforementioned two subsections 2-2-1 and 2-2-2 as reference, modular design multiphase machine and power converter is designed for the safety critical application in aircraft. Fig. 2-5 shows the structure of the integrated modular design power converter and machine. Integration of the machine and power electronics in one structure will improve the power density of the drive system. It also has the advantage of the reduced system weight [1].

2-2-3 Design of Drive Controller

In most of the motor drives single MC or DSP is used for the control of the power converter of the multiphase machine. To incorporate the modularity in the controller of drive structure, it is required to use multiple controllers [27]. Thereby it will also help to address fault in control circuitry described in the beginning of the section.

In the drive controller under consideration, two MC are used to control the multiphase machine. Distributed MCs are used to include redundancy in the system. In the case of a fault in one of MC, functional tasks can be handed over to the another MC. It also helps in the verification of the estimation of motor control parameters (rotor position, rotor speed, flux) using two MCs. Each MC will control three phases of the machine, which includes generating

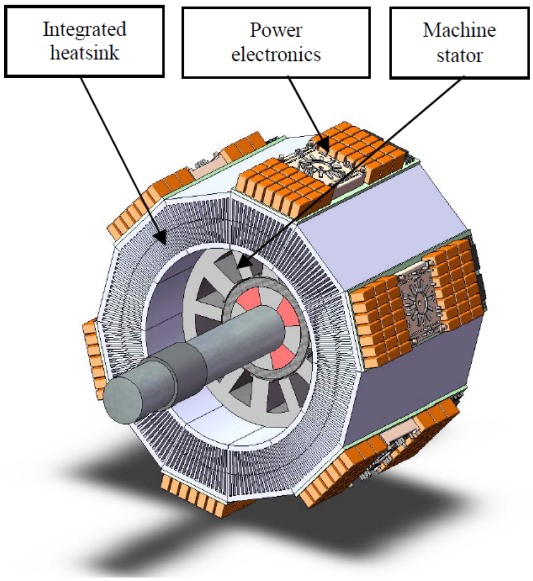

Figure 2-5: Integrated modular power converter and machine for aerospace application [1].

all the output signals and processing all the measurements. Fig. 2-6 shows the use of two MCs to control six phase machine.

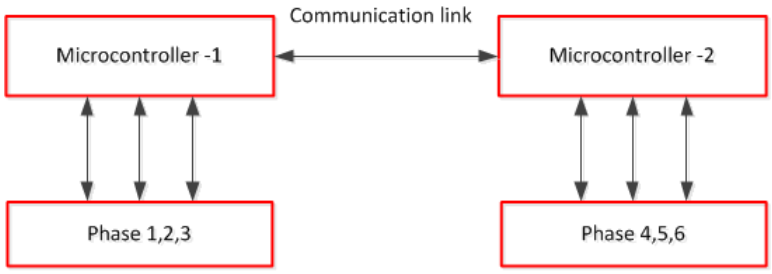

Figure 2-6: Controller for modular control drive architecture.

2-3 Permanent Magnet Rotor

The machine rotor has surface mounted permanent magnets. Plastic bonded rare earth type of magnets are used, they are injection moulded and magnetized in Halbach array with four magnetic pole pairs [3]. As a consequence of using surface mounted configuration, to reach very high-speed Carbon Fiber Reinforced Plastic (CFRP) retaining sleeve has to be used to avoid the magnet detaching from the shaft. Using retaining sleeve will also increase airgap and reducing the mutual coupling between the phases [3].

The Halbach array is a combination of radial magnet array and azimuthal magnet array. Flux distribution in Halbach array is a summation of the flux distribution in radial and azimuthal magnet array, as indicated in the Fig. 2-7. In the Fig. 2-7 it can be seen that flux lines are

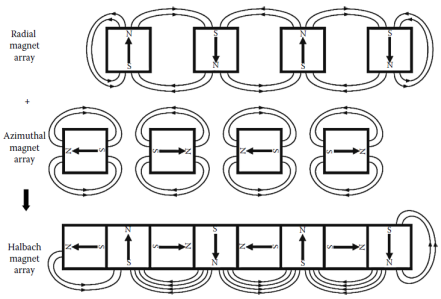

Figure 2-7: Halbach magnet array [2].

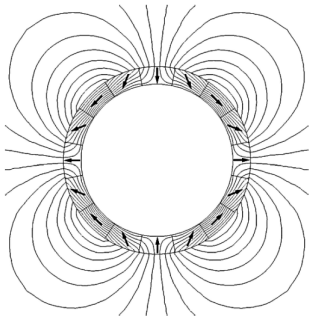

Figure 2-8: Flux distribution in Halbach array [2].

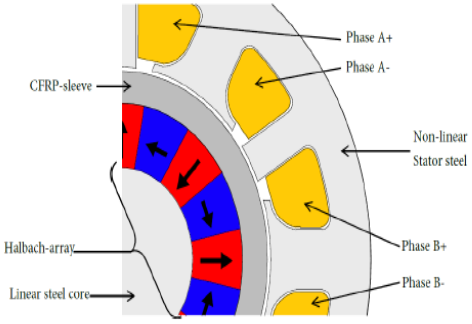

Figure 2-9: Section of modular design machine [3].

Figure 2-10: Rotor structure with Halbach array.

maximum at bottom of the magnet and very few lines on the top of the Halbach array magnet.

In the PM machine under consideration, using the same idea, of having the maximum flux distribution on one side of the arrangement (towards the stator) and few flux lines on another side of the array (towards the rotor), rotor cylinder with Halbach array is built. Flux distribution of the Halbach array magnet on the rotor can be seen in the Fig. 2-8. Section of the fractional pitch concentrated winding machine is indicated in Fig. 2-9, this is shown to provide the overview of the arrangement of CFRP sleeve on Halbach cylinder rotor. Fig. 2-10 shows the Halbach array on rotor structure used in modular design PMSM.

The advantage of using the Halbach array permanent magnet for rotor are as follows [2]:

- Air gap field produced by the Halbach array is nearly sinusoidal.
- No back iron is required, as flux lines are very minimal on the other side of the array. Bonding of the Halbach array can be performed on the nonferrous structure which has good structural properties.
- Torque ripple will be lower due to sinusoidal distribution of airgap flux.

2-4 Determination of Machine Parameters

For implementation of sensorless FOC using InstaSPIN Texas Instruments (TI) TMS320F28069x MC, knowledge of the machine parameters for the estimation of rotor position of machine is required. Following parameters were determined through experiment required for the sensorless control using microcontroller.

1. Stator Resistance.
2. d and q axis inductance
    - Stator self inductance.
    - Stator mutual inductance.
3. EMF constant.

2-4-1 Stator Resistance per phase

A multimeter was used to determine the stator resistance of each phase. Multimeter measurement : $R_s = 0.11\Omega$.

2-4-2 Measuring d and q axis Inductance

A permanent magnet has magnetic characteristics due to uniform and permanent alignment of its magnetic domains, they have the permeability close to 1. In surface mounted permanent magnet machine, poles on the surface of the rotor offer the same reluctance to magnetic flux has that of the air. Hence the inductance measured along the d and q axis will be same, $L_d = L_q$.

Stator Self Inductance

Sinusoidal voltage supply was applied phase one stator coil of the machine through variac, the coil would produce the pulsating field. Voltage and current response of excited phase measured using the oscilloscope, is shown in the Fig. 2-11. From the measured response, self-inductance is calculated which is a sum of magnetizing inductance and leakage inductance. Reactance of the phase one is calculated using equation 2-2 [28].

$$X_{11} = \sqrt{Z_{11}^2 - R_s^2} \tag{2-2}$$

$$X_{11} = \sqrt{\left(\frac{V_{11}}{i_1}\right)^2 - R_s^2} \tag{2-3}$$

Measured stator resistance is used in the equation 2-3.

$$L_{11} = \frac{X_{11}}{2 \cdot \pi \cdot f}. \tag{2-4}$$

where, X_{11} is Reactance of stator phase one. Z_{11} is Impedance of stator phase one. V_{11} is voltage applied across the stator phase one. i_1 is current through stator phase one, f is frequency of supply.

Table 2-1 shows the measurements using oscilloscope from self inductance measurement test.

Serial No.	Voltage $V_{11}[V]$	Current $i_1[A]$	Self Inductance $L_{11}[mH]$
1	0.44	1.30	0.99
2	0.855	2.5	1.03

Table 2-1: Stator self inductance.

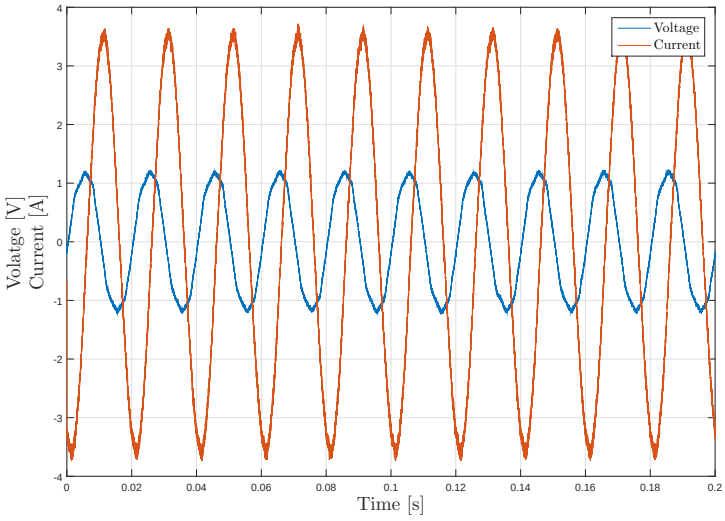

Figure 2-11: Voltage and current applied across phase five for measurement of the phase inductance. Frequency = 50 Hz, V_{rms} = 0.855 V, I_{rms} = 2.5 A.

Stator Mutual Inductance

To measure the mutual inductance between the phases of the machine, one of the machine phase was excited with the sinusoidal voltage supply (Variac) and rotor was kept stationary. The voltage induced in the all remaining phases was measured using the oscilloscope. Phase five was excited with the Variac, emf induced in all the remaining phases was measured and the mutual inductance was calculated. Flux linkage in phase one, due to the voltage applied to the phase five.

$$\lambda_{11} = L_{11} \cdot i_1 + L_{12} \cdot i_2 + L_{13} \cdot i_3 + L_{14} \cdot i_4 + L_{15} \cdot i_5 + L_{16} \cdot i_6 + \lambda_m. \tag{2-5}$$

Since current in the remaining phases are zero and also rotor is stationary in the experiment, so equation becomes.

$$\lambda_{11} = L_{15} \cdot i_5 \tag{2-6}$$

Using Faraday's law of electromagnetic induction

$$E_{51} = -\frac{d\lambda_{11}}{dt} \tag{2-7}$$

Solving equation 2-7 to calculate the mutual inductance will result in equation 2-8.

$$L_{51} = L_{15} = \frac{E_{51\_rms}}{I_{5\_rms} \cdot 2 \cdot \pi \cdot f} \tag{2-8}$$

where, λ_{11} is flux linkage in phase one. L_{12}, L_{13}, L_{14}, L_{15}, L_{16} are mutual inductance between the phase one and phase two, three, four, five and six respectively. λ_m is Flux linkage from the permanent magnet rotor on stator. i_2, i_3, i_4, i_5, i_6 are current through the stator phases two, three, four, five, and six respectively. E_{51}, $E_{52}, E_{53}, E_{54}, E_{56}$ is induced emf in the phase one, two, three, four, and six respectively due to voltage applied across phase five. L_{51}, L_{52}, L_{53}, L_{54}, L_{56} is mutual inductance between the phase one and phase two, three, four, five, and six respectively.

Using the equations 2-5 to 2-8 mutual inductance between the phases are calculated and tabulated in the table 2-2. Inductance matrix L is formed by the combination of the self

Phase 5		Phase 1		Phase 2		Phase 3		Phase 4		Phase 6	
V_{55} $[V]$	i_5 $[A]$	E_{51} $[mV]$	L_{51} $[\mu H]$	E_{52} $[mV]$	L_{52} $[\mu H]$	E_{53} $[mV]$	L_{53} $[\mu H]$	E_{54} $[mV]$	L_{54} $[\mu H]$	E_{56} $[mV]$	L_{56} $[\mu H]$
0.44	1.30	10	24.5	8.5	20.8	9.6	23.51	18.5	45.32	20	48.99
0.855	2.5	20	25.4	17	21.6	19	24.2	34	43.32	36	45.85

Table 2-2: Mutual inductance between the phases.

inductance obtained from stator self inductance test and the mutual inductance tabulated in the table 2-2. In the matrix it can be seen that non diagonal elements have negative sign, this is because of the 180° phase shift between the applied and induced voltage as shown in Fig. 2-12 and 2-13. Also phase lag of the induced voltage from the supplied current can also be seen using both the figures.

Looking into the table 2-2 and also any of the rows in the inductance L matrix, it can be seen that three different mutual inductance values exist. If the first row is considered, and Fig. 2-4 for reference then adjacent phases two and six have same mutual inductance value, phase five and phase three have same mutual inductance value due to their 120° spatial distance from phase one. Phase four, diagonally opposite to phase one has lesser mutual inductance compared to other phases. The reason for having different mutual inductance value is because no back iron is used for the Halbach array rotor cylinder, so the relative permeability of the rotor cylinder is equal to one, similar to that of the magnet. Reluctance to the flux path inducing on the other phases increases, which will reduce the induced emf and mutual inductance between the phases [29].

$$\mathrm{L} = \begin{bmatrix} 1mH & -46\mu H & -25\mu H & -21\mu H & -25\mu H & -46\mu H \\ -46\mu H & 1mH & -46\mu H & -25\mu H & -21\mu H & -25\mu H \\ -25\mu H & -46\mu H & 1mH & -46\mu H & -25\mu H & -21\mu H \\ -21\mu H & -25\mu H & -46\mu H & 1mH & -46\mu H & -25\mu H \\ -25\mu H & -21\mu H & -25\mu H & -46\mu H & 1mH & -46\mu H \\ -46\mu H & -25\mu H & -21\mu H & -25\mu H & -46\mu H & 1mH \end{bmatrix}$$

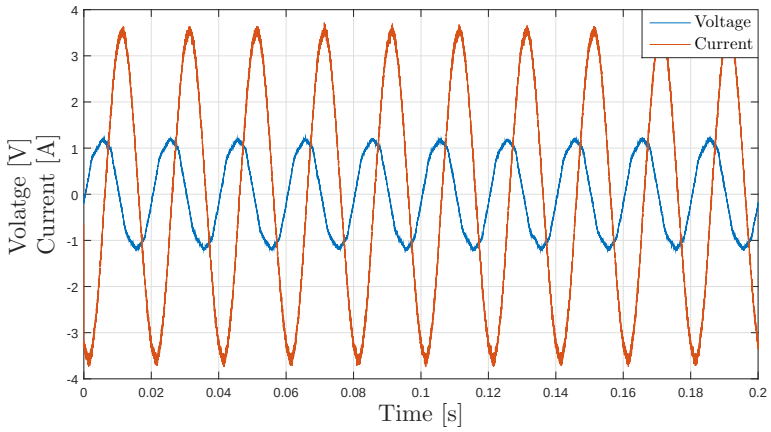

Figure 2-12: Voltage and current applied to the machine phase five. Frequency = 50 Hz, V_{rms} = 0.85 V, I_{rms} = 2.5 A.

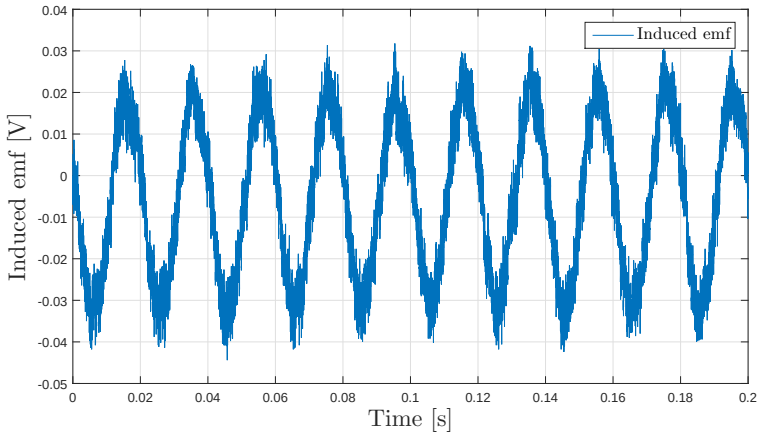

Figure 2-13: Induced emf in phase three. V_{rms} = 19 mV, frequency = 50 Hz.

From the inductance matrix (L) formed using the experiment, L_d and L_q inductance are calculated.

$$\lambda_{123} = L_{123} \cdot i_{123}. \tag{2-9}$$

where, λ_{123} is flux linkage vector of phase 1,2,3. L is inductance matrix corresponding to phase 1,2,3. i_{123} is current vector of phase 1,2,3.
Applying the Clarke's transformation (C) and Park's transformation (P) to equation 2-9, to

calculate the L_d and L_q [30].

$$C^{-1} \cdot P^{-1} \cdot \lambda_{dq} = L_{123} \cdot C^{-1} \cdot P^{-1} \cdot i_{dq}. \tag{2-10}$$

$$L_{dq} = P \cdot C \cdot L_{123} \cdot C^{-1} \cdot P^{-1} \tag{2-11}$$

For 3 phase machine, Clarke's transformation and Park's transformation.

$$C = \frac{2}{3} \cdot \begin{bmatrix} 1 & -\frac{1}{2} & -\frac{1}{2} \\ 0 & \frac{\sqrt{3}}{2} & -\frac{\sqrt{3}}{2} \\ \frac{1}{2} & \frac{1}{2} & \frac{1}{2} \end{bmatrix} \tag{2-12}$$

$$P = \begin{bmatrix} \cos p\theta_m & \sin p\theta_m & 0 \\ -\sin p\theta_m & \cos p\theta_m & 0 \\ 0 & 0 & 1 \end{bmatrix} \tag{2-13}$$

where, C is Clarke's transformation matrix. P is Park's transformation matrix. L_{dq} is inductance matrix in rotating reference frame.

As described in previous section, one MC would control the three phases of the machine, so L_d and L_q values are calculated for three phases.

$$L_{123} = L_{456} = \begin{bmatrix} 1mH & -46\mu H & -25\mu H \\ -46\mu H & 1mH & -46\mu H \\ -25\mu H & -46\mu H & 1mH \end{bmatrix}$$

Using equation 2-11 with P and C matrices. $L_d = L_q = 1$mH.

2-4-3 EMF Constant

The aim of this experiment is to determine the flux linkage in the stator winding from the rotor, which is always constant. Usually, this experiment is carried out by running the rotor of the machine whose EMF constant has to be measured using the another machine. Due to the limitation with the facility available to run the rotor of the PMSM machine under consideration using another machine shaft. The rotor of the PMSM machine under consideration was ran with the help of the three phases (1,2,3) of the machine. Taking advantage of low mutual coupling between the phases, induced emf in phase five is determined.

The magnitude of induced voltage is a function of the rate of change of flux according to Faraday's law is given by equation 2-14. Table 2-3 shows the induced voltage tabulated for the corresponding speed.

$$e_{55} = -\frac{d\lambda_m}{dt} \tag{2-14}$$

$\lambda = \lambda_m \cdot cos(2\pi ft)$ substituting value of λ in the equation 2-14.

$$e_{55} = \lambda_m \cdot 2 \cdot \pi \cdot f \cdot sin(2\pi ft) \tag{2-15}$$

Serial No.	Induced Voltage $[V]$	Frequency $[Hz]$	Speed $[rpm]$
1	1.72	20	300
2	3.36	40	600
3	4.24	50	750
4	5	60	900
5	6.64	80	1200
6	8.28	100	1500

Table 2-3: Induced voltage in phase five over the different rotor speed.

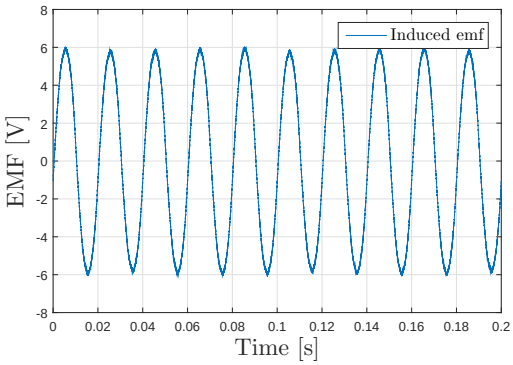

Figure 2-14: Induced emf in phase five at frequency of 50 Hz.

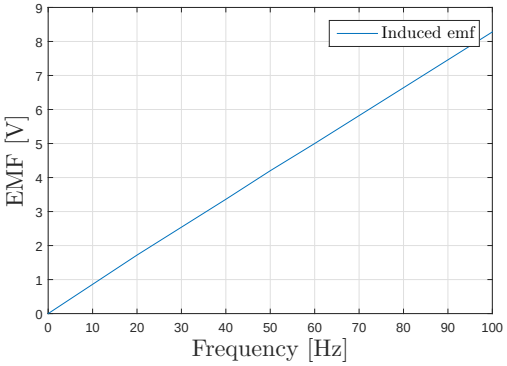

Figure 2-15: Induced emf in phase five over frequency.

$$e_{55\_rms} = \sqrt{2} \cdot \pi \cdot f \cdot \lambda_m \tag{2-16}$$

Since rotor of the machine was rotated with help of the three phases of the machine, induced EMF in phase five from three active phases has to be subtracted to know the exact value of the induced emf from the rotor on the stator. Using equation 2-8 and the inductance matrix calculated in the previous section. It was found that mutual coupling between the phases has very minimal effect on the magnitude of induced voltage from rotor to stator. It is illustrated in the example below, using one of the experiment result.

Example : Induced voltage = 4 V, speed = 750 rpm, frequency = 50 Hz.
Current through the stator excited phases : $I_1 = 107mA$,$I_2 = 120mA$,$I_3 = 102mA$.
Using the equation 2-8 and inductance matrix values.
Sum of the induced emf on the stator phase 1,2,3 = 2.5mV.
Subtracting the above sum with the induced emf in the phase 5 will result = 3.99V
This result is anticipated, because the machine is designed for very minimal mutual inductance between the phases.

Figure 2-15, shows the plot of the induced emf in V vs frequency of rotor rotation in Hz. The slope of the line, EMF constant in (V/Hz) would be 0.086 V/HZ.

2-5 Discussion

This chapter presented an overview of the design consideration for modular design six phase machine. Section 2.1 shows the typical electrical drive system architecture. Section 2.2 explained the method of application of modularity into the electrical drive system primarily for the fault tolerant application in the aerospace field. Section 2.3 discussed the permanent magnet used on the rotor. Details of the machine specification discussed above are summarized in the table 2-4 [3].

Description	Specification
Shaft output power	50 KW
Torque	8 Nm
Shaft Speed	60,000 rpm
Stator phases	6
Stator slots	12
Rotor poles	8
Bus voltage	+/-270 V

Table 2-4: Machine specification.

Section 2.4 provided the method and experimental results to determine the machine parameters used for implementing the sensorless control in the six phase machine. Measured machine parameters are tabulated in table 2-5.

Parameter	Value
Stator resistance	0.11 Ω
L_d,L_q	1 mH
EMF constant	0.086 V/Hz

Table 2-5: Machine parameters.

Chapter 3

Build and Test of Inverter Modules

Chapter summary *This chapter describes the power converter (Inverter) used in the drive system to implement the field oriented control (FOC) in the machine that follows in the subsequent chapters. The steps followed to build and test the inverter modules for machine phases are explained.*

3-1 Drive System of the Machine

Figure 3-1 shows the block diagram of the drive system used to power a single phase of the machine[1], each phase has system similar to the one indicated in the figure except one microcontroller (MC) controlling three phases of the machine. In the Fig. 3-1, blue dashed lines shows the stator voltage, current from PMSM machine stator winding, and DC link voltage fed to MC, this is necessary to estimation parameters, which will become apparent in the next chapter.

The procedure followed to build the power converter for one phase of the machine is explained through Fig. 3-2, for remaining phases, the same method was followed. Initially, PWM gate signals are generated through ePWM module of the MC (TMS320F28069x). Generated PWM signals are amplified using the driver circuit. These amplified signals are used to switch the inverter modules as indicated using blue dashed lines in the Fig. 3-2.

3-2 Inverter Module Build and Test

As it was described in the section 2-2-1, H-bridge inverter module should be used to supply the machine phases. Schematic diagram of H-bridge inverter used is indicated in the Fig.

[1]Initially, three phases of machine drive system were active, remaining phases of the machine were built with same design which was used earlier to build active phases.

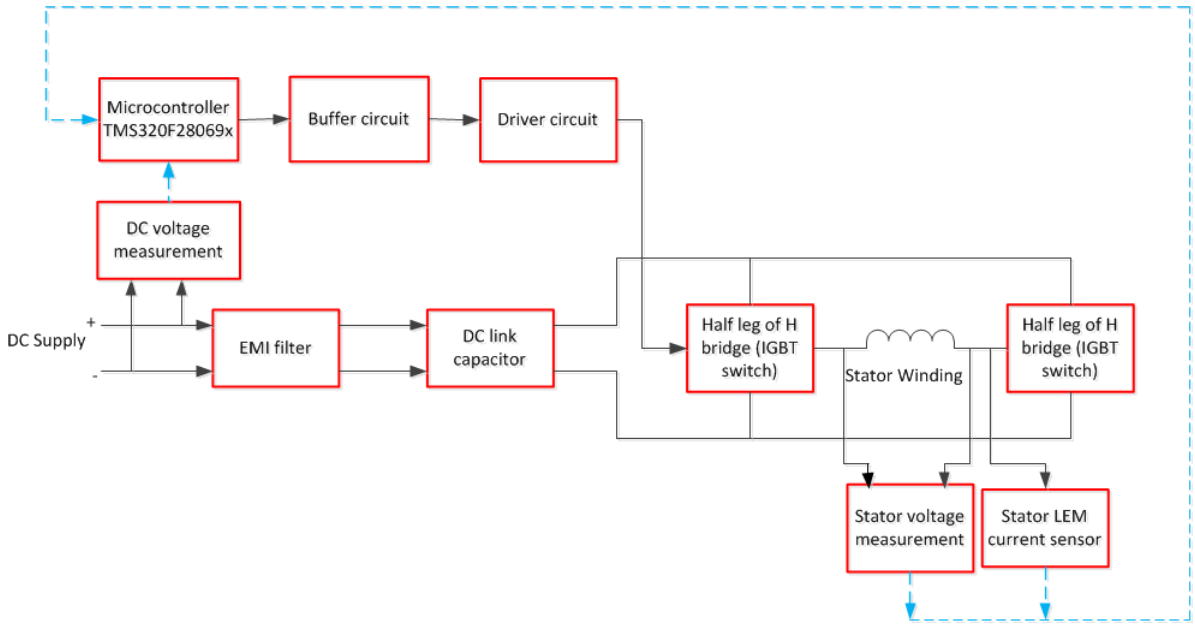

Figure 3-1: Block diagram of drive system of the machine.

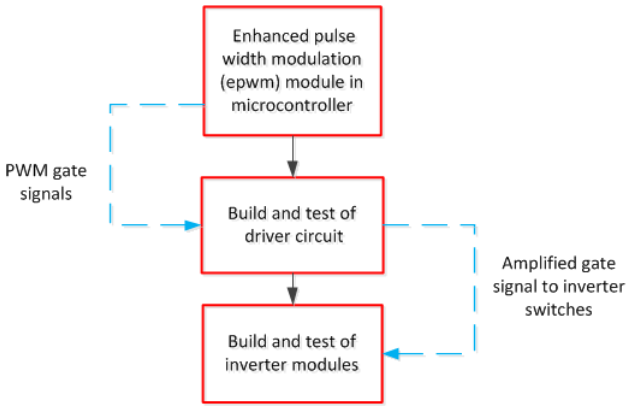

Figure 3-2: Procedure to develop power converter circuit of the machine.

3-3. For testing the single H-bridge inverter, single pulse width modulation voltage control technique is used. Fig. 3-2, will be explained in detail in following subsections.

3-2-1 Enhanced Pulse Width Modulator Module (ePWM)

Enhanced pulse width modulator (ePWM) module from MC is used for generating PWM signals to test the driver circuit and inverter module. The modulation technique used here is different from conventional modulation technique used to build the FOC in the machine. The modulation technique used for FOC will be explained in the next chapter.

ePWM module in MC is primarily used to generate the PWM signals for controlling the power converter modules. There are totally eight ePWM modules in MC. Each ePWM module has 2 outputs pins for high side and low side switch of the half H-bridge leg. Eight ePWM

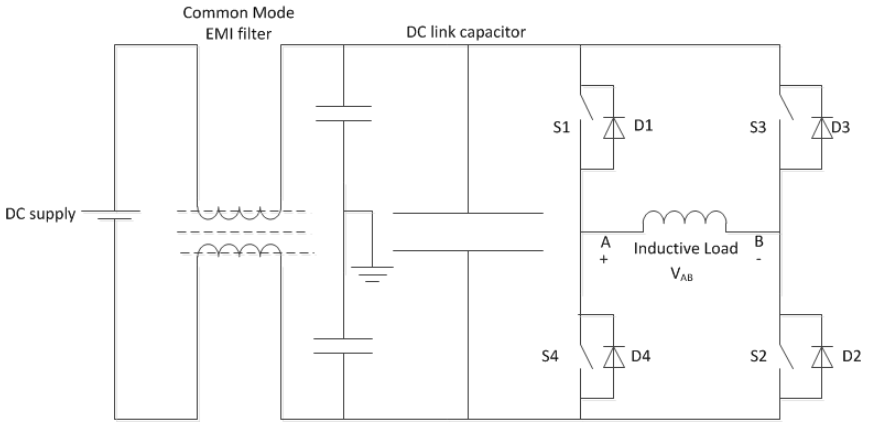

Figure 3-3: Single phase H bridge Inverter.

modules in MC are named has ePWMxA and ePWMxB[2].

Switching frequency of the PWM signals in MC is set using equation 3-1 [31].

$$\begin{aligned} T_{PWM} &= 2 \cdot TBPRD \cdot T_{TBCLK} \\ F_{PWM} &= \frac{1}{T_{PWM}} \end{aligned} \tag{3-1}$$

where, T_{PWM} is period of the PWM signal. $TBPRD$ is time base period. F_{PWM} is frequency of the PWM signal. T_{TBCLK} is time base clock, this is prescaled value of the CPU clock (SYSCLK = 90 MHz) and is used by all the submodules in the ePWM module, it is set to a value of 80 MHz.

To generate the triangular carrier signal, Up-down count mode is selected in MC. In this mode Time base counter (TBCTR) submodule in ePWM module will start counting until it reaches the time base period (TBPRD) value. When the counter reaches the TBPRD value, it starts decrementing until it reaches zero. Time base counter counts until it reaches TBPRD value and back to zero, hence it is named has Up-down count mode. This process is shown using the Fig. 3-4, here the TBCTR starts counting from zero until it reaches TBPRD with respect to the CPU clock. To set the duty cycle of the PWM signal, counter-compare submodule in ePWM module is used. In this submodule, a value is set with respect to TBPRD value. For 50% duty cycle half the value of the TBPRD is set in the counter compare register. When the time-base counter reaches the value of the counter compare, an ePWM signal is generated high or low. Using the active high complementary function, gate signals of ePWMxA and ePWMxB is made complementary to each other as indicated in the Fig. 3-4.

Fig. 3-5 shows the PWM signals generated from the MC, for inverter switches are shown. For selecting the switching frequency of PWM signals to 2kHz, TBPRD is set to value of 20,0000 and counter compare value is set to 9000 for setting the duty cycle of 45%.

[2]x = 1,2,3,4,5,6,7,8

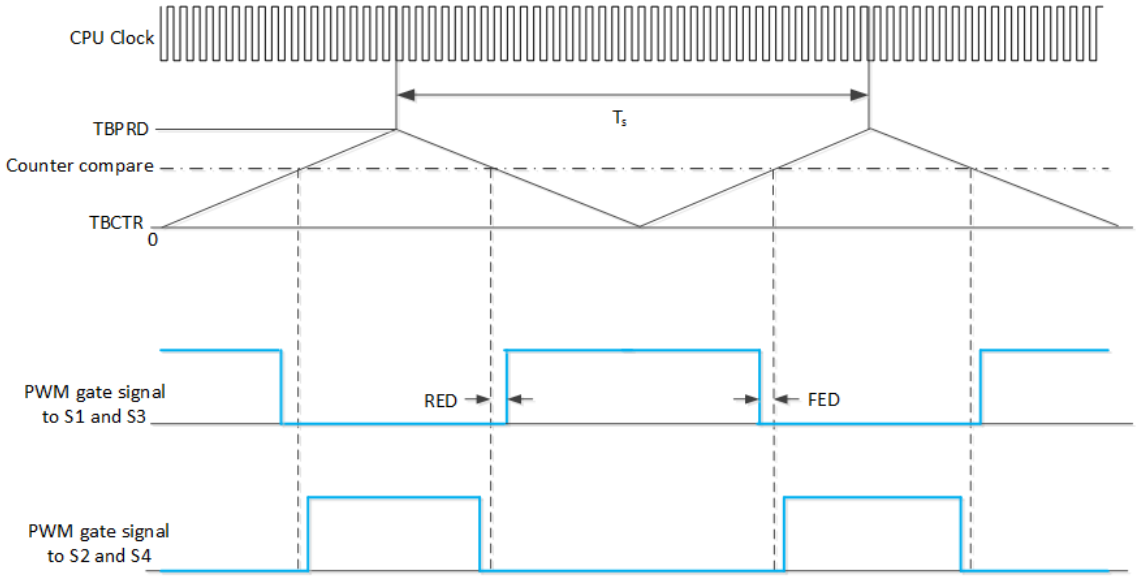

Figure 3-4: Up-Down count control method used for generating PWM signal.

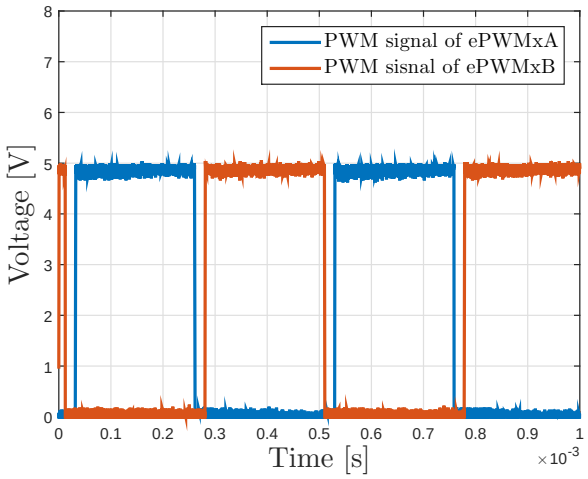

Figure 3-5: PWM signal generated by ePWM module of microcontroller. Switching frequency = 2 kHz, duty cycle = 45%.

3-2-2 Driver Circuit

The driver circuit in Fig. 3-1 is used to amplify the PWM gate signals obtained from the MC to required voltage level by the switches of the H-bridge inverter. It also provides the isolation between the MC and power converter circuit. Driver circuit uses the transformer for isolation between the MC (primary) and high voltage power circuit (secondary). During turn off the IGBT switch is maintained approximately at -10 V and at the IGBT turn-on gate voltage is kept at 15 V. IGBT is kept at the negative voltage at turn off, to avoid the dynamic latch up [32]. Driver circuit can also be used for the detection of the malfunctioning of the circuit, which includes detection of the overcurrent in the switch and supply voltage

monitoring[33].

In the Fig. 3-6 shows the output PWM gate signal obtained from the driver circuit. The input to the driver circuit is supplied through buffer circuit from ePWM module in MC, has indicated in the Fig. 3-5. The PWM signal to driver circuit from MC is at 5V during turn on and 0V during turn off. Driver circuit uses the isolated DC/DC converter to step up the voltage as per the requirement IGBT threshold voltage to turn it on and keeps the voltage negative during turn off.

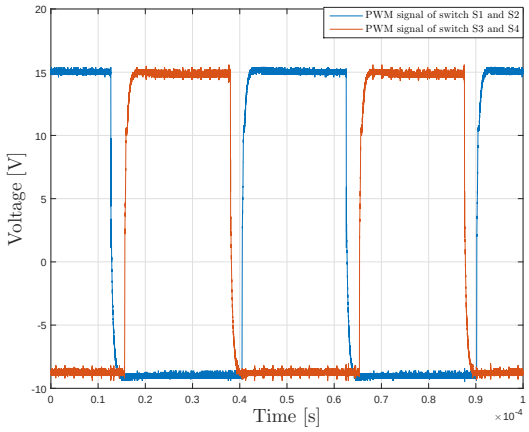

Figure 3-6: Driver circuit PWM signal to H bridge inverter. Switching frequency = 20 kHz, dead time = 2 μs, duty cycle = 44%.

3-2-3 H Bridge Inverter

For testing the H-bridge inverter, single PWM control technique is used. For this technique, PWM signals are generated from MC and stepped up using driver circuit as described in above subsections. Bipolar switching technique is used, here the diagonally opposite switches (S1,S2) and (S3,S4) in Fig. 3-3 are switched at the same time. Diodes are connected in antiparallel to the switches, here the diodes will conduct when the main switch is turned off. These diodes are known as freewheeling diodes.

R-L load was built with the inductance of 1.15mH and resistance of 2.15Ω. Load was connected between the two legs of H-bridge inverter as in the Fig. 3-3, for testing the Inverter [3]. To avoid the short circuit of the switches in the same leg, blanking time (dead time) between the switches is introduced.

Dead time (t_{dead}) depends on the gate resistance, driver circuit, and IGBT switch delay time. Dead time between the IGBT switches in one leg is calculated using the equation 3-2 [4] :

$$t_{dead} = [t_{D\_OFF\_MAX} - t_{D\_ON\_MIN} + (t_{PDD\_MAX} - t_{PDD\_MIN})] \cdot 1.2. \tag{3-2}$$

[3]Main idea behind building this specific value of inductance is to match the stator winding inductance of the machine.

where, $t_{D\_OFF\_MAX}$ is the maximal turn off delay time. $t_{D\_ON\_MIN}$ is the minimum turn on delay time. t_{PDD_MAX} is the maximal propogation delay of driver. t_{PDD_MIN} is the minimum propogation delay of driver. 1.2 is safety margin to be multiplied.

From equation 2-6 it can be seen dead time calculation is dependent on turn off and turn on delay times of switch. Definition of the turn on and turn off delay time can be referred using Fig. 3-7.

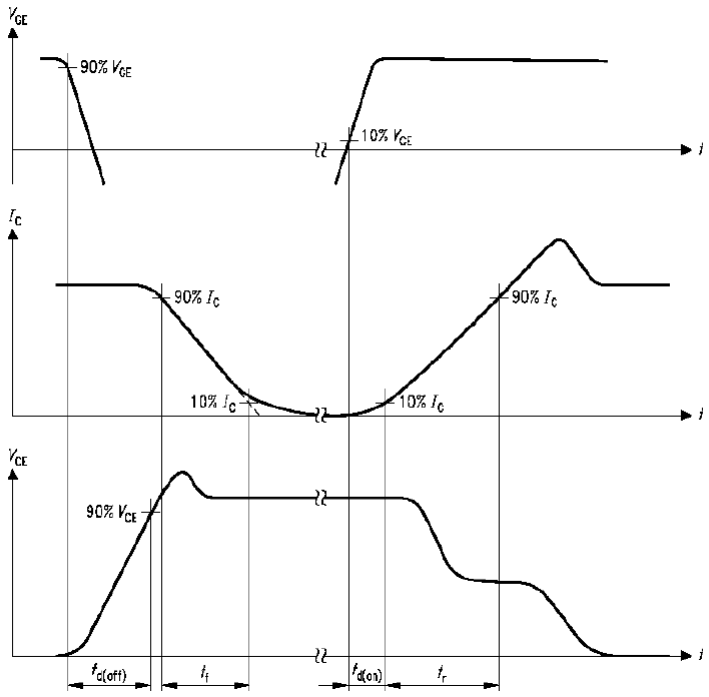

Figure 3-7: Definition of switching times [4].

Maximum turn off delay $t_{D\_OFF\_MAX}$ and the minimum turn on delay $t_{D\_ON\_MIN}$ time of the switch are not specified in IGBT Semikron datasheet [34]. So, typical values of turn off and turn on delay times mentioned in the datasheet are used for the calculation of the dead time in the equation 2-6. The value of the gate resistance in inverter is 10Ω. Time delay increases with the increase in the gate resistance [4]. This can also be observed from the characteristics plot of the switching times vs gate resistance in Semikron datasheet [34]. From the safety viewpoint, it is better to consider the higher value of the delay time, so for the calculation delay time mentioned for 15Ω is used. Typical values of the turn on and turn off delay time of IGBT switch are :
t_{d_on} = 63ns for gate resistance of 15Ω.
t_{d_off} = 521ns for gate resistance of 15Ω.

Second part of the equation depends on propagation delay time difference in the driver circuit. It means the delay time caused by the driver circuit gate signal from MC to switch. This value will be usually specified in the data sheet of the driver circuit [4]. Propagation time delay of the driver circuit 2SC0108T is 100ns [35].

Since the maximum value of the t_{d_off} wasn't specified in the datasheet. For improving the safety factor, fall time (t_f) is added to turn off delay. Fall time (t_f) is added to compensate for using typical turn off delay time instead of maximum turn off time. It will give t_{dead} value of 766ns.

Dead time value between the switches in the leg is set with the help of Dead band generator submodule in the ePWM module. This submodule used the programmable delay on rising and falling edges of the PWM signals generated by the ePWM module [31]. By controlling the values of Falling edge delay (FED) and Rising edge delay (RED) in ePWM module, deadtime value is set for ePWM modules, as indicated in the Fig. 3-5.
Formula for calculating Falling edge delay (FED) and Rising edge delay (RED) in MC.

$$\begin{aligned} FED &= DBFED \cdot T_{TBCLK} \\ RED &= DBRED \cdot T_{TBCLK} \end{aligned} \tag{3-3}$$

where, FED is Falling edge delay. RED is Rising edge delay. DBFED is Dead band rising edge delay. DBRED is Dead band falling edge delay, T_{TBCLK} is a period of TBCLK, prescaled version of CPU clock (SYSCLK).

Keeping the dead time calculated above has a reference, the dead time value is set between the two switches. DBRED and DBFED are set to a value of 165 and the T_{TBCLK} is $\frac{1}{80MHz}$, in equation 3-3 which will result in the dead time of 2μs. Switching frequency of the PWM signals generated by MCU is set to 20KHz, using the equation 3-1, TBPRD is set to value of 2000.

The output voltage and current measured across the inductor for above mentioned configuration is shown Fig. 3-8. By varying the duty cycle of the reference signal output V_{o_rms} is controlled. The duty cycle of the all the switches are set at 44%, excluding the dead time, rms value of the output voltage V_{o_rms} is 9.17 V. Current through the inductive load lags the output voltage due to an inductive nature of the load this can be seen in the Fig. 3-8.

During dead time, both the switches previously conducting will stop and the load connected between the legs of the H-bridge will be floating. But the energy stored in the inductor will start conducting through the freewheeling diodes connected antiparallel to the switches. If current is flowing through the switches S3 and S4 (from point B to A) before the dead time, to maintain the current in the same direction during dead time. Diodes D1, D2 will conduct and negative voltage will appear across the load [36]. If the current is flowing through the switches S1 and S2 (from point A to B) before dead time. During the dead time to maintain the current in the same direction diodes D3, D4 will conduct and positive voltage will appear across the load. Both the effects can be seen in the Fig. 3-8.

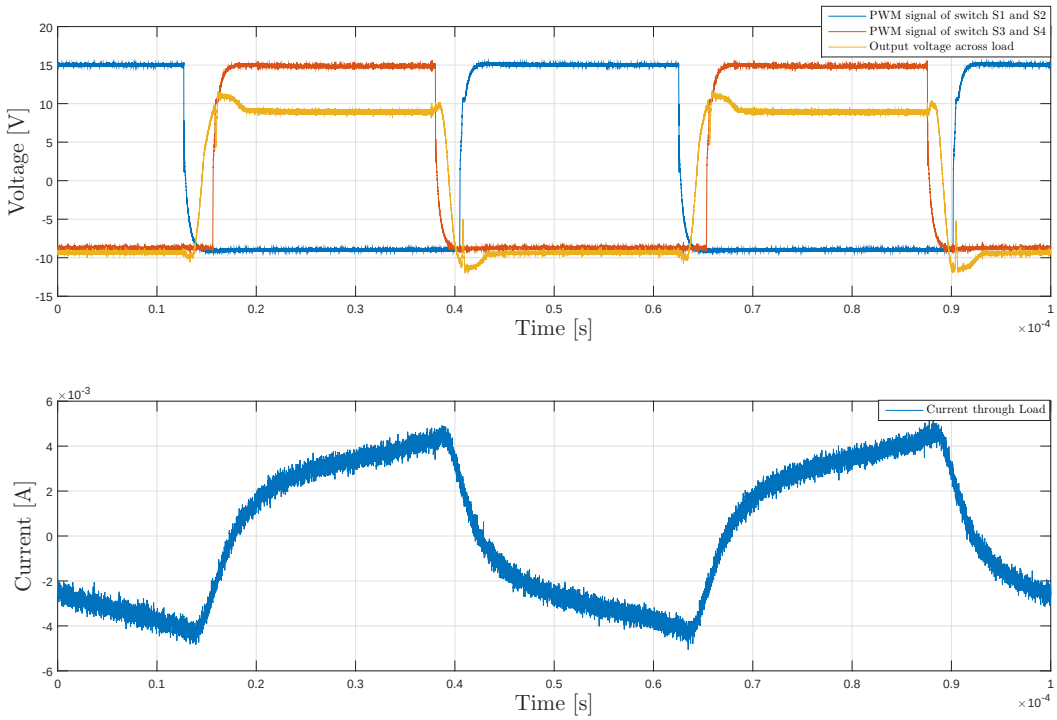

Figure 3-8: H bridge inverter output voltage and current plots, with gate signal. Switching frequency = 20 kHz, dead time = 2 μs, duty cycle = 44%, dc supply = 10 V.

3-3 Discussion

This chapter has focussed on building and testing of the drive circuit of the PMSM machine. It also gives insight into the power converter of drive system of the machine. Fig. 3-9 and 3-10 shows the built front and rear view of the single phase H-bridge module. As indicated in the two figures numbering is used to indicate the components in the full bridge inverter 1a - EMI Filter Inductor, 1b - EMI filter Capacitor, 2 - DC link Capacitor, 3 - Driver circuit, 4 - Output terminals of H-bridge, across this machine stator winding is connected, 5 - Buffer IC, 6 - Half leg IGBT switches. 7. Slot for interconnection between microcontroller and power converter, connection is formed through wire to board connector and PCB connector.

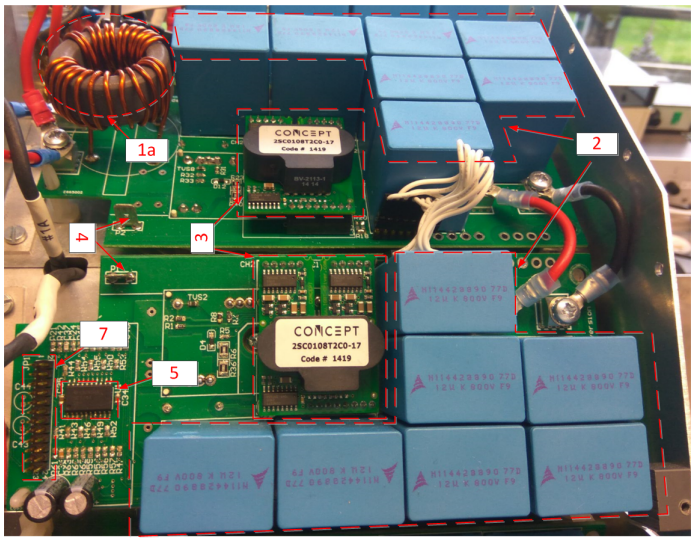

Figure 3-9: Single phase H bridge module front view.

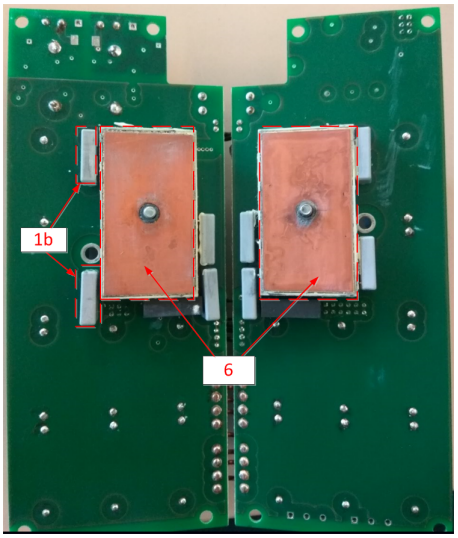

Figure 3-10: Single phase H bridge module rear view.

Chapter 4

Implementation of Sensorless FOC for Three Phases of Machine

Chapter summary *This chapter aims at building the sensorless field oriented control (FOC) in the three phases of the machine. First, sensorless FOC is explained and dq theory is applied to the PMSM machine. Thereafter, InstaSPIN algorithm in the microcontroller used for implementing the direct FOC is described with the drive setup. This is followed by Analog to digital conversion module (ADC) and enhanced Pulse width modulation (ePWM) module applied to dual two level inverter is explained. Use of the model based current control for the PI controller of the current controller is discussed. Finally, experiments results of the sensorless control for the three phase is shown.*

4-1 Sensorless FOC

4-1-1 Field Oriented Control

Motor control performance can be characterized to be effective if it has a smooth rotation and good torque control over the entire speed range, fast acceleration, and deceleration. In FOC stator current is decomposed into the magnetic field generating component and torque generating component, for controlling the machine[37].

FOC is based on projections which transform a three phase time and speed dependent system into a time-independent two coordinate system. Three phase voltages and currents supplied to the motor, is represented by complex space vector, with regard to the current space vector it is represented by $\vec{i}_s$. Current space vector is represented by instantaneous sinusoidal current i_a,i_b and i_c given by equation 4-1 and Fig. 4-1 indicates stator current space vector with its

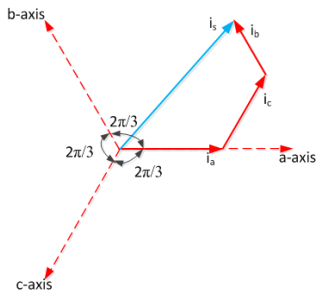

Figure 4-1: Stator current space vector and its three phase variables i_a,i_b and i_c.

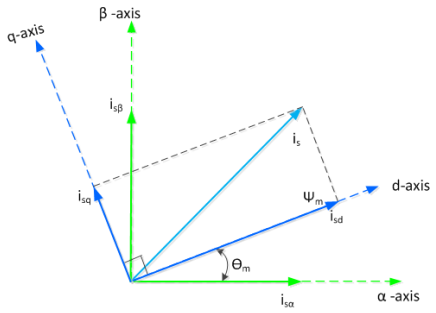

Figure 4-2: Stator current space vector and its component in α, β and d,q reference frame.

current component.

$$\vec{i}_s = i_a + i_b \cdot e^{j\frac{2\pi}{3}} + i_c \cdot e^{-j\frac{2\pi}{3}} \tag{4-1}$$

To convert from three phase system to two phase time invariant system, two transformations are followed.

Clark's transformation (C) : This projection will converts the a,b,c system into two dimensional orthogonal system (α, β), after this transformation current $i_{s\alpha}$ and $i_{s\beta}$ still depends on the time and speed.

$$i_{\alpha\beta 0} = C \cdot i_{abc} \tag{4-2}$$

$$\begin{bmatrix} i_{s\alpha} \\ i_{s\beta} \\ i_0 \end{bmatrix} = \frac{2}{3} \cdot \begin{bmatrix} 1 & -\frac{1}{2} & -\frac{1}{2} \\ 0 & \frac{\sqrt{3}}{2} & -\frac{\sqrt{3}}{2} \\ \frac{1}{2} & \frac{1}{2} & \frac{1}{2} \end{bmatrix} \begin{bmatrix} i_a \\ i_b \\ i_c \end{bmatrix} \tag{4-3}$$

$$\begin{aligned} i_{s\alpha} &= \frac{2}{3} \cdot i_a - \frac{1}{2} \cdot i_b - \frac{1}{2} \cdot i_c \\ i_{s\beta} &= \frac{1}{\sqrt{3}} \cdot i_b + \frac{2}{\sqrt{3}} \cdot i_c \end{aligned} \tag{4-4}$$

Park's transformation (P): This transformation modifies the projection from the two phase orthogonal system (α, β) into the d,q rotating reference frame. It also converts two co-ordinate time varying system into two co-ordinate time invariant system.

$$i_{dq0} = P \cdot i_{\alpha\beta 0} \tag{4-5}$$

$$\begin{bmatrix} i_d \\ i_q \\ i_0 \end{bmatrix} = \begin{bmatrix} \cos p\theta_m & \sin p\theta_m & 0 \\ -\sin p\theta_m & \cos p\theta_m & 0 \\ 0 & 0 & 1 \end{bmatrix} \begin{bmatrix} i_{s\alpha} \\ i_{s\beta} \\ i_0 \end{bmatrix} \tag{4-6}$$

$$\begin{aligned} i_d &= i_{s\alpha} \cdot \cos p\theta_m + i_{s\beta} \cdot \sin p\theta_m \\ i_q &= -i_{s\alpha} \cdot \sin p\theta_m + i_{s\beta} \cdot \cos p\theta_m \end{aligned} \tag{4-7}$$

The two transformations described above are also pictorial represented in the Fig. 4-2. Currents i_d and i_q are always constant under steady state. During transient conditions, values of current varies with the time. Conversion of the stator system into rotor reference frame and basic structure of FOC is algorithm is shown in the schematic Fig. 4-3.
Following steps describe briefly the algorithm of FOC in PMSM.

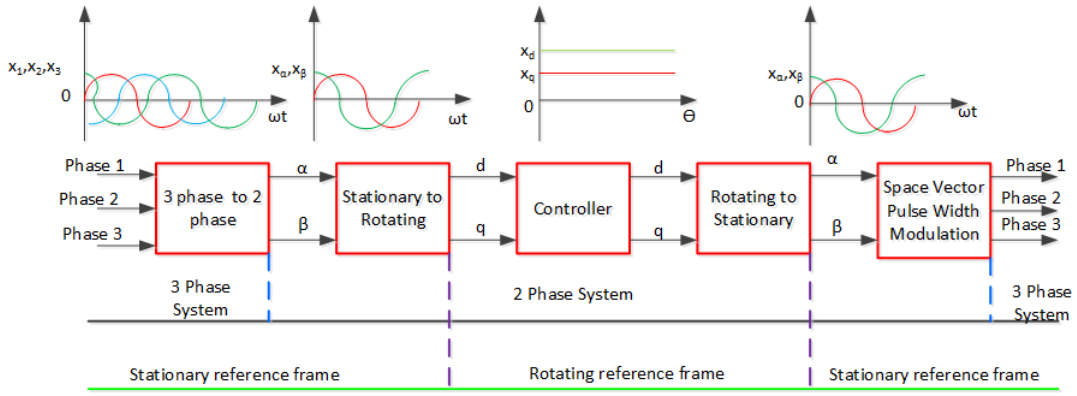

Figure 4-3: Field oriented control transformation.

- Three phase motor quantities voltage and current are measured.
- Using Clarke's transform three phase system is converted to two phase i_α and i_β currents.
- Rotor flux space vector angle and magnitude is calculated.
- Stator currents are transformed into rotor reference frame i_d and i_q currents using Park's transform
- The current i_d acts has flux producing component and current i_q is torque producing the component, they are controlled independently.
- Using PI controller, torque current component i_q is controlled.
- By using inverse Park's transform, currents i_d and i_q are converted back to the two phase stationary reference system.
- Three phase output voltage is generated from space vector pulse vector modulation, corresponding to the output from the two phase transformation.

4-1-2 Sensorless Control Technology

Machines employing FOC technique for its control would require accurate rotor position information all the time. Rotor position is required for the decomposing the stator current into the torque producing current component and flux producing current component. And it is also required for the Park's transformation used in the FOC. Inaccurate rotor position

in the control would result in poor performance and in some cases it will lead to complete drive failure. The position/speed sensor used for rotor position information in FOC [1] technique may result in problems such as complexity of hardware, difficulties in application to the unfriendly atmospheres, increased cost, decreased reliability due to cables and sensors, difficulties of attachment of the sensor to electrical machine, electromagnetic interference and increased axial length [38]. To solve described problems with conventional position sensor, many sensorless control techniques are employed for control of AC machines.

Sensorless control for the AC machines can be classified into three groups [39].

- Linear method.
- Non Linear method.
- High-frequency injection method.

In the linear method measured terminal voltage and currents are used to calculate the rotor position. This technique uses classical control theory with the basic machine equations. This work is limited to this method and the other two methods are beyond the scope of this work. Sensorless control is implemented in PMSM machine, based on the linear method.

Using the concept of rotor position feedback from sensorless control and FOC, angle control (and field orientation) is introduced. Here, the instantaneous control of the stator current (i_d, i_q) is done in rotor reference frame. Controlled current supply to the machine, using FOC maintains relative field orientation condition for transient changes in the machine speed as well as under steady state conditions [37].

4-2 Permanent Magnet Synchronous Machine Model

When applying the dq theory to the machine, some assumptions have been made, stator winding has to be sinusoidally distributed and the magnetic circuit shouldn't saturate. Florence Meier showed that torque and steady state operation can be accurately calculated using the dq model if the magnetic circuit isn't saturated for PMSM machine with the non-overlapping concentrated winding, and even if the sinusoidally distributed winding is violated [40].

Magnetic, electrical and physical isolation between all the stator phases, each machine phase can be considered has single decoupled circuit. Each stator phase is represented by resistor R_s, inductor L_s and the induced back-emf e_1 from the rotor magnet, circuit schematic is indicated in the Fig. 4-4.

As it was explained in the thesis objective, initially sensorless control was implemented for three phases of the machine and later it was extended to six phases of machine. Hence, dq model for three phases of the machine is developed [5]. Electrical equation for the three phases of the circuit in a,b,c reference frame, is converted to dq rotor reference frame rotating

[1] This type of FOC is known has Indirect FOC, because rotor position sensor is used for measuring the rotor position

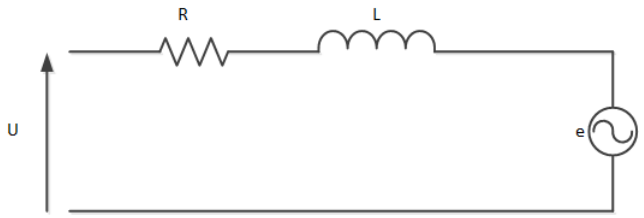

Figure 4-4: Equivalent circuit of single phase modular design machine.

at synchronous speed.

$$\begin{aligned} u_1 &= R_s \cdot i_1 + L_s \cdot \frac{di_1}{dt} + e_1 \\ u_2 &= R_s \cdot i_2 + L_s \cdot \frac{di_2}{dt} + e_2 \\ u_3 &= R_s \cdot i_3 + L_s \cdot \frac{di_3}{dt} + e_3 \end{aligned} \tag{4-8}$$

where, u_1, u_2, u_3 is voltage applied across the stator phases one two and three respectively. i_1, i_2, i_3 is the current through the stator phases one, two, and three respectively. R_s is stator resistance. L_s is stator inductance. e_1, e_2, e_3 is induced emf in the stator phases one,two, and three respectively.

Applying the Clarke's transformation(C) matrix to the equation 4-8

$$u_{\alpha\beta 0} = C \cdot u_{123} \tag{4-9}$$

$$\begin{aligned} u_\alpha &= R_s \cdot i_\alpha + L_s \cdot \frac{di_\alpha}{dt} + e_\alpha \\ u_\beta &= R_s \cdot i_\beta + L_s \cdot \frac{di_\beta}{dt} + e_\beta \end{aligned} \tag{4-10}$$

For obtaining the machine model in rotor reference frame, Park's transformation (P) is applied to the equation 4-10.

$$\begin{aligned} u_{dq0} &= P \cdot u_{\alpha\beta 0} \\ u_{dq0} &= P \cdot C \cdot u_{123} \end{aligned} \tag{4-11}$$

$$\begin{aligned} u_d &= R_s \cdot i_d + L_d \cdot \frac{di_d}{dt} - p \cdot w_m \cdot L_q \cdot i_q \\ u_q &= R_s \cdot i_q + L_q \cdot \frac{di_q}{dt} + p \cdot w_m \cdot L_d \cdot i_d + \psi_m \cdot p \cdot w_m \end{aligned} \tag{4-12}$$

$$T = \frac{3}{2} \cdot p \cdot \psi_m \cdot i_q \tag{4-13}$$

where, T is electromagnetic torque. p is number of pole pairs. ψ_m is the rotor flux. i_d, i_q is current in d and q axis of rotor reference frame. u_d, u_q is the voltage in d and q axis of the rotor reference frame. L_d, L_q is inductance in d and q axis of rotor reference frame.

In the dq model, the d-axis stator current is aligned with the rotor flux axis and q axis

current is perpendicular to rotor flux axis. By controlling the d-axis current field weakening can be achieved in the PMSM. From the equation 4-13, torque in surface mounted PMSM machine, depends on the rotor flux ψ_m and q axis current i_q. Since the amplitude of the rotor flux is always constant, torque has a linear relationship with the current component i_q.

4-3 Sensorless FOC Control Using TI instaSPIN Algorithm

Sensorless FOC is implemented in the PMSM machine using Texas instruments (TI) InstaSPIN FOC motor control algorithm in TMS320F2806xF MC device. TI introduced the InstaSPIN FOC, this device employs the FAST software observer[2]. FAST observer uses measured stator terminal voltage and currents from motor, for the estimating the rotor flux angle or rotor position (θ_m) [22]. FAST observer works on principle of back-emf model with open-loop operation at low speed [41]. Open loop operation is employed to avoid the problem of evaluating the flux vector at low speed, which is one of the demerits of using the back-emf method. By using both the methods in the InstaSPIN algorithm, motor control can be built for entire speed range.

4-3-1 Principle of Back-emf Approach

In the back-emf model approach, for estimating the rotor position, measured three phase voltage and currents are used [22]. In this method estimated voltage vector is calculated using the motor equation in vector form, it is defined in [42].

$$\begin{aligned} \vec{e_s} &= \vec{u_s} - R_s \cdot \vec{i_s} \\ \vec{e_s} &= \frac{d\vec{\psi_s}}{dt} \end{aligned} \tag{4-14}$$

where, e_s is voltage vector. ψ_s is stator flux linkage vector. $\vec{u_s}$ is stator voltage vector. $\vec{i_s}$ is stator current vector.

Equation 4-14 shows that voltage vector can be estimated using the stator resistance, voltage, and currents measured across stator of the machine. Integration of the estimated voltage vector, will give estimated stator flux linkage as shown in the equation 4-15.

$$\vec{\psi_s} = \int \vec{e_s} \cdot dt \tag{4-15}$$

Rotor flux position and magnitude is calculated using equation 4-16 with the knowledge of the stator inductance and the measured current [22]. Fig. 4-5, shows space vector diagram for rotor position estimation method.

$$\vec{\psi_m} = \vec{\psi_s} - L_s \cdot \vec{i_s} \tag{4-16}$$

[2]FAST observer is TI proprietary technology, literature available is limited only to application notes

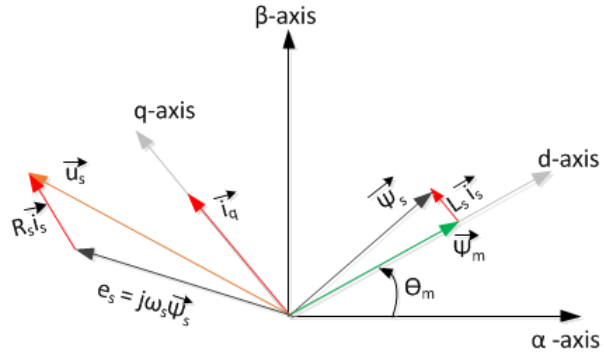

Figure 4-5: Space vector diagram for estimation of voltage emf vector.

4-3-2 Drive Setup using InstaSPIN Module

Fig. 4-6 shows the schematic of the standard drive setup for building sensorless control using the InstaSPIN algorithm [41]. In the system under consideration, similar drive setup is employed to implement sensorless control in machine. Measured stator current, stator voltage, and DC link voltage using the sensors, are the fed to the ADC module of the MC. Further the analog input signal is converted into a digital output, method of conversion to digital output will be explained in the following section.

Output of ADC is fed to Clarke's transform module, here i_1, i_2, i_3, u_1, u_2, and u_3 are transformed to $i_\alpha, i_\beta, u\alpha$, and u_β. Clarke's module output values with the DC link voltage (V_{DC}) from ADC module is fed to FAST observer. MC houses the FAST software observer in the ROM of the device. This module also requires access for the measured stator resistance R_s and stator inductance L_s value. With these inputs to the observer module described above, FAST software encoder will estimate the rotor position (θ_m), rotor flux amplitude (ψ_m), speed of the rotor (ω_m), and Torque (T) using back emf method described in section 4-3-1. Rotor speed and position obtained from FAST, will be used for building the FOC for PMSM machine.

In drive setup, two control loops are used for controlling speed and torque of the machine. Torque equation 4-13, shows that torque can be controlled directly by current in q axis of the rotor reference frame, through the inner current controller loop. Inner current control loop is superimposed by the outer speed control loop for controlling the shaft speed of the machine. This type of control is known has cascaded control approach, inner control loop is for current control and outer control loop for the speed.

In the outer speed control loop, estimated speed $\left(\widetilde{\omega}\right)$ is compared with the user reference speed (ω_{ref}). The resulting error signal is fed to speed PI controller, the output of the controller represents the reference torque T_{ref} or i_{qref} (current reference). Measured current i_1, i_2, and i_3 fed to the ADC module are converted to i_d and i_q, using the estimated rotor position, Clarke and Park's transform. Measured current (i_q) is compared with the reference current (i_{qref}) from the speed controller, deviation in the value is fed to the PI current controller. This controller uses the model-based current control for generating the voltage reference u_q. Inverse Park transformation on reference voltage, with space vector pulse width

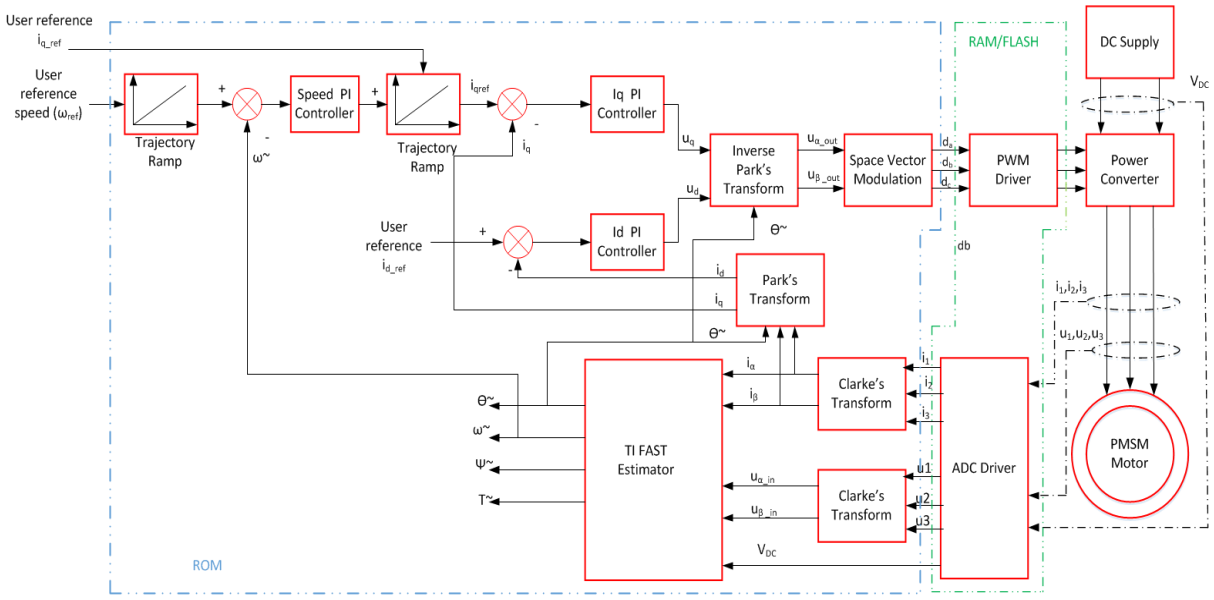

Figure 4-6: Drive setup using InstaSPIN-FOC.

modulation using PWM driver circuit module duty cycle values required by the power converter are generated through MC [22]. Current reference (i_{dref}) is always kept zero, because field weakening mode of operation is out of the scope of the research.

Employing the cascaded control loop discussed, machine would produce required electromagnetic torque, necessary to achieve the user reference speed. In the next section, detail working of the PI controller modules and the PWM modules will be explained.

PI Antiwindup

During transients when control variables reach actuator limits, the feedback loop breaks and the system will run on the open loop because actuator will remain at its limits irrespective of the process output. Integrator action present in the PI controller will produce the error due to deviation in reference and output value. Integration of this error will result in the large integral term value and it winds up [43].

In the system under consideration, two control loops are used one for speed control and another one for torque control. Windup will occur when the reference voltage generated by the PI controller exceeds the maximum value of the voltage that can be delivered by the power converter. Under this circumstance, the current error occurs at the input of the controller, which will further increase PI controller reference voltage output.

The anti-windup feature in the PI controller will limit the integrator action to user defined limit (user defined voltage reference) when it has reached. This is done through the static integrator clamping. In the speed controller limit is set to maximum speed motor can reach and for the current controller, it is set through maximum voltage per sample.

4-3-3 Microcontroller Board

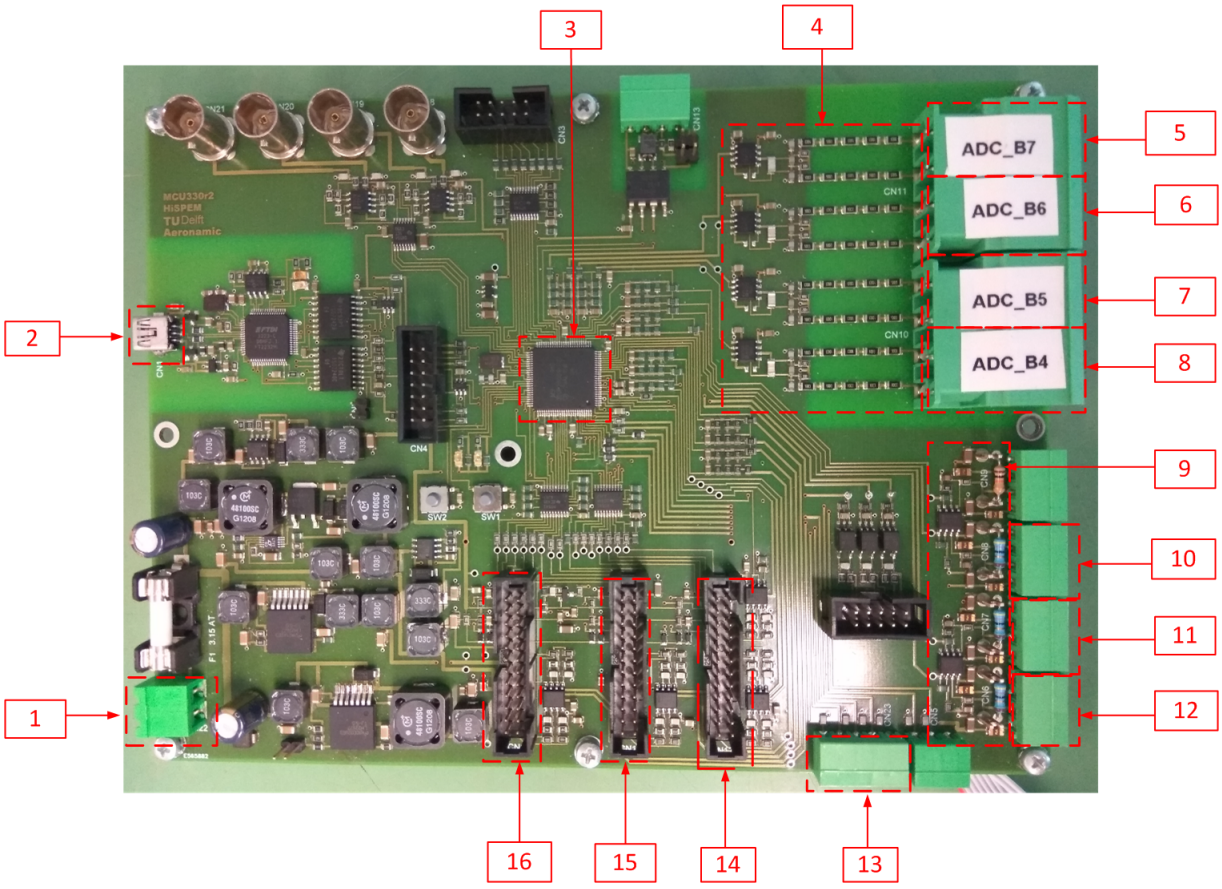

Figure 4-7: Micrcontroller board used for the sensorless control.

Fig. 4-7 shows the MC board used for implementing the senorless control in PMSM machine. Modules/Components numbers indicated in MC board are as follows :

1. 24V DC power supply port to MC.

2. Universal Serial Bus (USB) port used to flash the program to MC board.

3. TMS320F28069x MC chip.

4. Voltage scale down and filter circuit for DC voltage (from inverter), three phase stator voltage (from motor phases) fed to ADC module in MC.

5. DC link supply to inverter fed to ADC module in MC through this external port.

6,7,8. Voltage across the phase one (8), two (9) and three (10) stator winding are fed to ADC module in MC through this external port.

9. Voltage transformation and filter circuit for current from the stator winding fed to ADC

module in MC.

10,11,12. Current through the phase one(12), two (11), and three (10) stator winding are fed to ADC module in MC through this external port.

13. SPI module external port of MC.

14. ePWMx5 and ePWMx6 module external ports.

15. ePWMx1 and ePWMx2 module external ports.

16. ePWMx3 and ePWMx4 module external ports.

4-4 Analog to Digital Converter (ADC) Measurement Unit

Analog to Digital converter (ADC) module is used to convert the analog input signal to digital output. The purpose of this module in FOC is to convert the analog real-time variation of the stator phase voltage, stator phase current, and DC link voltage to digital binary numbers. Converted digital values are used by FAST observer, to estimate the rotor position, rotor flux magnitude, torque and rotor speed as described in the previous section. ADC module has 12 bit ADC core with the maximum digital output value of 4096 ($2^{12} = 4096$) for analog input of 3V at MC ADC pin.

Before the signal is sent to ADC pin of MC to convert it to the digital signal, it has to be scaled down to the voltage range of 0 to 3V. Circuits used to scale down the voltage, current and procedure followed to convert analog to digital signal are explained in the following two subsections.

4-4-1 Stator Phase Voltage - ADC Module

The conversion circuit for ADC module is designed for the voltage range of -306V to +306V. This voltage range is scaled down to the voltage range of 0 to 3V required by the ADC pin in MC [31].

Circuit used to scale down the voltage is indicated using the block diagram shown in the Fig. 4-8. Initially, the input voltage (+306V to -306 V) is divided by the ratio of 1/51, using the voltage divider circuit. This would result in the voltage reduction of +6 to -6V. Scaled down voltage signal is passed through the low-pass RC filter to remove higher order harmonic signals. After a high harmonic signal is removed, using level shifter -6V to 6V signal is converted to the 0 to 3V. Analog input voltage in the range of 0 to 3V is fed to MC ADC pin for digital conversion.

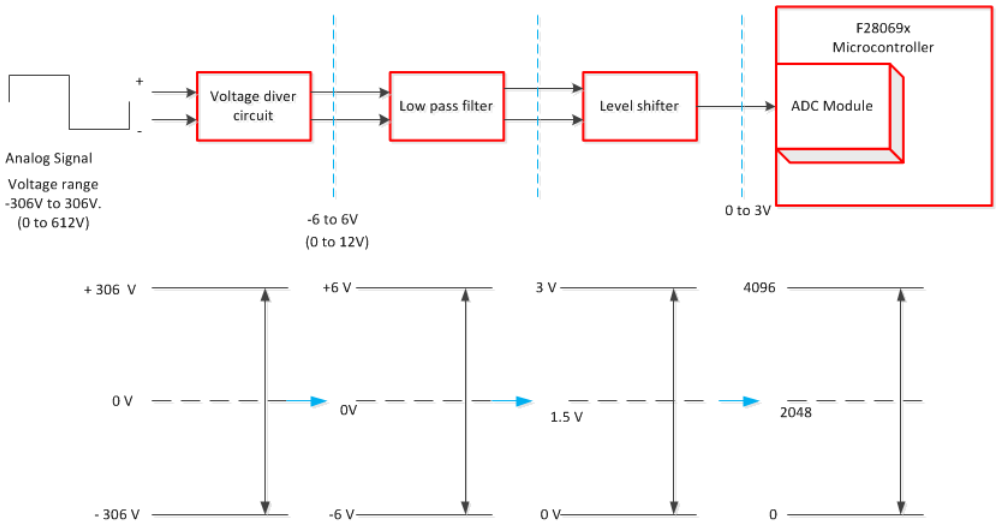

Figure 4-8: Block diagram of the voltage scale down circuit for ADC module used in the microcontroller board.

Digital Conversion Method for Voltages in MC

ADC module in the MC uses the Bipolar Offset Binary (BOB) coding method to convert the analog signal to the digital value [44]. In this method, the analog input voltage is both positive and negative. Digital output counting begins with zero for negative analog input full scale value $(-306V \rightarrow 0V)$[3]. As the digital value increments and reaches half the digital maximum value (2048) for analog input voltage equivalent to zero $(0V \rightarrow 1.5V)$[4]. After analog input zero crossing occurs at digital value of 2048, digital output value increases proportionally to positive analog input signal until input reaches its positive full-scale value $(+306V \rightarrow 3V)$[5].

Digital code for the corresponding analog input voltage can be determined analytially using equations below [45]:

$$V_{in} = \text{Digital Code} \cdot \text{LSB Size} \tag{4-17}$$

$$\text{LSB Size} = \frac{\text{Full scale voltage}}{2^N} \tag{4-18}$$

where, V_{in} is analog input voltage. Digital Code is output digital value of ADC module. LSB Size is value or weight of the least significant bit (LSB) in the ADC code. Full scale voltage is analog to digital full scale input voltage. N is number of bits of the ADC output code.

Experiment Results - ADC Module

Experiment was conducted to verify the ADC module, digital values obtained for respective analog input signals is shown in the table 4-1.

[3] -306V represents voltage measured across the stator and 0V represents scaled down voltage for ADC pin
[4] 0V represents voltage measured across the stator and 1.5V represents scaled down voltage for ADC pin
[5] +306V represents voltage measured across the stator and 3V represents scaled down voltage for ADC pin

Analog input voltage [V]	Digital output code [Decimal format]
-20	1889
-15	1920
-10	1955
-5	1986
0	2020
5	2054
10	2085
15	2120
20	2150

Table 4-1: ADC module digital output for corresponding analog input voltage.

Using the equations 4-17 and 4-18, digital output code can be analytically calculated for analog DC input voltage shown below.

Example 1 : Analog input voltage = 20V.

$$\text{LSB Size} = \frac{612}{2^{12}} = 0.14941.$$

Using the LSB size in the equation 4-17 for input voltage of 20V.

$$\text{Digital code} = \frac{20}{0.14941} = 134.$$

BOB method is used for conversion in ADC module, it will result in the digital value in decimal format output 2154 ($2020 + 134 = 2154$).

Both the positive and negative signal are amplified, it will result offset in the half the digital ADC range [46].

DC Voltage - ADC module

Scale down and digital output conversion procedure for DC voltage fed to inverter, is same as in the stator phase voltages. Here, conversion is always unipolar (positive voltage).

4-4-2 Stator Phase Current - ADC Module

The conversion circuit used for conversion is designed for the analog input current range of +30A to -30A. This input current range is scaled down to the voltage range of 0 to 3V required by the ADC pin in MC [31].

Block diagram of the current sensor and the corresponding circuits used for the measurement of the current is shown in the Fig. 4-9. ABB current sensor is used, it works on the principle of the closed loop Hall effect technology, with the galvanic isolation between the primary and secondary of the circuit [47]. The primary current (I_P) is current flowing through

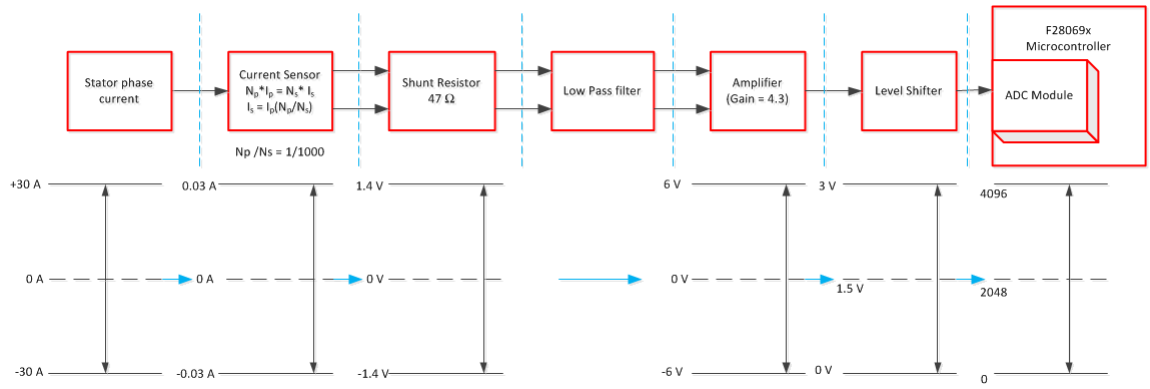

Figure 4-9: Block diagram of the current sensor with corresponding current scale down circuit for ADC module used in the microcontroller board.

the stator phase. Secondary current is the output from the sensor is related to primary current by $N_p \cdot I_p = N_s \cdot I_s$, ratio of number of turns in primary to secondary is $\frac{N_P}{N_s} = \frac{1}{1000}$. Secondary current from the current sensor will flow through the shunt resistor of value 47Ω [48]. The voltage measured across this resistance is the proportional secondary current output from the current sensor. The voltage measured across the resistor will be in the range of -1.4V to +1.4V, this signal is amplified using amplifier by a gain of 4.3. This would result in the voltage in the range of +6V to -6V. Using the level shifter, +6V to -6V will be converted to the ADC module requirement of 0 to 3V.

Digital Conversion Method for Current in MC

In this method, the digital output value of current measurement in ADC module is proportional to the voltage drop across shunt resistance. Hence, the digital method of conversion here is same as the method described for analog input voltages in the previous subsection.

Experiment Results - ADC Module

Experiment was conducted to test the ADC module, digital values obtained for respective analog input currents signals is shown in the table 4-2.

Digital output code of ADC module can be analytically calculated for analog input current shown below.

Example 1 : Primary current (I_p) through the current senor = 1.2 A.

Secondary current related to primary current $I_s = \frac{N_p \cdot I_p}{N_s}$ $\left(\frac{N_P}{N_s} = \frac{1}{1000}\right)$
Secondary current of the current sensor = 1.2 mA.
Voltage acorss the resistor will be V = I · R. ($R = 47\Omega$)

$$V = 1.2 \cdot 10^{-3} \cdot 47 = 0.0564V.$$

Analog input current [A]	Digital output code [Decimal format]
-2.0	1880
-1.6	1906
-1.2	1936
-0.8	1968
-0.4	1990
0	2020
0.4	2045
0.8	2075
1.2	2104
1.6	2130
2.0	2162

Table 4-2: ADC module digital output for corresponding analog input current

Using equation 4-18, Full scale voltage = 2.8V (Voltage range = -1.4V to +1.4 V).
LSB size = $\frac{2.8}{4096} = 6.835 * 10^{-4}$.

Using equation 4-17.
Digital code = $\frac{56.4 \cdot 10^{-3}}{6.835 \cdot 10^{-4}} = 83$.

BOB method used for conversion in ADC module, it will result in the digital code 2103 ($2020 + 83 = 2103$).
Offset can be seen here too, as in the voltage measurement at the half the value of the digital ADC range.

4-5 SVPWM

4-5-1 Dual Two Level Inverter Configuration

PWM inverters used to drive the motor will generate the common mode voltage, which will cause motor bearing currents. PWM also produces leakage current which will be the source of conducted electromagnetic interference (EMI) in the drive system [49]. These problems can be avoided by employing the switching strategy which will eliminate the common mode voltages in the drive system. Electrostatic coupling produced through common mode voltage, will result in the bearing and leakage current is also avoided [49].

In the system under consideration, each machine phase is powered using H-bridge inverter, so this configuration supplying three phases of the machine can be assumed to be the combination of conventional dual two-level inverter (VSI1 and VSI2) scheme as shown in the Fig. 4-10. In Fig. 4-10 switches used in the inverter are named based on the ePWM pins supplying the PWM signals from MC. Switch S_{3a}, S_{3b} means the ePWM3a and ePWM3b pins from MC are used to supply the PWM gate signal to the switches.

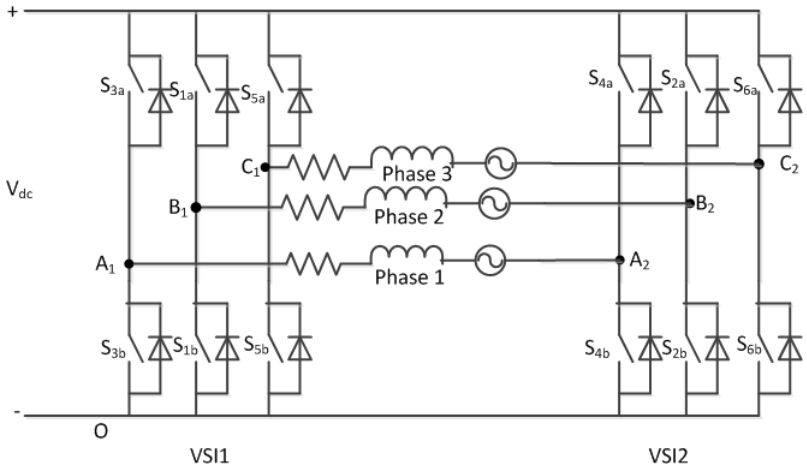

Figure 4-10: Schematic of dual inverter fed three phases of the machine.

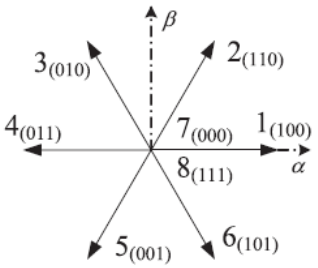

Figure 4-11: Voltage space vector of inverter 1 (VSI1).

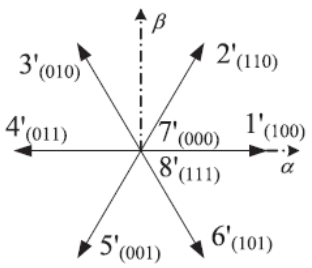

Figure 4-12: Voltage space vector of inverter 2 (VSI2).

Fig. 4-11 and 4-12 indicates the individual active space vector generated by the dual two level inverter respectively. In the two-level converter module, eight possible switching states exist, out of which two of them are zero switching state and six other combinations are active switching states. V_{A1O},V_{B1O},V_{C1O} are the pole voltage of inverter 1 ($VSI1$) and V_{A2O},V_{B2O},V_{C2O} are the pole voltages of inverter 2 ($VSI2$). The voltage available across the machine phase, is given by the equation 4-19 and it will be $-V_{DC}$,0,$+V_{DC}$.

$$\begin{aligned} V_1 &= V_{A1O} - V_{A2O} \\ V_2 &= V_{B1O} - V_{B2O} \\ V_3 &= V_{C1O} - V_{C2O} \end{aligned} \tag{4-19}$$

V_1,V_2,V_3 are the voltages across the machine phases 1,2 and 3.

Voltage space vector produced by both the inverter is given by equation 4-20.

$$\begin{aligned} V_{s1} &= \frac{2}{3} \cdot \left(V_{A1O} + V_{B1O} \cdot e^{j\frac{2\pi}{3}} + V_{C1O} \cdot e^{-j\frac{2\pi}{3}} \right) \\ V_{s2} &= \frac{2}{3} \cdot \left(V_{A2O} + V_{B2O} \cdot e^{j\frac{2\pi}{3}} + V_{C3O} \cdot e^{-j\frac{2\pi}{3}} \right) \end{aligned} \tag{4-20}$$

From equation 4-19 and 4-20, resulting voltage vector for dual inverter combination is given by equation 4-21.

$$V_s = V_{s1} - V_{s2} \tag{4-21}$$

In this type of configuration, common dc bus used for both the inverters (VSI1 and VSI2), which provides the path for the zero sequences current[50]. Presence of common mode voltage is the main cause for the zero sequence currents in the system.
Common mode voltages will be present in the system from following sources[50][51] :

- PWM technique.
- Voltage drop in the semiconductor power devices.
- Dead time used to avoid short circuit of the switches in one leg.

Common mode voltage generated by inverter 1 and inverter 2 is given by equation 4-22:

$$\begin{aligned} V_{com1} &= \frac{V_{A1O} + V_{B1O} + V_{C1O}}{3} \\ V_{com2} &= \frac{V_{A2O} + V_{B2O} + V_{C2O}}{3} \end{aligned} \tag{4-22}$$

V_{com1},V_{com2} are the common mode voltage generated by the inverter 1 and inverter 2.

The combination of the dual two level inverter will result in 19 difference space voltage vector as shown in the Fig. 4-13, which includes 18 active vectors and one zero vector [5]. The zero vector is indicated in the center of the Fig. 4-13 and the active vectors are distributed around the hexagon. Out of these 19 voltage vectors from the combination of the two inverter VSI1 and VSI2, 7 voltage vectors (HJLNQS) will not contribute to the common mode voltage in the machine phase winding [49] as shown in the Fig. 4-14. Using these 7 voltage vectors common mode voltage generated through PWM is avoided.

Voltage space vector OS is obtained, from the two combinations of inverter 1 and inverter 2. The first combination is state 1 one from inverter 1 and state 3' from inverter 2, the second combination is state 2 from inverter 1 and state 4' from inverter 2, as shown in the Fig. 4-15 and 4-16 respectively. Two combinations 13' and 64' are indicated in the Fig. 4-14 next to the vector OS head. Phasor combination for the remaining five active vectors (HJLNQ), is obtained similarly.

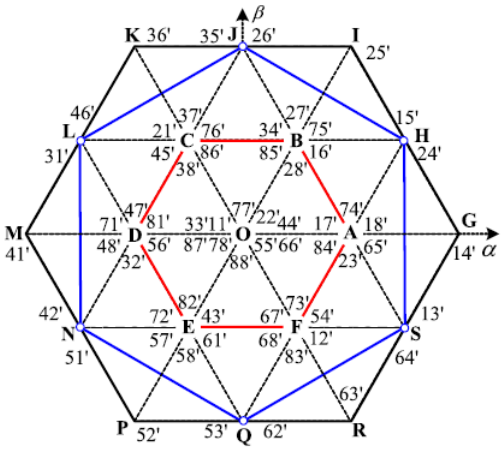

Figure 4-13: Voltage space vector of dual inverter [5].

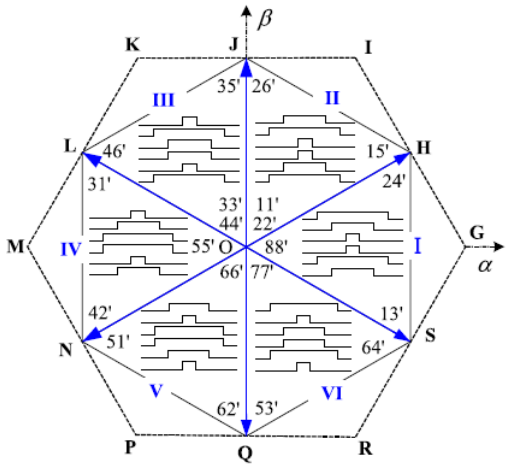

Figure 4-14: Voltage space vector of dual inverter which don't contribute to the common mode voltages [5].

4-5-2 SVPWM unit in InstaSPIN

Fig. 4-17 shows the block diagram of the SVPWM unit used in the drive system of InstaSPIN module. Current controller in the rotor reference frame will generate reference voltages $\left(u_d^{ref}, u_q^{ref}\right)$ based on model based current control method [42]. The inverse Park's transformation on the reference voltage $\left(u_d^{ref}, u_q^{ref}\right)$ will give the revolving reference vector in the stationary reference frame $\left(u_\alpha^{ref}, u_\beta^{ref}\right)$. This reference vector is converted to three-phase reference signals $\left(u_1^{ref}, u_2^{ref}, u_3^{ref}\right)$, using inverse Clarke's transform. Three reference signals are fed to pulse centering module. This module is used to obtain space vector pulse width modulation (SVPWM) like performance with carrier-based reference sinusoidal PWM method, by adding a suitable offset voltage to the sinusoidal reference voltage [52]. For two-level inverter, the common mode offset voltage is given by equation 4-23 [52]

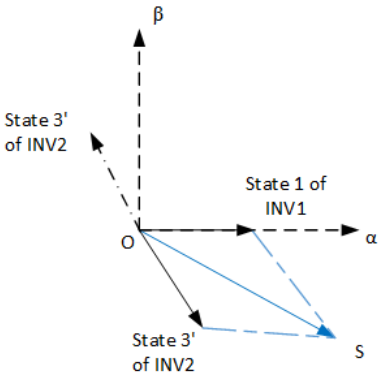

Figure 4-15: Voltage space vector OS by combination of VSI1 and VSI2 : Combination one.

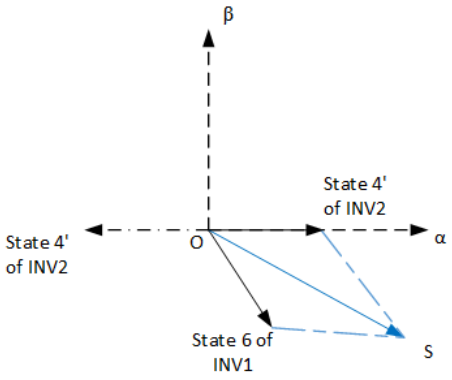

Figure 4-16: Voltage space vector OS by combination of VSI1 and VSI2 : Combination two.

$$V_{comm} = -\frac{V_{max} + V_{min}}{2} \tag{4-23}$$

where, V_{max} and V_{min} are the maximum and minimum reference voltages of the three phases at that sample time.

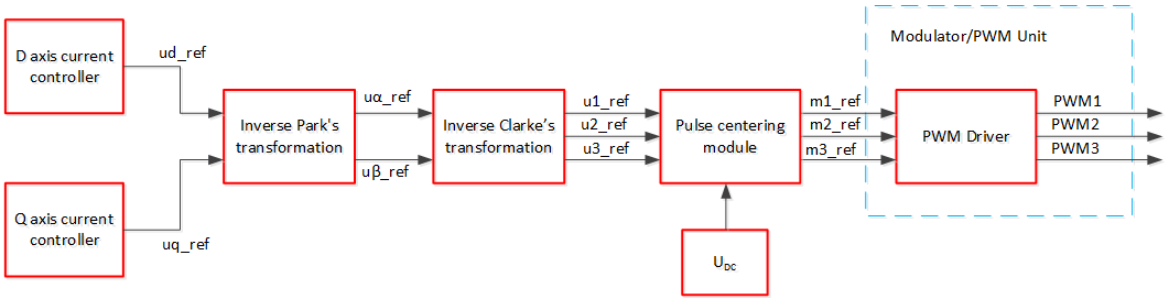

Figure 4-17: Space vector PWM unit in InstaSPIN algorithm.

This equation is based on the concept that the reference voltage with the lowest magnitude, will cross the triangular carrier waveform first and its switching will take place first. Reference voltage with the maximum amplitude will cross the carrier wave last, so it will switch at last as shown in the Fig. 4-18. Using this modified reference waveform SVPWM like switching is achieved from sinusoidal waveform [52]. The advantage of using the pulse centering module, is it symmetrizes the references with respect to the time axis [52].

Reference signals are scaled by DC link voltage which would give modulation indices $\left(m_1^{ref}, m_2^{ref}, m_3^{ref}\right)$, this values are fed to the PWM unit[6]. Utilizing the modulation indices reference values the duty cycle of the switches are calculated using the equation 4-24, where

[6]Modulation index M is defined as the ratio of the reference voltage space vector, generated by three reference phase to the applied DC link voltage [52]

i makes references to each of the phases.

$$d_i^{ref} = \frac{1 + m_i^{ref}}{2} \cdot \text{TBPRD} \qquad \text{for i =1,2,3} \tag{4-24}$$

Duty cycle values for three phases are compared with the triangular carrier signal of amplitude one, to generate the gate logic signals using the comparator function in the MC devices as shown in the Fig. 4-18.

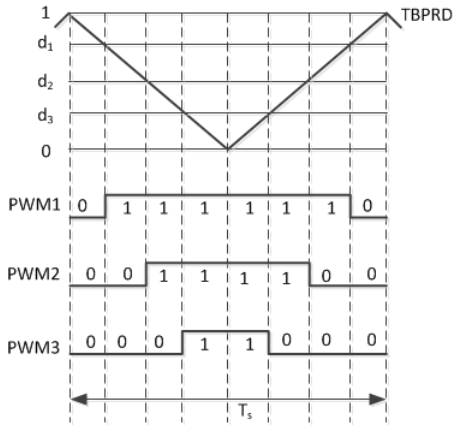

Figure 4-18: PWM gate signal.

Switching technique

According to Fig. 4-14, in sector of the vector (HJLNQS) the switching states of the two legs in dual two level inverter will be same as follows [5] :

- $S_3 = S_2$
- $S_1 = S_6$
- $S_5 = S_4$

where, S_3 is switching state of inverter leg 1 of VSI1. S_2 is switching state of inverter leg 2 of VSI2. S_1 is switching state of inverter leg 2 of VSI1. S_6 is switching state of inverter leg 3 of VSI2. S_5 is switching state of inverter leg 3 of VSI1. S_4 is switching state of inverter leg 1 of VSI2.

Using this switching technique, vectors H,J,L,N,Q and S is obtained from states 13',24',35',46',51' and 62' with VSI1 and VSI2 combination. This combination can be seen in the table 4-3. There is another alternative switching sequence available, to switch the dual two level inverter for vectors H,J,L,N,Q and S using states 64',15' 26',31',42',53' with VSI1 and VSI2 combination. To obtain alternative switching sequence, two different legs switching states in dual two level inverter are set same compared to the first sequence.

- $S_3 = S_6$
- $S_1 = S_4$
- $S_5 = S_2$

This is also shown in the table 4-3. In the present motor control algorithm, the first sequence is followed.

Using the first technique in SVPWM algorithm for the system under consideration for generating gate logic switching signals for three phase H-bridge. Gate logic signals $(1, 0)$ for three phases is generated based on the comparison of the triangular carrier signal with the reference signal as shown in the Fig. 4-18. Gate logic signal zero corresponds to lower switch of the inverter leg is on and gate logic signal one corresponds to upper switch of inverter leg is on. Combination of the switching states in VSI1 and VSI2 to obtain the voltage vector (HJLNQS) which don't contribute to common mode voltage in machine phase winding is shown in the Table 4-3. In the table 4-3 a,b,c represents switching states of VSI1 $(a = S_3, b = S_1, c = S_5)$

Vector	Phasor combination	Inverter 1			Inverter 2			Output Voltage		
V_{vector}		a	b	c	a'	b'	c'	V_1	V_2	V_3
OS	13'	1	0	0	0	1	0	V_{DC}	$-V_{DC}$	0
	64'	1	0	1	0	1	1	V_{DC}	$-V_{DC}$	0
OH	24'	1	1	0	0	1	1	V_{DC}	0	$-V_{DC}$
	15'	1	0	0	0	0	1	V_{DC}	0	$-V_{DC}$
OJ	35'	0	1	0	0	0	1	0	V_{DC}	$-V_{DC}$
	26'	1	1	0	1	0	1	0	V_{DC}	$-V_{DC}$
OL	46'	0	1	1	1	0	1	-V_{DC}	V_{DC}	0
	31'	0	1	0	1	0	0	-V_{DC}	V_{DC}	0
ON	51'	0	0	1	1	0	0	-V_{DC}	0	V_{DC}
	42'	0	1	1	1	1	0	-V_{DC}	0	V_{DC}
OQ	62'	1	0	1	1	1	0	0	-V_{DC}	V_{DC}
	53'	0	0	1	0	1	0	0	-V_{DC}	V_{DC}
O	77'	0	0	0	0	0	0	0	0	0
	88'	1	1	1	1	1	1	0	0	0

Table 4-3: Voltage space vector combination producing zero common mode voltage in the motor phase winding.

and a',b',c' represents switching states of VSI2 $(a' = S_4, b' = S_2, c' = S_6)$.

In order to know switches conducting in the three-phases when it receives the gate signal from the ePWM module of MC, for output voltage space vector OS $(13')$ Fig. 4-19 is shown. This switching state is arbitrarily chosen to show how the combination of VSI1 and VSI2 works for generate voltage space vector OS. In the Fig. 4-19, switches with red color indicates that it is conducting and direction of the current is indicated using the dotted line. For the vector OS $(13')$, a =1 $(S3 = 1)$, a'=0 $(S4 = 0)$, b = 0 $(S1 = 0)$, b' = 1 $(S2 = 1)$, c = 0 $(S5 = 0)$ and c' = 0 $(S6 = 0)$. For this combination of states output voltage across the machine phases, $V_1 = V_{DC}$, $V_2 = -V_{DC}$ and $V_3 = 0$.

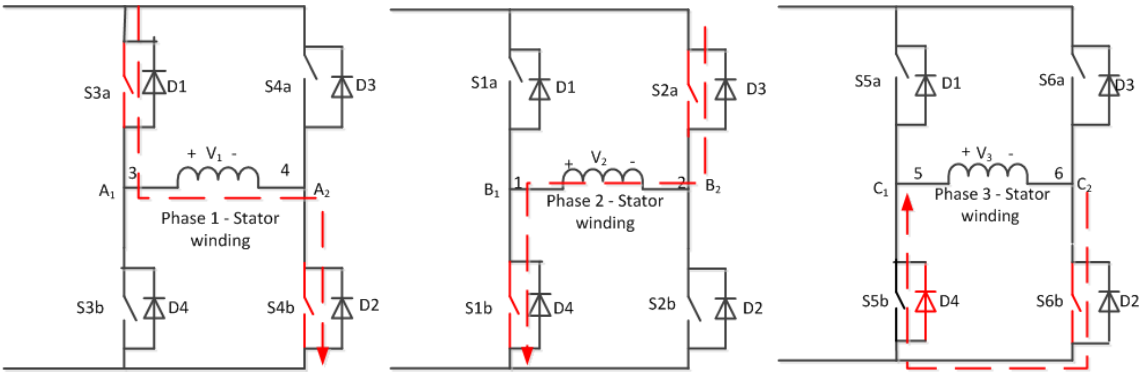

(a) Phase 1 (Leg 3 and 4). (b) Phase 2 (Leg 1 and 2). (c) Phase 3 (Leg 5 and 6).

Figure 4-19: Switching states for voltage vector OS (13')for combination VSI1 (a = 1,b = 0, and c = 0) and VSI2 (a'=0 ,b'= 1, and c'= 0).

4-6 Data Acquisition and Execution of Control Algorithm

In previous sections 4-4 and 4-5, ADC module and PWM module working principle were explained individually. In this section, PWM and ADC module synchronization with the CPU clock for the instaSPIN algorithm is explained.

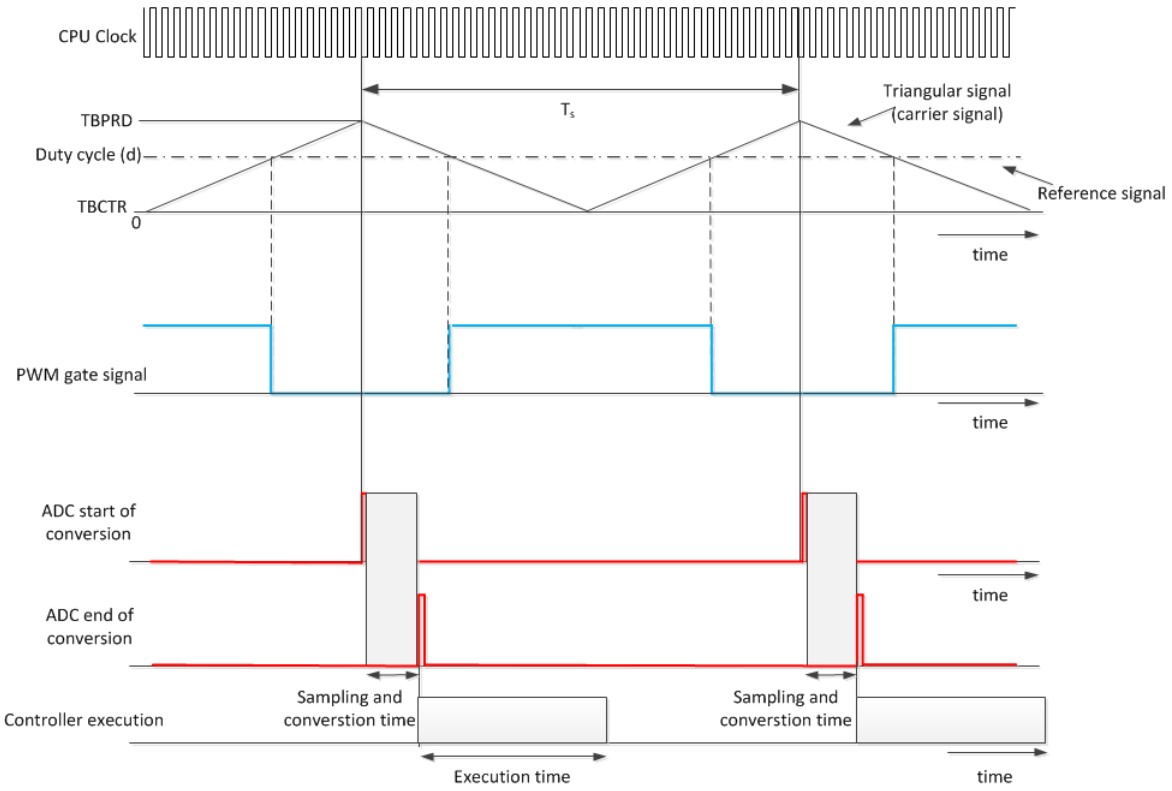

Figure 4-20: Data acquisition using ADC module and PWM generation.

In the motor control application, Up-down count mode is used to generate the PWM signals. Switching frequency of the triangular signal is set to 20KHz , Sampling period = 0.05ms [7]. For setting this switching frequency value in the ePWM module equation 4-25 is used [31]. This equation is same as equation 3-1.

$$\text{TBPRD} = \frac{T_s \cdot \text{CPU CLK}}{2} \tag{4-25}$$

where, TBPRD is time base period value set in the ePWM for selecting the switching frequency of the triangular signal. CPU CLK is CPU clock of MC (CPU CLK = $90MHz$). T_s is sampling time.

TBPRD value is set to 2250 in ePWM module from equation 4-25. Using set TBPRD value, triangular reference signal is generated similar to procedure explained in the section 3-2. Triangular signal is compared with the duty cycle values, to generate the PWM gate signals has explained in the section 4-5 and indicated in the Fig. 4-20.

Sampling time is set to start at TBPRD value, it is also peak value of the triangular signal. At the beginning of each sampling period, data acquisition of the stator voltage, current and DC link voltage starts through ADC module in MC. This is marked by ADC start of conversion in Fig. 4-20. After the data acquisition is complete, it is sampled by ADC module. After data sampling is complete and it's ready for processing marked by the ADC end of conversion in the Fig. 4-20. Using this sampled data, FAST observer will give the estimated values required and InstaSPIN FOC algorithm executes. This part takes places during the execution time indicated in the Fig. 4-20.

4-7 Current Control Loop Gains

InstaSPIN algorithm employs the model based current control method to implement the PI current controller in FOC [42]. The main task of the PI current controller is to reduce the deviation between the feedback and reference current. In the regularly sampled system under consideration, the control objective driving the error to zero in every sample is represented by the equation [22].

$$\vec{i_{k+T_s}} = \vec{i^*_{t_k}} \tag{4-26}$$

where, $\vec{i_{t_k+T_s}}$ is actual current in the next sampling period T_s, $\vec{i^*_{t_k}}$ is reference current in the present sampling period of t_k, T_s is given sampling period.

Aforementioned condition in the equation 4-26 is satisfied by the controller through switching the modulator to reach the average voltage reference space vector. The average reference voltage vector is given by equation 4-27 [42].

$$\vec{U^*}(t_k) = \frac{1}{T_s} \int_{t_k}^{t_k+T_s} \vec{u}(\tau) \cdot d\tau \tag{4-27}$$

[7] Sampling period is inverse of the switching frequency $\left(T_s = \frac{1}{f_{sw}}\right)$

where, $\vec{u}(\tau)$ is instantaneous voltage applied to the machine. phase. $U^*\vec{(t_k)}$ is reference average voltage per sample.
Voltage applied across the motor phases is represented by

$$\vec{u_s} = R_s \cdot \vec{i_s} + L_s \cdot \frac{d\vec{i_s}}{dt} + \vec{e_s} \tag{4-28}$$

Transformation of equation into rotor reference frame, as described in the section 4-2, will result in equation 4-29.

$$\begin{aligned} \vec{u}_d &= R_s \cdot \vec{i}_d + L_d \cdot \frac{d\vec{i_d}}{dt} - p \cdot w_m \cdot L_q \cdot \vec{i}_q \\ \vec{u}_q &= R_s \cdot \vec{i}_q + L_q \cdot \frac{d\vec{i_q}}{dt} + p \cdot w_m \cdot L_d \cdot \vec{i}_d + \psi_m \cdot p \cdot w_m \end{aligned} \tag{4-29}$$

Using equation 4-29 in equation 4-27.

$$\begin{aligned} U_d^*(t_k) &= \frac{R_s}{T_s} \cdot \int_{t_k}^{t_k+T_s} i_d(\tau) \cdot d\tau + \frac{L_d}{T_s} \cdot \int_{i_d(t_k)}^{i_d(t_k+T_s)} di_d - \frac{1}{T_s} \cdot \int_{t_k}^{t_k+T_s} p \cdot \omega_m \cdot L_q \cdot i_q(\tau) \cdot d\tau \\ U_q^*(t_k) &= \frac{R_s}{T_s} \cdot \int_{t_k}^{t_k+T_s} i_q(\tau) \cdot d\tau + \frac{L_q}{T_s} \cdot \int_{i_q(t_k)}^{i_q(t_k+T_s)} di_q + \frac{1}{T_s} \int_{t_k}^{t_k+T_s} (p \cdot \omega_m \cdot L_d \cdot i_d(\tau) + u_e(\tau)) \cdot d\tau \end{aligned} \tag{4-30}$$

Since the integrand in the above equation, will be known only in the sampling period of the controller, using the first order approximation on the equation 4-30, will give us [42].

$$\begin{aligned} U_d^*(t_k) &\cong \frac{R_s}{T_s} \cdot \sum_{ij=0}^{ij=k-1} (i_d^*(t_{ij}) - i_d(t_{ij})) + \left(\frac{L_d}{T_s} + \frac{R_s}{2}\right) \cdot (i_d^*(t_k) - i_d(t_k)) + p \cdot \omega_m \cdot L_q \cdot i_q \cdot (t_k) \\ U_q^*(t_k) &\cong \frac{R_s}{T_s} \cdot \sum_{ij=0}^{ij=k-1} (i_q^*(t_{ij}) - i_q(t_{ij})) + \left(\frac{L_q}{T_s} + \frac{R_s}{2}\right) \cdot (i_q^*(t_k)) - i_q(t_k)) + p \cdot \omega_m \cdot L_d \cdot i_d(t_k) + u_e(t_k) \end{aligned} \tag{4-31}$$

From equation 4-31, propositional and integral controller gain for both the d and q current controllers as below [22]

$$\begin{aligned} K_p &= \frac{L}{T_s} + \frac{R_s}{2} \\ K_i &= \frac{R_s}{T_s} \end{aligned} \tag{4-32}$$

Since $\frac{L}{T_s} >> \frac{R_s}{2}$, so propositional controller gain term reduces to $K_p = \frac{L}{T_s}$.

4-8 Three Phase of PMSM Experiment Results

Initially, sensorless FOC control for the three phases of the multiphase machine was implemented using InstaSPIN algorithm with the TMS320F28069x MC device described in the above section. Later the sensorless FOC was extended to the six phases of the machine, which is explained in the next chapter. Fig. 4-21 shows the experiment setup in the TU-Delft Electrical machines laboratory. Number indicated in Fig. 4-21 are as follows.

1. Code composer software used to flash the MC.
2. Power source for MC.
3. DC power supply for the Inverter.
4. MC board shown in Fig. 4-7 used for controlling the motor.
5. Six phase PMSM motor.
6. Wires connecting from the DC power supply to H-bridge inverters on motor.
7. Oscilloscope used for measuring voltage and current.
8. Wire used to transmit the PWM signal from the MC to H-bridge inverter.

Here, it can be seen that inverter modules are integrated over the surface of the machine. This type of system integration will increase the power density of the whole system [1]. Due to the limitation in the facilities available in the lab, experiments were carried out on no load conditions.

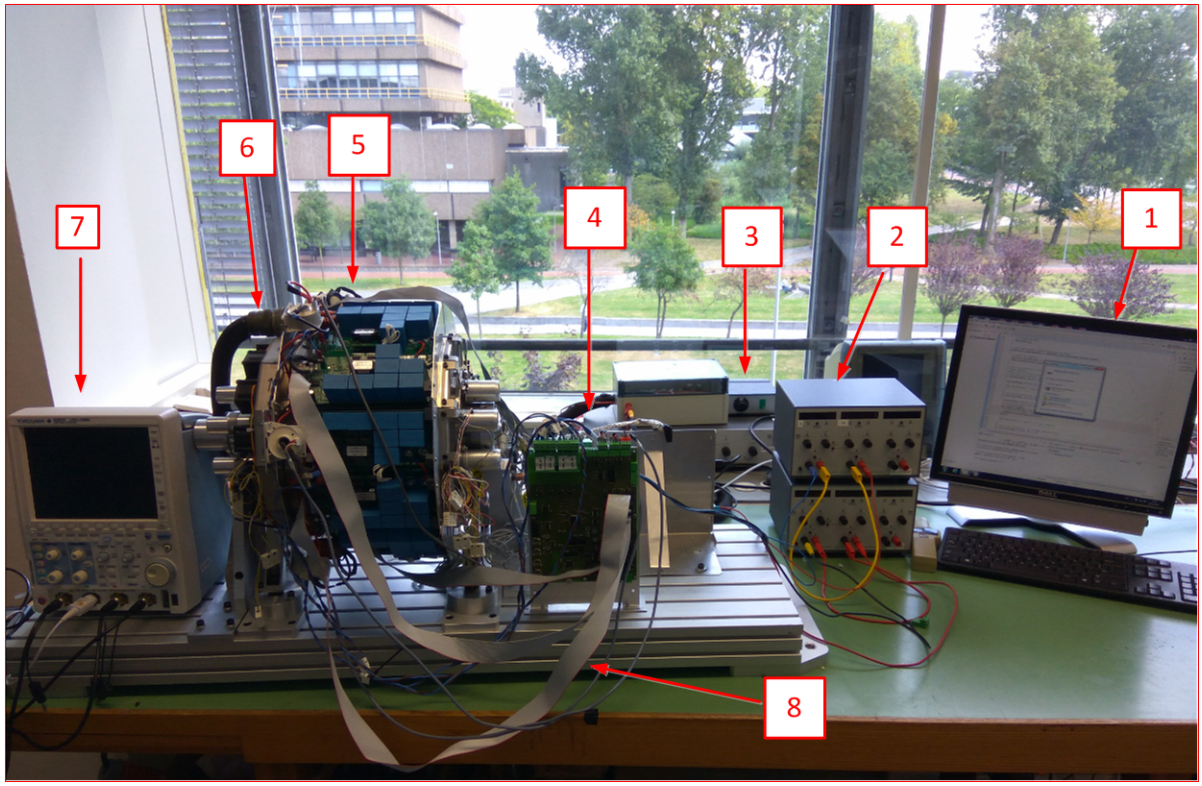

Figure 4-21: Experiment setup in electrical machines lab at TU Delft.

4-8-1 No Load Test

The test was carried out at no load to check whether the machine would reach the reference speed input given to the controller. Voltage and current were measured across the machine

phases using the differential voltage probe and the current probe. Measured voltage and current using these devices were viewed using the oscilloscope. Table 4-4 shows the results of the voltage and current measured during the no load test.

Speed [rpm]	Frequency [Hz]	Voltage V_{rms1} [V]	Voltage V_{rms2} [V]	Voltage V_{rms3} [V]	Current I_{rms1} [mA]	Current I_{rms2} $[mA]$	Current I_{rms3} $[mA]$
200	13.34	8.21	8.33	8.87	72	78	70
300	20	9.56	9.67	9.93	80	88	83
400	26.7	10.65	10.76	10.87	89	95	92
500	33.33	11.41	11.65	11.99	94	102	98
600	40	12.13	12.47	12.79	104	108	102
700	46.67	13.07	13.25	13.58	110	112	113
800	53.34	13.75	13.99	14.15	120	125	126
850	56.67	14.31	14.29	14.66	128	130	131

Table 4-4: No Load Test : Three phases of machine.

Observations from the experiment results:

- Equation 4-8, in the steady state form is rewritten as

$$\begin{aligned} \vec{u}_s &= R_s \cdot \vec{i}_s + \vec{e}_s \\ \vec{e}_s &= \frac{\omega_m \cdot N_s \cdot \psi_m}{\sqrt{2}} \end{aligned} \tag{4-33}$$

  Neglecting the resistive voltage drop, assuming only dominant induced voltage term in the equation 4-33, which reduces to equation 4-34.

$$\begin{aligned} \vec{u}_s &= \vec{e}_s \\ \vec{u}_s &= \frac{\omega_m \cdot N_s \cdot \psi_m}{\sqrt{2}} \end{aligned} \tag{4-34}$$

  From the equation 4-34 it can be seen that speed of the rotor increases with the applied voltage across the stator winding, which also holds with the results obtained in the table 4-4.

- Fundamental frequency of the voltage and current is same as the rotor speed frequency. Voltage and current at no load through three stator phases applied across the machine stator winding is indicated in Fig. 4-22 and 4-23, for the case machine running at 600 rpm speed.

- Magnitude of the rms value of the voltage and current through all the stator phases is same at all motor speeds.

- Current waveform is nonsinusoidal because of the no load applied to the rotor shaft, the effect of the semiconductor device voltage drop, and the effect of dead time. Effect of the device voltage drop and dead time on the current waveform will be explained in the section 4-8-3.

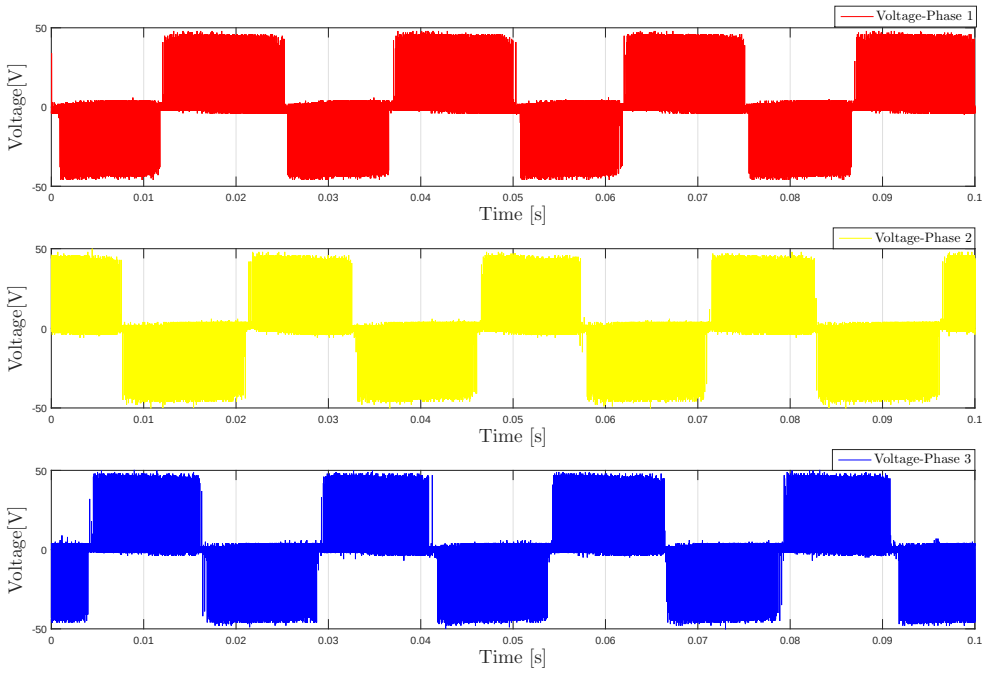

Figure 4-22: Voltage measured across the machine phases. Speed = 600 rpm, frequency = 40 Hz, V_{rms1} =12.13 V, V_{rms2} =12.47 V, V_{rms3} =12.79 V .

- When the manual load is applied to the rotor shaft, current through the machine phases, becomes more sinusoidal as shown in the Fig. 4-24.

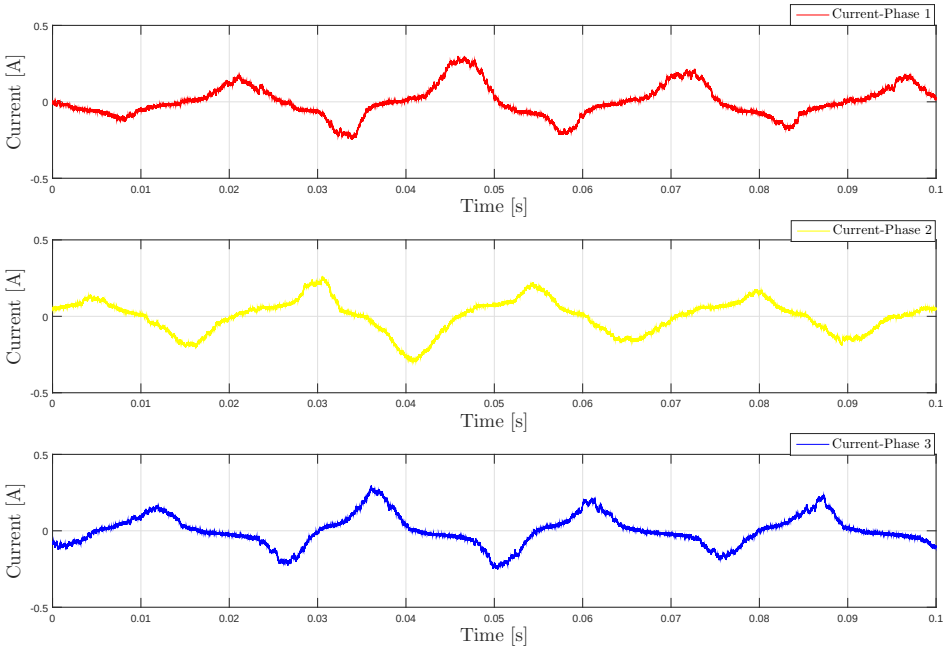

Figure 4-23: Current through the machine phases. Speed = 600 rpm, frequency = 40 Hz, I_{rms1} =104 mA, I_{rms2} =108 mA, I_{rms3} =102 mA .

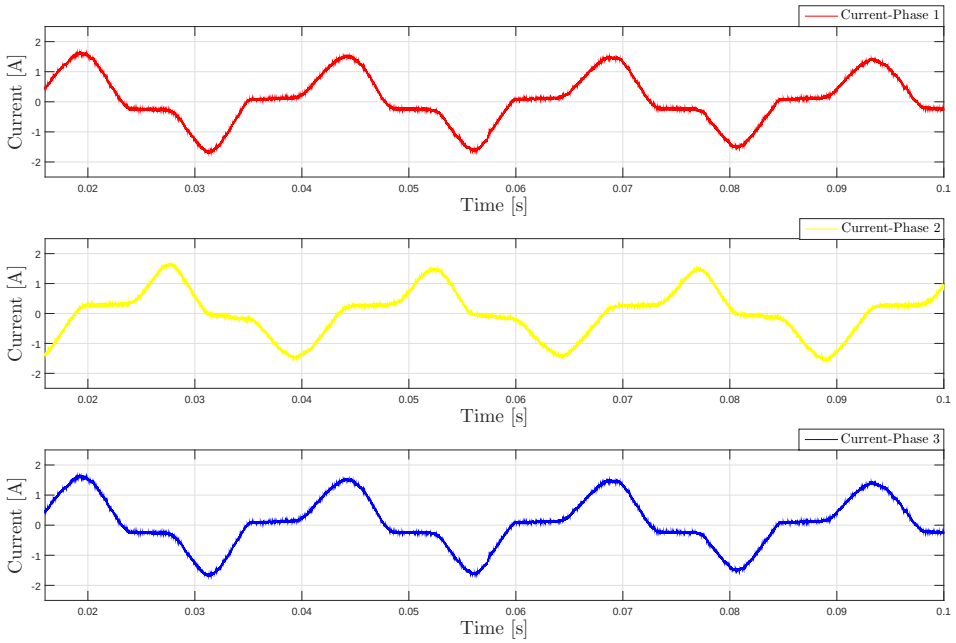

Figure 4-24: Current through the machine phases, when manual load was applied. Speed = 600 rpm, frequency = 40 Hz, I_{rms1} =0.818 A, I_{rms2} = 0.811 A, I_{rms3} = 0.819 A.

4-8-2 Acceleration Test

To check the motor performance and controller response during acceleration, following tests are performed.

Case 1 : Acceleration 200 rps

In this experiment, motor reference speed was increased from 200rpm to 800rpm using the inbuilt ramp generator with the slope of 200rps. Fig. 4-25 and Fig. 4-26 show the voltage and current through the stator winding phases with respect to the ramp generator to accelerate shaft speed from the initial reference speed of 200rpm to 800rpm.

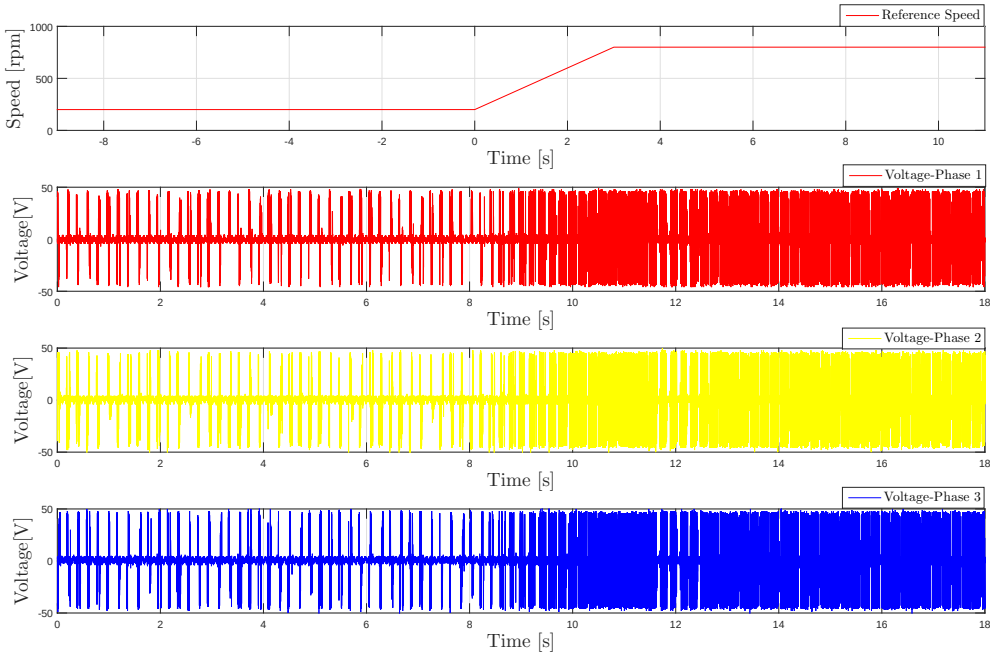

Figure 4-25: Variation of voltage across machine phases during acceleration 200 rpm to 800 rpm, at acceleration of 200 rps.

Observation from acceleration plot

- Due to the difference in reference and the actual speed of the rotor, the motor will start to accelerate. To accelerate the rotor, the duty cycle of the PWM waveform will increase, resulting in the increase in the output voltage amplitude as shown in Fig.4-25. This is anticipated due to increase in the EMF from the rotor.
- For accelerating the machine there will transient current drawn from the stator winding through the power converter, as shown in the Fig. 4-26.
- Once the machine reaches the reference speed, current will start reducing and it reaches close to zero when the machine has reached the reference speed. This can be seen in the Fig. 4-26.

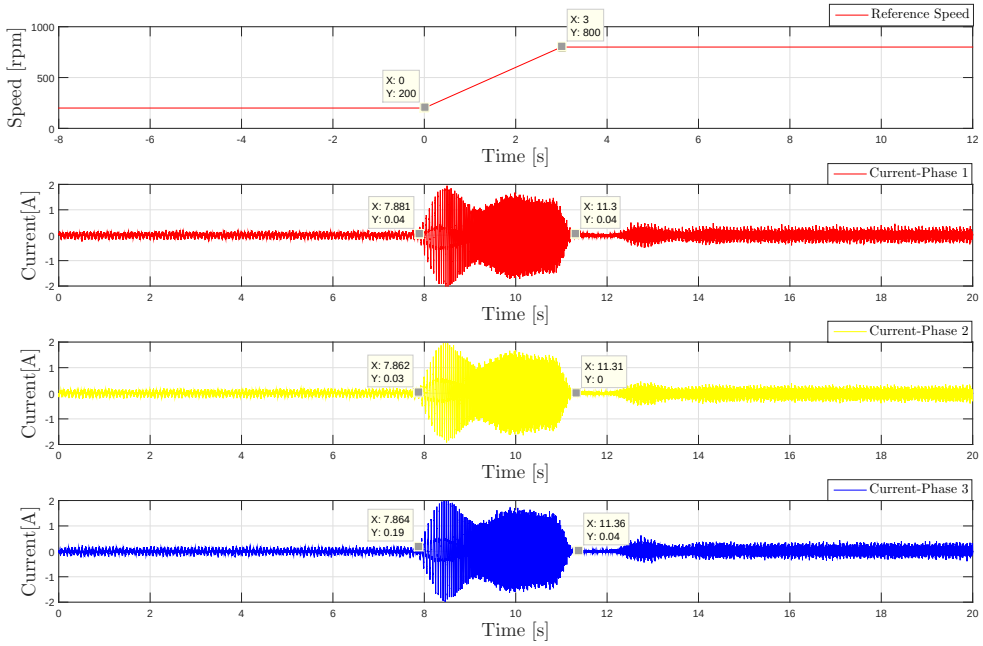

Figure 4-26: Variation of current through machine phases during acceleration 200 rpm to 800 rpm, at acceleration of 200 rps.

- Time taken by the ramp generator to reach reference speed of 800 rpm from 200rpm with the slope of 200 rps is 3s. Current through stator winding would follow the same trend in terms of the time to accelerate the machine shaft to reach reference speed.

Case 2 : Acceleration 100 rps

In this experiment, acceleration of the motor controller was reduced from 200 rps to 100 rps, to check the motor and controller performance, when the motor reference speed was increased from 200 rpm to 800 rpm. The variation of the current in three phases of machine obtained from this experiment is compared with the results obtained in the previous section when the acceleration was set to 200rps.

Observation from experiment.

- Variation of the current during acceleration is same in both the scenarios, even when the acceleration is reduced.
- Time taken by the motor to reach reference speed of 800 rpm from 200 rpm is twice when the acceleration was reduced from 200 rps to 100 rps. This is due to the reduction in the current drawn by half during acceleration. Increase in time to reach the reference speed and reduction in the current drawn during acceleration can be seen in the Fig. 4-27, when it is compared with Fig. 4-26.

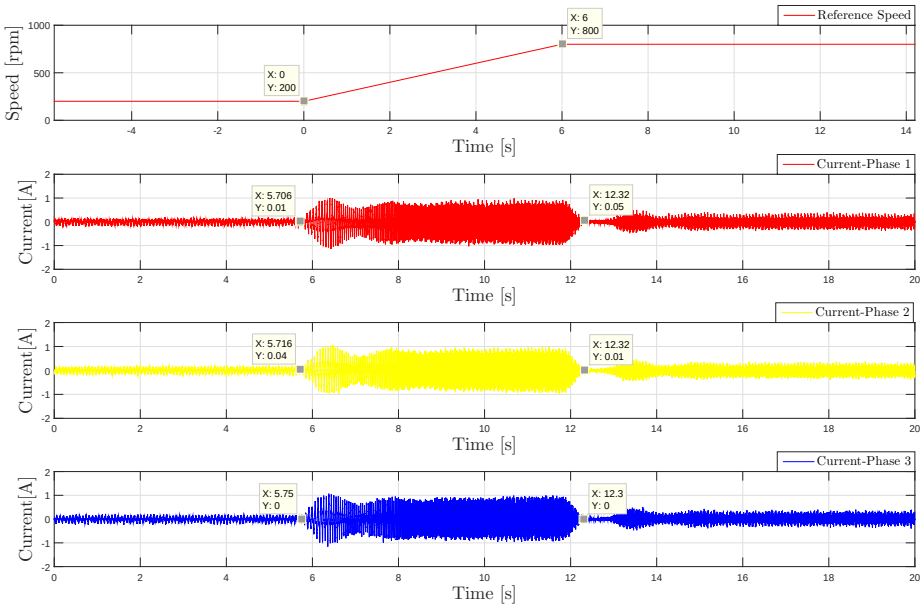

Figure 4-27: Variation of current through machine phases during acceleration 200 rpm to 800 rpm, at acceleration of 100 rps.

- Fig. 4-28 shows the variation of the fundamental voltage across the motor phase one, during both the acceleration values in the controller. Time taken by the motor reach 800 rpm is twice when acceleration is set to 100rps compared to 200rps.

4-8-3 Zero sequence current

It was mentioned in section 4-5-1, zero sequence current was produced due to the common mode voltage present in the system. Common mode voltages produced due to PWM was avoided by using selected voltage vector combination from VSI1 and VSI2 as explained in the section 4-5-1. However, other two effects which will cause the common mode voltage in the system, are the voltage drop in the semiconductor power device and dead time between the switches in the leg. Common mode voltage will be of the frequency of three times the fundamental frequency, this will produce the zero sequence current of frequency three times the fundamental frequency [51].

Effect of Dead Time

To avoid the short circuit of the switches, deadtime is introduced between the switches in a leg. During the dead time, common mode voltages across the machine phases depend on the current direction [5][51]. Common mode voltages across the machine phases during dead

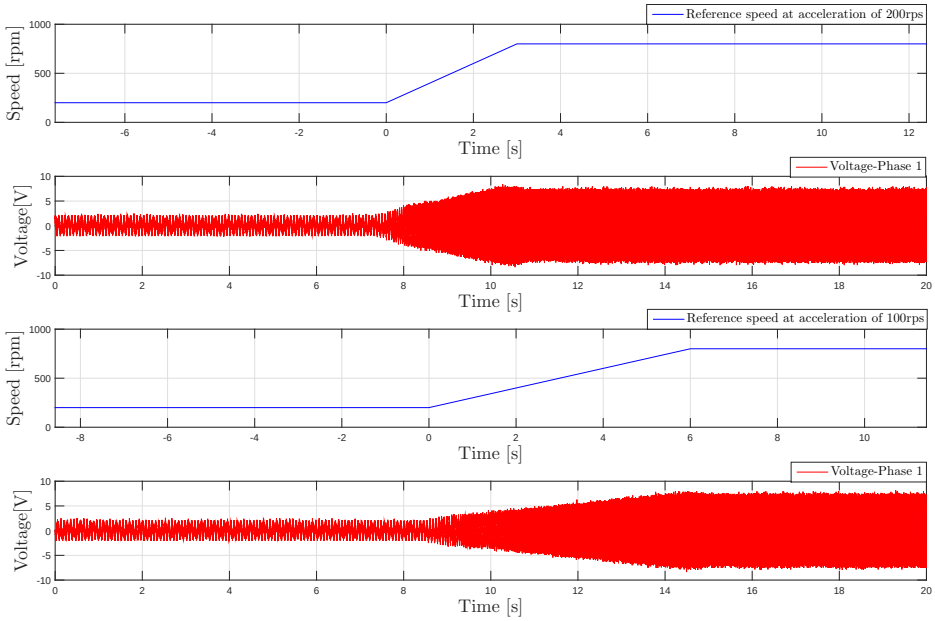

Figure 4-28: Variation of fundamental voltage through machine phases during acceleration 200 rpm to 800 rpm, at acceleration of 200 rps and 100 rps.

time is given by equation 4-35 [5][51].

$$\begin{aligned} V_{com} &= \left(\frac{2 \cdot T_d \cdot V_d}{T_s \cdot 3}\right) && \text{for one positive and two negative current direction} \\ V_{com} &= -\left(\frac{2 \cdot T_d \cdot V_d}{T_s \cdot 3}\right) && \text{for two positive and one negative current direction} \end{aligned} \tag{4-35}$$

where, V_{com} is common mode voltage across machine phase. T_d is dead time between the switches in one leg. V_d is DC voltage applied across the inverter. T_s is switching period.

Dead Time [μs]	First harmonic order	Second harmonic order	Third harmonic order	Fifth harmonic order
1.5	1	0.177	0.2624	0.085
2	1	0.1826	0.3315	0.081
3	1	0.1958	0.3846	0.118

Table 4-5: Normalized harmonic order amplitude to fundamental frequency amplitude of 40 Hz.

Fig. 4-29 shows the FFT of the phase one current at different dead time values. In table 4-5, harmonic amplitude values are normalized with fundamental frequency of (40 Hz). Here, it can be seen that with the increase in the dead time, lower order harmonic components amplitude values increases. Compared to all the other lower order harmonic, value of the third harmonic is of higher magnitude and it increases with the dead time between the switches, due to increase in the common mode voltage as per the equation 4-35. It also indicates the increase in the amplitude of the zero sequence current with increase in the dead time [51].

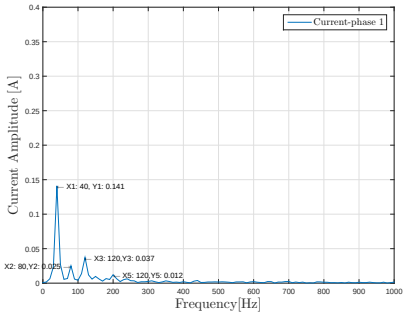

(a) FFT on phase one current, T_d =1.5 μs.

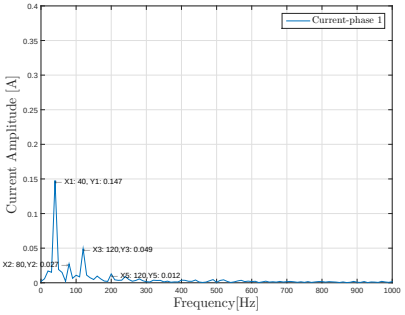

(b) FFT on phase one current, T_d = 2 μs.

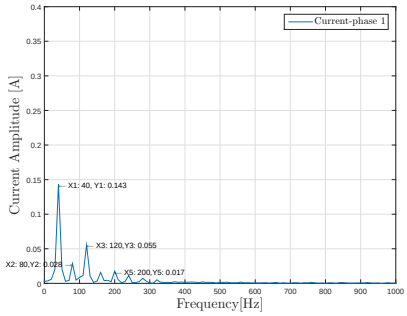

(c) FFT on phase one current, T_d = 3 μs.

Figure 4-29: FFT on phase one current at different dead time values.

Effect of Device Voltage Drops

To know the effect of the semiconductor device voltage drop on common mode voltage across the machine phases Fig. 4-30 is shown. In the Fig. 4-30 conduction of the semiconductor device in all three phases is for output voltage vector OS in Fig. 4-14 is indicated in the dual two-level inverter configuration. The voltage drop across semiconductor device during conduction is also indicated in the Fig. 4-30.

Pole voltage across three phases is given by equation 4-36.

$$\begin{aligned} V_{A1O} &= V_d - V_{CE} \\ V_{B1O} &= 0 + V_{CE} \\ V_{C1O} &= 0 - V_{FD} \\ V_{A2O} &= 0 + V_{CE} \\ V_{B2O} &= V_d - V_{CE} \\ V_{C2O} &= 0 + V_{CE} \end{aligned} \tag{4-36}$$

where, V_{CE} is the collector emitter on state voltage, V_{FD} is the diode forward voltage drop. Values of the V_{CE} = 2.05V and V_{FD} = 1.5V from the datasheet of the IGBT used [34].

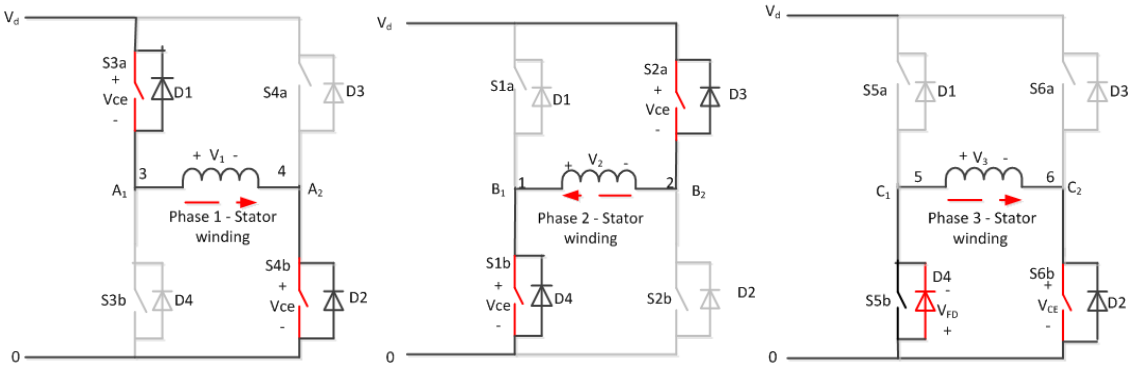

(a) Phase 1 (Leg 3 and 4). (b) Phase 2 (Leg 1 and 2). (c) Phase 3 (Leg 5 and 6).

Figure 4-30: Voltage drop across semiconductor device in VSI1 and VSI2, for output voltage vector OS

Using the equation 4-36 in equation 4-19.

$$\begin{aligned} V_{com1} &= \frac{V_d - V_{FD}}{3} \\ V_{com2} &= \frac{V_d + V_{CE}}{3} \end{aligned} \tag{4-37}$$

V_{com} is the common mode voltage across the machine phases [51].

$$\begin{aligned} V_{com} &= V_{com1} - V_{com2} \\ V_{com} &= -\left(\frac{V_{FD} + V_{CE}}{3}\right) \end{aligned} \tag{4-38}$$

In [51] it is shown that irrespective of the voltage vector, common mode voltage across the machine phases is dependent on the current direction in all the phases, given by equation 4-39.

$$\begin{aligned} V_{com} &= -\left(\frac{V_{FD} + V_{CE}}{3}\right) && \text{for two positive and one negative current direction} \\ V_{com} &= \left(\frac{V_{FD} + V_{CE}}{3}\right) && \text{for one positive and two negative current direction} \end{aligned} \tag{4-39}$$

Acceleration = 1 krps

Acceleration of the machine was changed from the previously set value of 0.2 krps to 1 krps and machine reference speed was increased from 200 rpm to 800 rpm. Acceleration is set to value of 1 krps to increase the magnitude of the current drawn by the stator winding. Because of the increase in the magnitude of the current, the effect of the voltage drop across the semiconductor device is reduced, with the increase in the applied voltage, due to increasing back emf of the motor. Variation of the voltage and current across the machine phase one and two during acceleration in detail can be seen in the Appendix A.

In Fig. 4-31 highlights the portion of maximum amplitude of the current drawn through machine phase during acceleration from 200rpm to 800rpm at 1krps, this part of the waveform

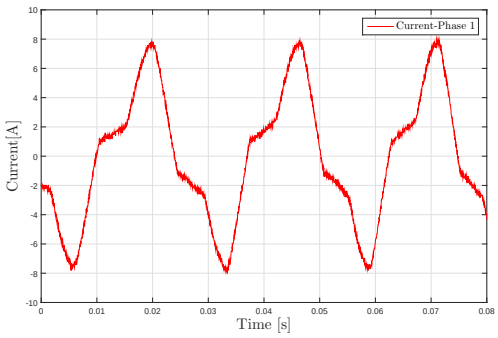

Figure 4-31: Variation of current drawn during the acceleration from 200 rpm to 800 rpm at acceleration 1000rps.

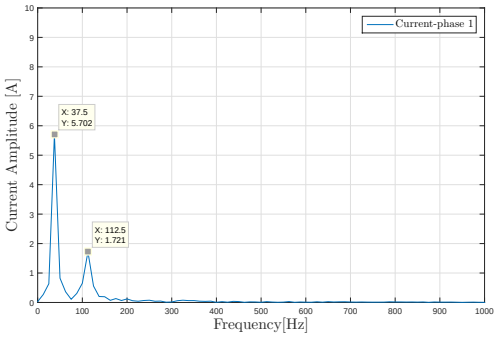

Figure 4-32: FFT on the current measured during acceleration from 200 rpm to 800 rpm at acceleration of 1000rps.

was chosen to show the effect of the semiconductor device on common mode voltage. It can be seen here that current through machine phase is more sinusoidal. It also indicates the effect of the common mode voltages due to semiconductor device reduced when the machine draws the high current. FFT on this current waveform shows that lower order harmonic value is zero except for the third harmonic . Normalized third order harmonic value with the fundamental harmonic value of 37.5 Hz gives the value 0.3018. When this value is compared with the normalized third harmonic results obtained at 40 Hz for the same dead time value of 2μs is 0.3315 from table 4-5, it shows the decrease in the third harmonic component when the machine is loaded and draws high current.

4-9 Discussion

This chapter focussed on the development of the sensorless field oriented control (Vector control) in the three phases of the six-phase machine. Section 4.2 describes the application of dq theory to PMSM machine.
Section 4.3 discussed the concept of Back-emf method used in the sensorless control in InstaSPIN algorithm and the drive setup used for the prototype machine.
Section 4.4 describes ADC module conversion principle, the circuit used in the MC board.
Section 4.5 explains the application of SVPWM modulation technique which will avoid the common mode voltage produced due to the PWM in dual two level inverter configuration.
Section 4.6 explain the process of data sampling and PWM generation for H-bridge inverter in synchronization with CPU clock.
Section 4.8 shows the experiment results of no-load test, acceleration test for the three phase machine with sensorless FOC. Further, the effect of the voltage drop across the semiconductor device during PWM and dead time, which will cause the common mode voltage across the machine stator windings is shown .

Chapter 5

Implementation of Sensorless FOC for Six phase machine

Chapter summary *This chapter aims at implementing sensorless field oriented control (FOC) for the six phase machine. At first, the concept of extending the FOC from the three phase machine to six phase is explained. Further, using Serial Peripheral Interfaces (SPI) module to establish the communication between two microcontrollers is explained. Subsequently, sensorless FOC is implemented in six phase machine is described. Finally, experiment results of the sensorless control for six phase machine are shown.*

In Fig. 5-1 shows the drive architecture employed in the prototype multiphase machine. Here two MCs are used to control the six phase machine, with each MC has control over the three phases of the machine. In this control structure, each MC will have full control over three phases of the machines, in term of generating the output signals for the machine phases and processing of the measured data. It should be noted that in this drive architecture, each MC has its own ADC module and ePWM module. ADC module is used for the measuring and processing machine real time data stator voltage, current and DC-link voltage. ePWM module for generating the PWM signals for the gate of the power converters.

It was initially described in section 2-2-3 that application of modularity to the controllers to the electrical drive system, will address the fault tolerance in the control circuitry. The advantage of having the distributed (modularity) controller architecture in critical applications like the aerospace field. Failure of one MC will have another MC would continue the control of the three phases of the machine, this will introduce the redundancy in control architecture. When this happens, even though the full performance of the machine won't be achieved, at least half the performance can be attained until the next service.

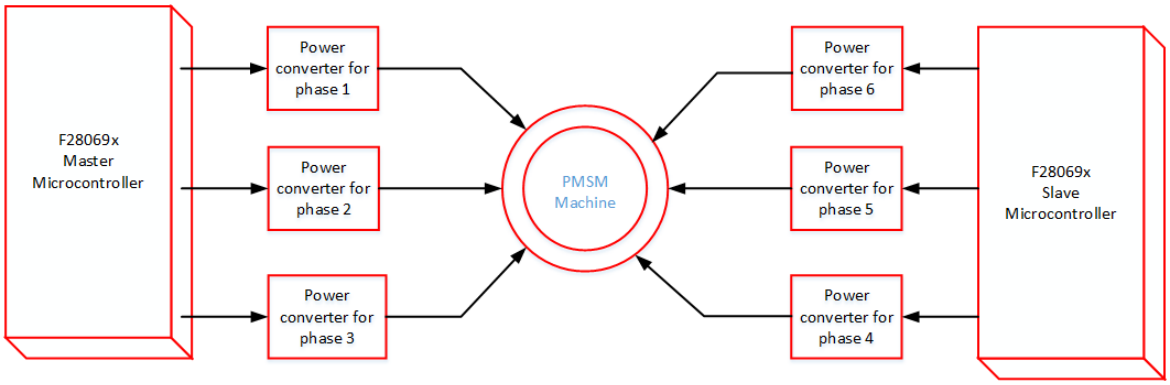

Figure 5-1: Six phase drive architecture.

5-1 Field Oriented Control in Six Phase Machine

Field oriented control (FOC) for the six phase machine is built on the same concept as in the three phase machine of decomposing the stator current into the flux generating component and torque component. In the distributed electrical drive system architecture discussed, one method to achieve FOC in six phases, using the master-slave MCs configuration in the controller structure. In Fig. 5-3 indicates the master-slave controller configuration for the control of the six phase machine.

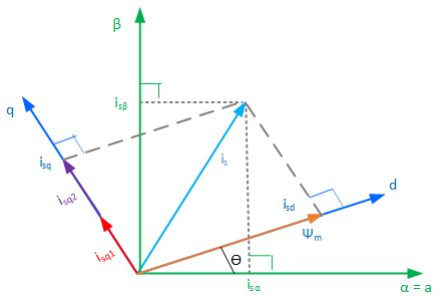

Figure 5-2: Space vector diagram for rotor -oriented control for six phase machine.

In this master-slave control architecture the user reference speed given to the master MC, reference speed is compared with FAST estimator rotor speed feedback as discussed in the section 4-3-2. Error in the speed is fed to the speed controller which would produce the current reference. Reference current from master MC is transmitted to the slave MC using Serial Peripheral Interface (SPI) communication. Reference current obtained in both the MCs is compared with measured current and error is fed to the PI current controller, which will produce the voltage reference (V_d and V_q) based on the model-based current control. Voltage reference in rotor reference frame is fed to the SVPWM module in both the master and slave MC. PWM gate signals from the master-slave MCs are generated similar to method explained in the section 4-5. By using this technique, it would result in torque current component's i_{q1} by the master MC and i_{q2} by slave MC in the same direction, two vectors get added to produce the resultant current component iq as indicated in the Fig. 5-3.

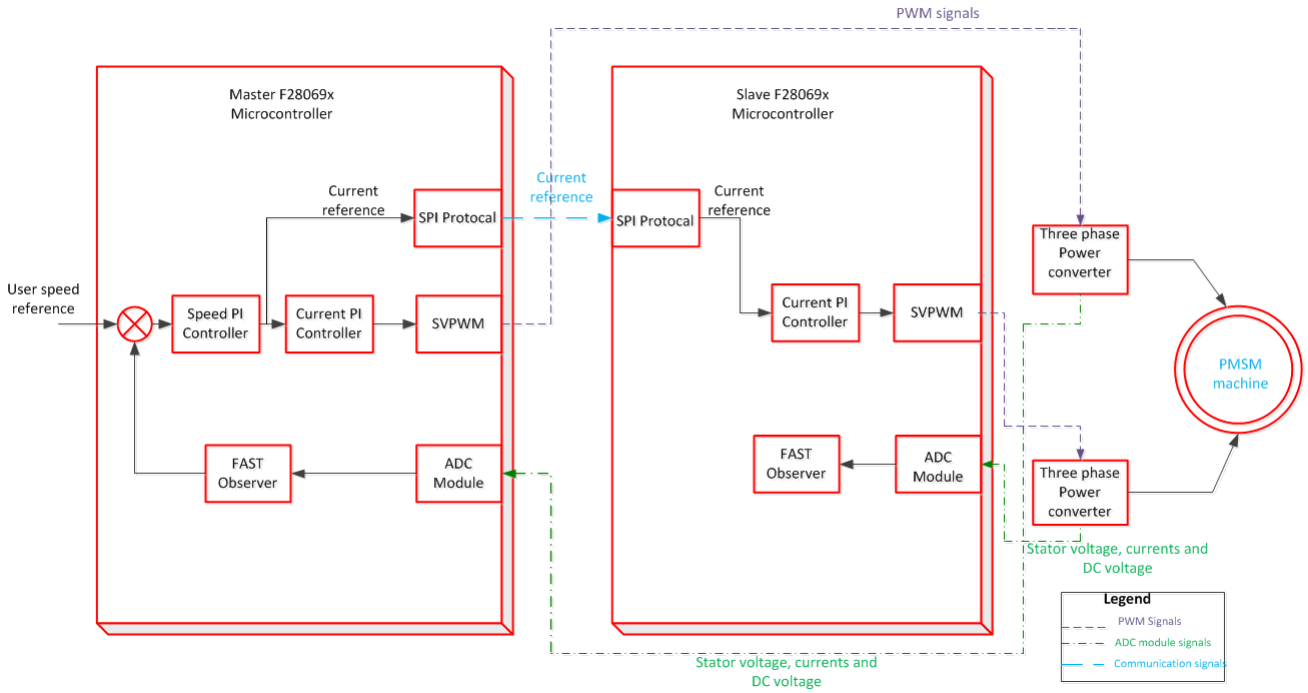

Figure 5-3: Master slave control architecture of six phase machine.

In Fig. 5-3, communication using SPI protocol between the two MC's is represented by the light blue dashed line. SVPWM gate signals required to trigger the three-phase power converters are indicated by the purple line and measured signals for the for the MC for sampling and processing from is indicated by the green line.

5-2 SPI Communication between Two Microcontrollers

Serial Peripheral Interface (SPI) is a built-in feature in the TMS320F28069x device. This module is synchronous serial input/output port which will shift a serial bit stream of variable length data into and out of the device at the certain programmed bit transfer rate. Here "synchronous" means bit transfer is synchronized to a CPU clock (System clock) signal. For data transfer between two MCs devices using SPI module, the master-slave configuration has to be used. In this arrangement, the master will control the clock signal required for data transfer between two devices. Data transfer between both the controllers using SPI module can be bidirectional or unidirectional.

Fig. 5-4 shows the schematic of single master-slave SPI implementation, the same arrangement is used for establishing motor control using distributed controllers as explained in the previous section. In this arrangement, five wires have to be connected between two MCs SPI module. SPICLK (SPI system clock) pin is used to transfer the system CPU clock to slave for data transfer. SPISOMI (SPI slave output master input) is used to transmit the data from slave to master using SPI clock. SPISIMO (SPI slave input master output) is used to transmit the data from master to slave using SPI clock. SPISTE (SPI slave transmission enable pin) is

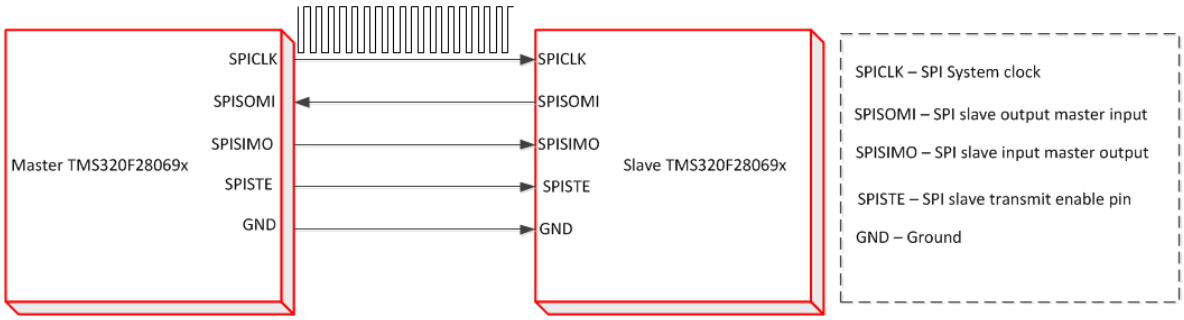

Figure 5-4: Single master, single slave SPI implementation.

used for initiating the data transfer between two devices. When SPISTE pin is made low both master and slave will start transmitting and receiving data using SPISOMI and SPISIMO pins. The direction of the lines in the Fig. 5-4 indicates the data transmission direction between two MCs in SPISOMI and SPISIMO pins. Ground connection in SPI modules of two devices is used to keep both the SPI modules at same potential.

Data transfer rate between two MCs is controlled by baud rate register (SPIBRR) in SPI module. SPIBRR register is used to set the frequency of the SPICLK using the Low speed peripheral clock prescale register (LSPCLK) [31]. As name defines LSPCLK is used for generating the prescaled clock signals to the peripheral in the MC. Recommendation from Texas Instruments for efficient master-slave communication between two devices using SPI should have the clock frequency set less than 10MHz [53]. Hence, LSPCLK is set to 7.5MHz. SPIBRR is defined by equation 5-1 [31]. SPIBRR in equation 5-1 is set to value 21.

$$\begin{aligned} \text{SPI Baud Rate} &= \frac{\text{LSPCLK}}{\text{SPIBRR}+1} \\ \text{SPIBRR} &= 3 \text{ to } 127 \end{aligned} \tag{5-1}$$

$$\begin{aligned} \text{SPI Baud Rate} &= 340909. \\ \text{Bit per second} &= 2.93 \cdot 10^{-6} bps \end{aligned} \tag{5-2}$$

For transmitting one bit of data from master to slave and vice versa, SPI module would require $2.93 \cdot 10^{-6} s$ from equation 5-2 from master to slave MC. The current reference value is 32-bit data size, SPI module would require the total time of $93.86 \cdot 10^{-6} s$ to transfer data from the master to slave MC. The sampling period is set to 50μs in both master and slave MC, data acquisition in ADC module and triggering of ePWM module takes every 50 μs once in both MCs. The reason for the delay in the slave MC is due to the hardware issue in SPI module, which will be described in the next chapter.

5-2-1 Impact of the delay

The impact of the delay in the communication in the FOC of the six phase can be seen using the Fig. 5-5. Here master MC will generate the current reference every sample, which is 50μs once. Once the current reference is generated it is transferred to the slave MC using the SPI communication. SPI communication would take 93.86μs to the full current reference from

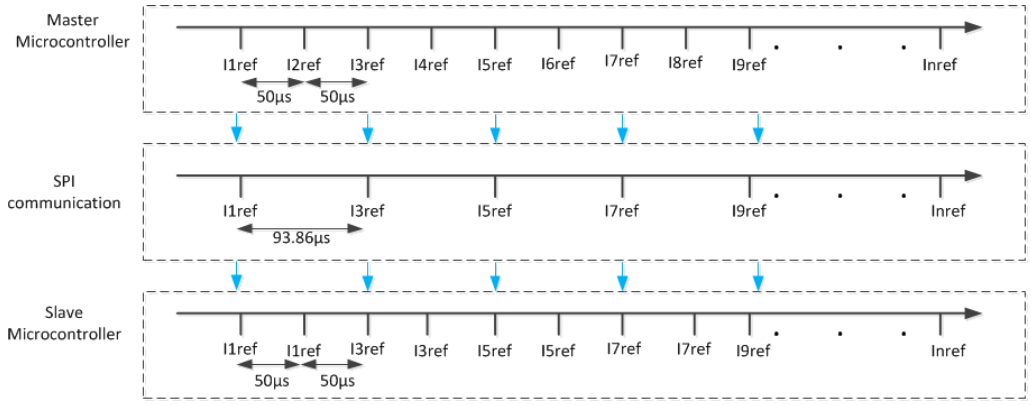

Figure 5-5: Delay in the communication of current reference.

master to slave MC. Only after the communication is complete the SPI module in the master MC will take the next current reference data to be transmitted. Due to this delay in the communication master MC will be able to transmit the alternate current reference to slave MC. So the slave MC uses same current reference for the present and next sampling time as shown in the Fig. 5-5. Since the machine is operating at a frequency very low compared to the switching frequency (Sampling time), the impact of the delay in FOC of the six phase machine is very low.

5-2-2 EMI Interference on SPI Communication Lines

While establishing SPI communication between two MCs for current reference data transmission. It was found that data received on the slave MC was corrupted. Later, it was detected that magnetic field produced by the permanent magnet on the rotor was producing EMI noise on communication lines between two MCs. This specific problem was solved by shielding the SPI communication lines with the household aluminum foil for effectively blocking of EMI noise [54]. Using this conductive material for shielding provides reflection, absorption, and transmitting EMI noise to ground [54]. In Fig. 5-6 shows the experimental setup for SPI communication using aluminum foil for EMI shielding between two MCs.
In Fig. 5-6 numbering specifies following :

1. Master MC Board.
2. Slave MC Board.
3. SPI module external pins in master MC.
4. SPI module external pins in slave MC.
5. Aluminum foil for EMI shielding over the SPI communication lines.

5-2-3 SPI- Experiment

Fig. 5-7 shows the SPI data transfer between two MCs, using master-slave configuration. SPI system clock is generated by the master MC. With respect to the master SPI clock (SPICLK),

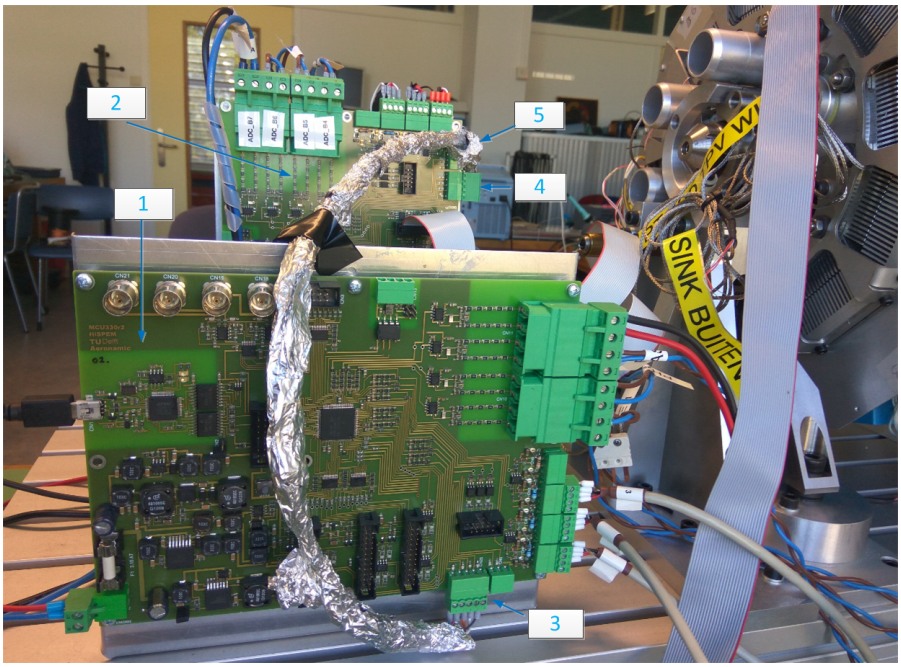

Figure 5-6: SPI module connection between master and slave MCs.

data transmission between master-slave takes place. SPI module is configured to transmit a 16-bit message, using SPISOMI, SPIMOSI pins. As explained in the beginning of the section, data transmission starts when SPISTE pin goes low, as indicated in Fig. 5-7. When the 16-bit data transfer is completed, SPISTE pin state goes high. SPISTE will go low when the data exchange between two MC starts again. In the present built master-slave, configuration data transfer from master to slave is set on rising edge of the system clock and vice versa is set on falling edge of the system clock. Selection of the clock edge for data transfer from master to slave and another way around can be selected interchangeably.

5-3 Six Phase Motor FOC-Experiment Results

SPI communication was established between the two controllers, to implement the FOC for six phase machine as discussed in the section 5-1. Using this communication lines, a current reference from the master was transmitted to slave MC.

5-3-1 No Load Test

No load test was carried out for the six-phase machine to check whether the machine is able to reach the reference speed applied to the master controller, with the distributed controller configuration. In this experiment, voltage and current were measured across two, three, five and six phase of the machine using the differential voltage and current probe. Measurement obtained from these probe were viewed using oscilloscope. Results obtained through the experiment are tabulated in the Table 5-1.

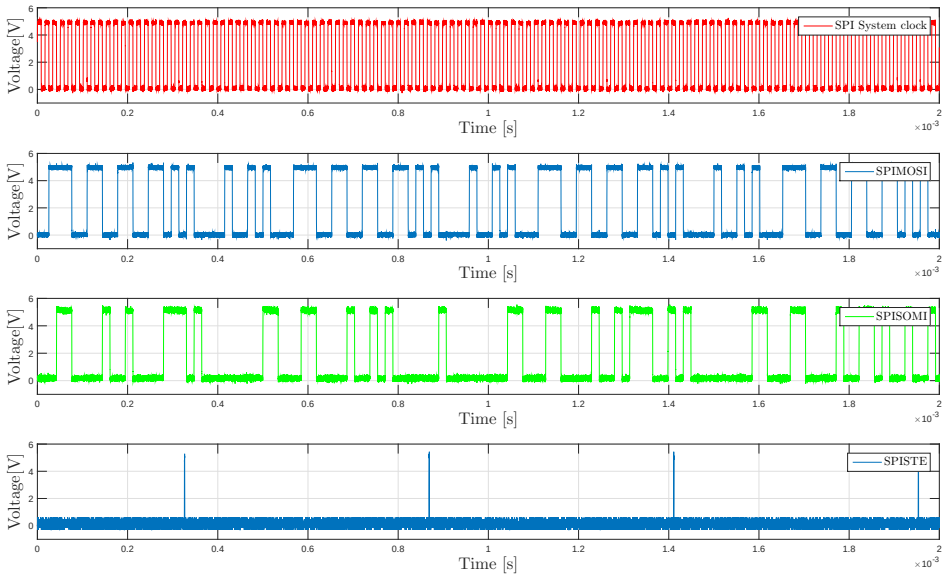

Figure 5-7: Transmission of data between two master and slave MC using SPI communication.

Speed [rpm]	Frequency [Hz]	Voltage V_{rms2} [V]	Voltage V_{rms3} [V]	Voltage V_{rms5} [V]	Voltage V_{rms6} [V]	Current I_{rms2} [mA]	Current I_{rms3} [mA]	Current I_{rms5} [mA]	Current I_{rms6} [mA]
200	13.34	8.27	8.20	8.10	8.01	34	35	44	32
300	20	9.34	9.32	9.12	9.10	40	38	46	36
400	26.67	10.37	10.28	10.12	10.20	43	37	50	38
500	33.37	11.37	11.56	11.24	11.34	52	40	58	40
600	40	12.22	12.43	12.02	12.19	55	44	65	42
700	46.67	13.04	13.20	12.98	13.05	61	49	66	46
800	53.36	13.80	14	13.56	13.63	68	55	71	53
850	56.67	14.19	14.41	13.98	14.13	71	60	77	58

Table 5-1: No Load Test : Six phase machine.

Number of observation from experiment results :

- RMS value of the voltage applied across the stator machine phases increases with the speed of the machine. Variation of the voltage across all the stator windings is same as in the three phase machine shown in previous chapters.
- Fig. 5-8 and 5-9, shows the measured value of the voltage and current at no load for the machine speed of 600 rpm.
- FFT on the voltage measured across the machine phases shows the amplitude of the fundamental value of voltage measured across four machine phases is same. Fig. 5-10 and 5-11 shows the FFT plot of the voltage measure across machine phase two and five at a rotor speed of 600 rpm.

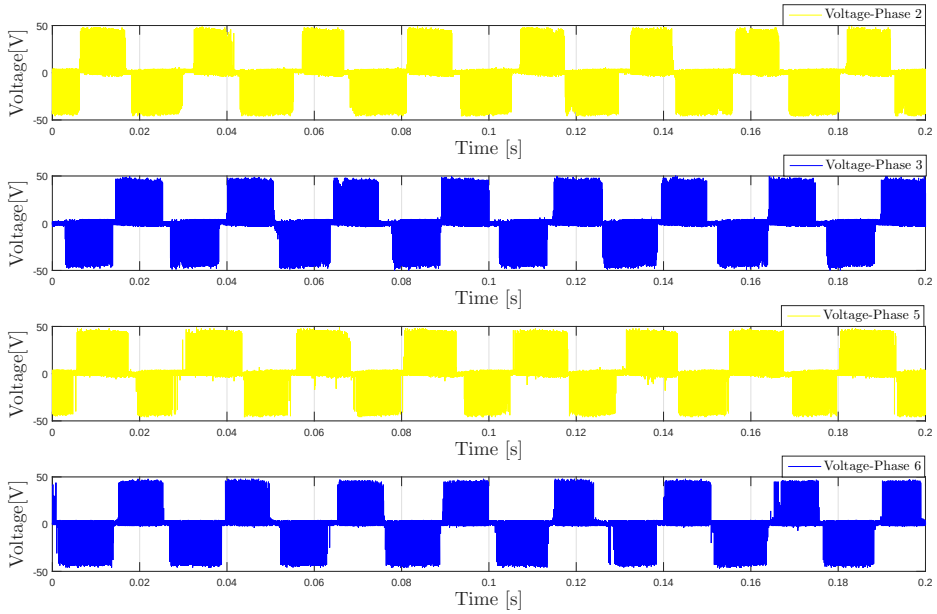

Figure 5-8: Voltage measured across the four phases of the machine. Speed = 600 rpm,frequency = 40 Hz, V_{rms2} = 12.22 V, V_{rms3} = 12.43 V, V_{rms5} = 12.02 V, V_{rms6} = 12.19 V.

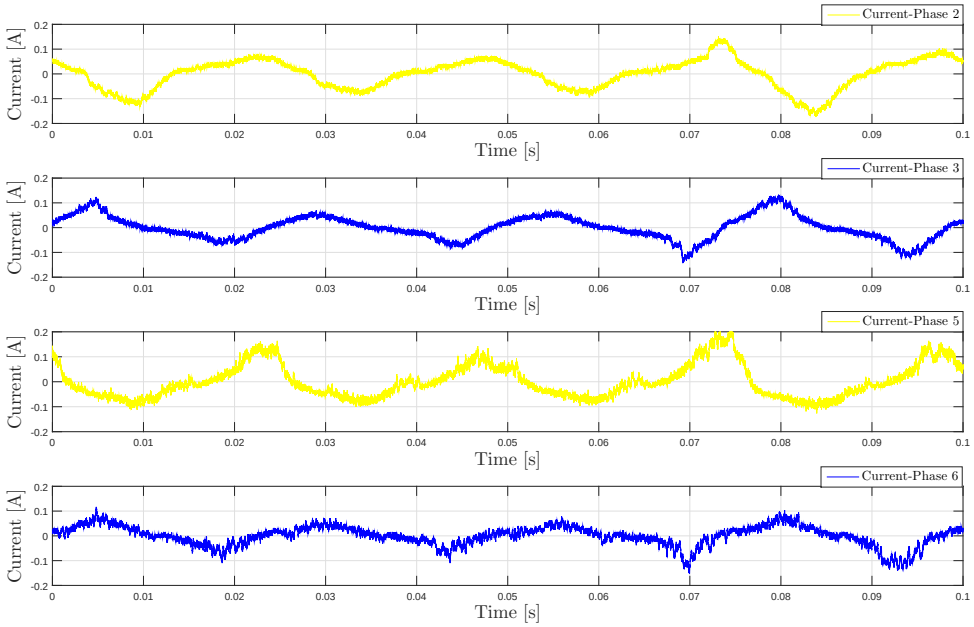

Figure 5-9: Current through through the four phases of the machine. Speed = 600 rpm,frequency = 40 Hz, I_{rms2} = 55 mA, I_{rms3} = 44 mA, I_{rms5} = 65 mA, I_{rms6} = 42 mA.

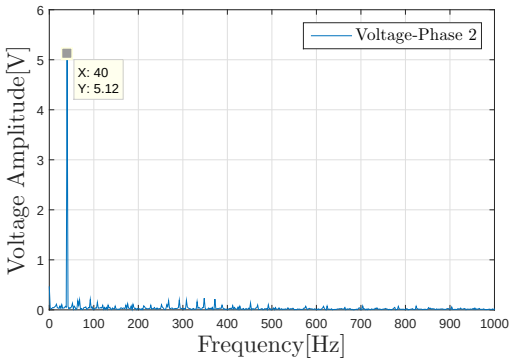

Figure 5-10: FFT on the voltage measured across machine phase two at rotor speed of 600 rpm.

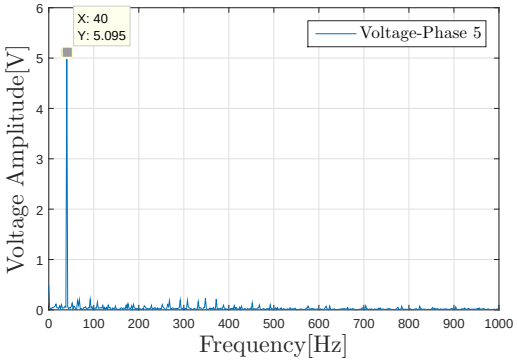

Figure 5-11: FFT on the voltage measured across machine phase five at rotor speed of 600 rpm.

- FFT plot from the Fig. 5-10 and 5-11 also shows the frequency of the fundamental component is same as the user speed reference frequency.
- When the manual load is applied to the rotor shaft, current through the machine phases becomes more sinusoidal as shown in the Fig. 5-12.

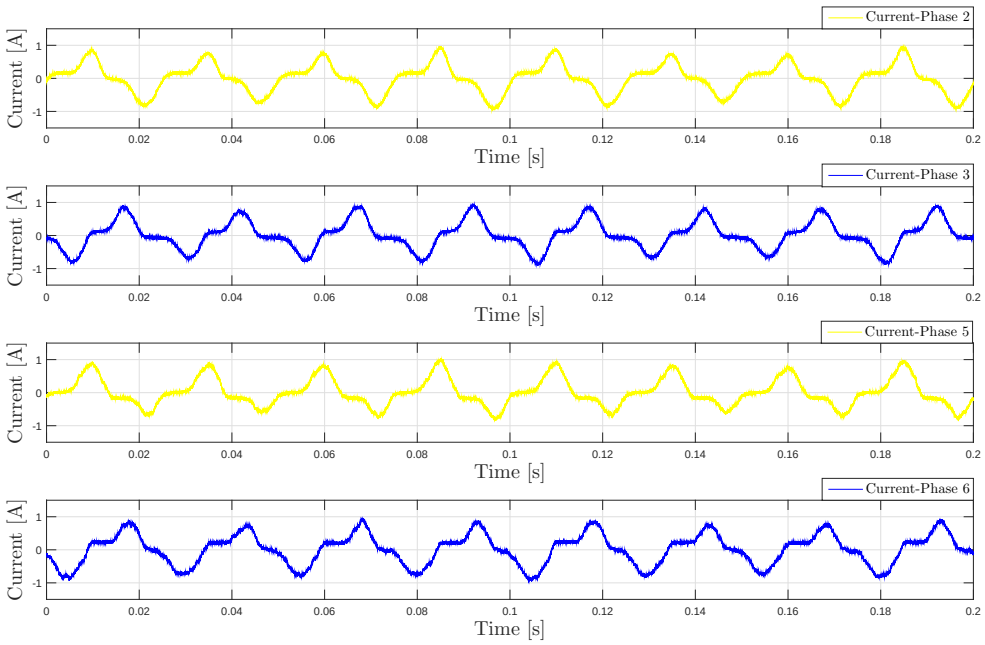

Figure 5-12: Current through through the four phases of the machine. Speed = 600 rpm,frequency = 40 Hz, I_{rms2} = 0.426 A, I_{rms3} = 0.419 A, I_{rms5} = 0.408 A, I_{rms6} = 0.430 A.

5-3-2 Acceleration Test

Acceleration test was performed for six phases of the machine, similar to the three phase described in the section 4-8-2.

Case 1 : Acceleration 200 rps

Acceleration was set to 200 rps and the machine reference speed was changed from 200 rpm to 800 rpm and observations from the test are as follows :

- Due to the deviation in the value of the difference between reference speed and actual speed, the controller will start to accelerate. To accelerate the rotor, the amplitude of the output voltage across the stator winding phases starts increasing. This is done by increasing the duty cycle of PWM gate signal fed to all stator phases as shown in Fig. 5-13.

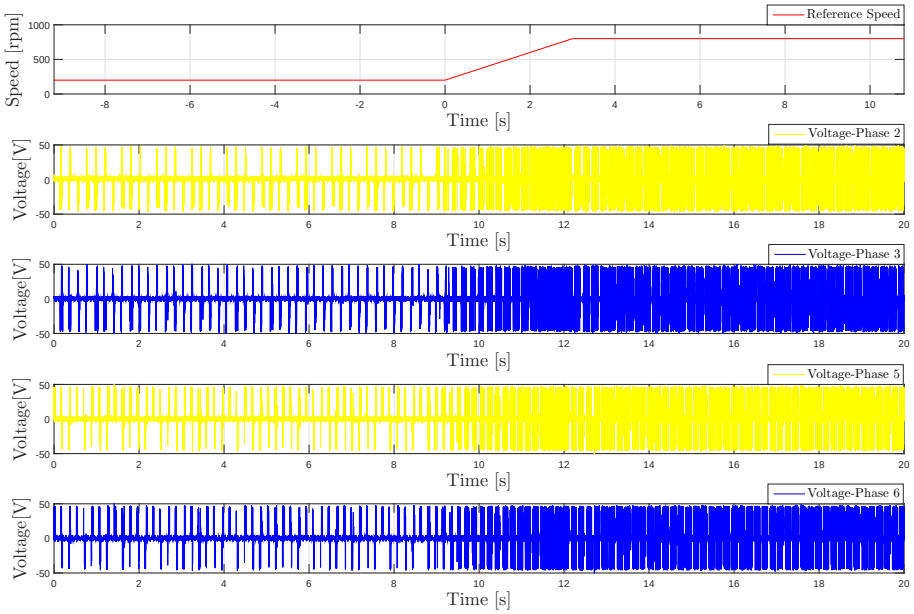

Figure 5-13: Variation of the voltage during acceleration from 200 rpm to 800 rpm, at acceleration of 200 rps.

- For accelerating, the motor will draw initially transient current. When the machine reaches the reference speed, current drawn for accelerating will start reducing. It will reduce until the machine has enough current to run the machine at reference speed. In Fig. 5-14 both the effects of the current transient and current reduction after machine reaches reference can be seen in all phases.
- Magnitude of the transient current drawn during acceleration is reduced by almost half in the six phase compared to the three phase during acceleration.

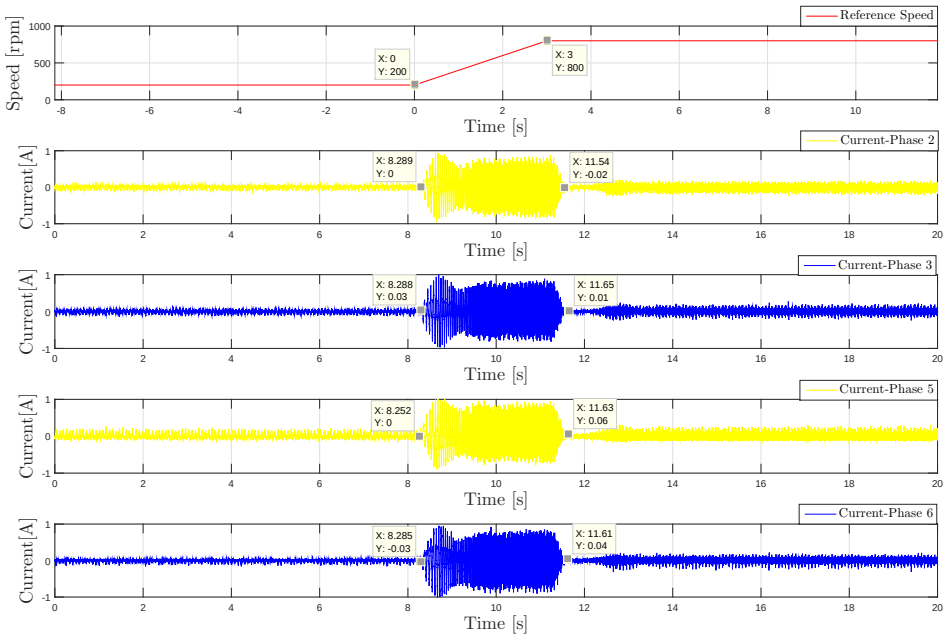

Figure 5-14: Variation of current through machine phases, during acceleration from 200 rpm to 800 rpm, at acceleration of 200 rps.

- Time taken by the ramp generator to reach the reference speed of 800 rpm from 200rpm, is 3s with acceleration set to 200rps. Current drawn by the stator winding, during this period will follow the similar trend in terms of time taken to reach reference speed as shown in the Fig. 5-14.

Case 2 : Acceleration 100 rps

In this experiment, acceleration was reduced to 100 rps in both the master and slave MC from the previously set value of 200rps. observation from experiment.

- Time taken by the controller to reach 800 rpm is doubled, due to the reduction in the acceleration by half, resulting in the lower value current drawn. Current through the stator follows same trend in terms of the variation as shown in the Fig. 5-15.

5-4 Discussion

This chapter focussed on the development of sensorless control of the six phase prototype machine, using microcontroller based FAST observer. Section 5.1 provides the schematic of the drive architecture of PMSM prototype system.
Section 5.2 explained the concept of extending the three phase FOC to six phase machine in the PMSM using distributed controllers.

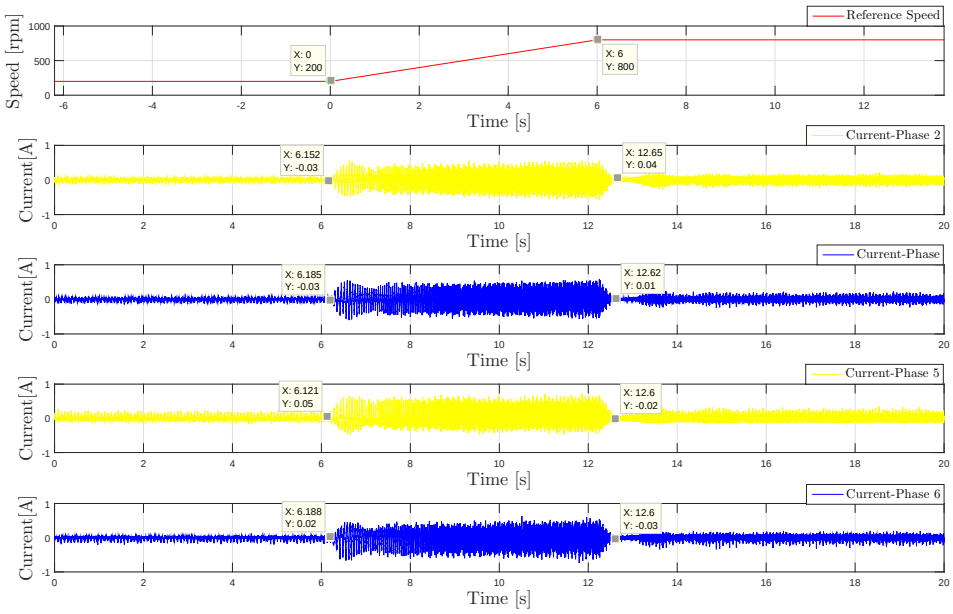

Figure 5-15: Variation of current through machine phases, during acceleration from 200 rpm to 800 rpm, at acceleration of 100 rps.

Section 5.3 describes the practical implementation of the using the SPI communication between two MCs. Further, the method employed to avoid the EMI noise from the permanent magnet rotor.
Section 5.4 shows the experiment results carried out on the six phase machine for the no-load test and also for the step change in the reference speed using the internal digital ramp generator.

Chapter 6

Hardware Implementation Issues

Chapter summary *This chapter aims to give an overview about hardware issues in Microcontroller board, H-bridge inverter and motor control during the implementation of sensorless control FOC in six phase.*

6-1 Microconrtoller Board

6-1-1 SPI Communication

Problem description

In the SPI module of the MC, there will be five pins as explained in the in the section 5-2. These five pins are SPICLK (SPI system clock), SPISOMI (SPI slave output master input), SPISIMO (SPI slave input master output), SPISTE (SPI slave transmission enable pin), Ground pin. These pins in the two MCs are interconnected using the wires to establish the communication between them.

MC will be usually equipped following serial communication modules, two serial peripheral interface (SPI) modules, one inter-Integrated circuit ($I2C$) modules and two Serial communication interfaces (SCI) modules. In the customized MC board under consideration, only one SPI module is built for the communication in both master and slave MC. In this presently MC board, other serial communication protocols (SCI and I2C) are used for other functions. Reason being each MC pin will be designed to have two to three functionalities, for instance single pin will have both inbuilt functionalities of PWM and ADC. So while designing the MC for the control, care has to be taken to design well to use all the functionalities thoroughly.

In this SPI module, SPISTE pin from the MC isn't connected to the external port of SPI.

SPITE pin (pin number 77) of SPI module is left unused, this can be seen from the MC board design in the Appendix BB-1. SPISTE is an important pin in SPI module because it is primarily used to enable the slave MC to receive/sending the data when the communication between two MCs starts.

Remedy

To solve the aforementioned problem, the general purpose input/output (GPIO58 - pin number 98) pin was used, this pin was programmed to act as the SPISTE pin in both the master and slave MCs. These two GPIO pins in both master and slave were interconnected through the wire for communication, as other pins in the SPI module.

Hypothesis on delay

Theoretically, SPI module can transmit the 32-bit data from master to slave and vice versa in 17.06μs [31]. Using the equation 5-1, by setting SPIBRR to minimum value of 3. However, practically data transmission resulted in error when SPIBRR value was set to value less than 21. Setting SPIBRR value to 21 will result in the delay of 43.96 μs, as described in the section 5-2. This might be maximum speed possible practically from SPI module, for communication or GPIO pin programmed to be used as SPISTE pin can also be the reason for this delay.

6-1-2 ADC Module issue

Problem description

During testing of the FOC for three phases of the machine using both MCs individually. It was found that motor reference speed given to MC was not equal to the actual speed. Motor speed was always lagging by almost 200 to 300 rpm compared to the reference speed given to the controller.

Remedy

To solve this problem, MC external modules present in the MC board was tested. After verifying all the modules, it was found that ADC module voltage scale down digital output results wasn't matching with analog input. The reference voltage of 3V required for the conversion in the ADC module wasn't function properly. Due to this measured voltage across the stator phases weren't accurate, so it was resulting in the speed difference between the reference and actual speed of the motor. Later the defect chip was replaced with the new chip, motor FOC was functioning properly.

Note

It must be noted that this is not the only issue if the motor control isn't functioning properly. There can be other possible problems too, but this is one of the potential areas to be checked if the motor speed is lagging reference speed by a large value.

6-2 Power Converter

6-2-1 H-bridge inverter

During the testing of H-bridge inverter modules, the output voltage across inverter wasn't square wave for single pulse width modulation technique used in the controller. Bipolar voltage switching technique is used, so switches diagonally opposite in H-bridge will conduct in a pair. Output voltage and current waveforms observed is as shown in the Fig. 6-1.

In the Fig. 6-1 it can be seen that voltage and current waveforms are completing only the

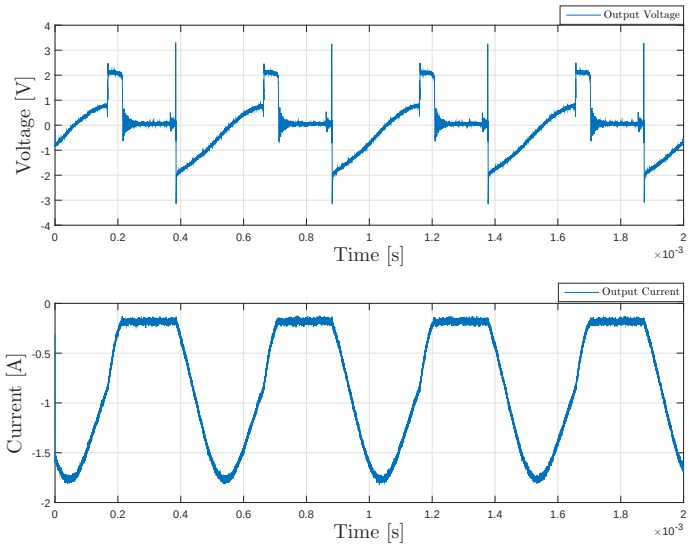

Figure 6-1: Inverter output voltage and current.

half cycle. It shows that one switch pairs aren't functioning properly. Later when both the legs were checked individually, it was found that IGBT switch S_2 was not turning on, even with driver circuit feeding the gate signals properly.

6-3 In Motor Control

6-3-1 Driver Circuit

Problem Description

In the FOC of the motor, current through motor phase one was in low magnitude compared other two phases of the machine and it was not conducting in the negative cycle fully, as shown in the Fig. 6-2.

Remedy

Initially, H-bridge inverter connected across each phase of the machine was tested for its operation. In testing, it was found that driver circuit in the machine phase one wasn't

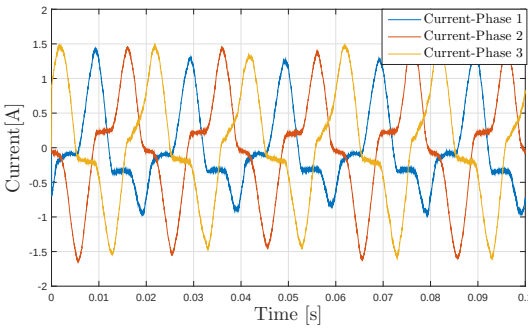

Figure 6-2: Current through the machine phase one, two and three, during the driver circuit malfunctioning. I_{rms1} = 0.6 A, I_{rms2} =0.80 A, I_{rms6} = 0.796 A.

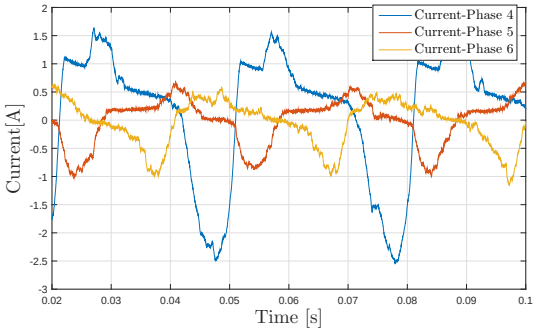

Figure 6-3: Current through machine phase four, five, six. during the current measurement error. I_{rms4} = 1.27 A, I_{rms5} = 0.39 A, I_{rms6} = 0.45 A.

functioning properly for the duty cycle value less than 0.25, when the results obtained were compared with the other phase inverter. The driver circuit is used to step up the gate voltage signal obtained from the MC to IGBT switches in the inverter. Later the driver circuit was replaced with the new one and FOC was tested again. It was observed that the current through machine phase one was same as the other phases and it was conducting fully in both positive and negative cycle.

6-3-2 Current Measurement

Problem Description

The magnitude of the current through phase four of the machine was two times higher compared to the phase five and phase six, as shown in the Fig. 6-3.

Remedy

While checking all the driver and power converter circuit of phase four, it was found that wire connecting from the current sensor to the MC board wasn't functioning in phase four, which resulted in the higher magnitude of the current the phase four. Later wire was repaired than the current through machine phases were of equal magnitude.

Chapter 7

Conclusion and Recommendations

7-1 Conclusion

This master thesis project aims at implementing the sensorless field oriented control on the prototype modular design six phase permanent magnet synchronous machine with the distributed control architecture. The main conclusions drawn from the thesis are presented as follows.

At first, modular design of the PMSM and power converter under consideration is explained using literature. Further, application of the modularity to the whole electrical drive system including the control circuit is presented. Integration of modularity will make system suitable for the safety critical application, which is very important for the system to be considered for the "More Electric Aircraft" application in future.

Subsequently, thesis focussed on the measurement of machine parameters such as stator resistance, rotor flux, stator self and mutual inductance through experiments. Measured machine parameters are used for estimating the rotor position information in sensorless FOC. H-bridge inverter required for powering the machine phase is built and tested, using the (enhanced Pulse Width Modulation) ePWM module in the microcontroller.

At first sensorless FOC (Direct FOC or Vector Control), was implemented in the three phases of the machine using the inbuilt InstaSPIN FOC algorithm in microcontroller (MC) TMS320F28069x device. In this algorithm, the microcontroller will act has software position encoder, InstaSPIN estimates the back emf of the machine, using the machine parameters $(R_s, L_d, L_q, \lambda_m)$ and also the real-time measured voltage, current. From the machine back emf, rotor position information is estimated. Using this rotor position information speed of the rotor is also estimated and used for the control for the motor. FOC has two controllers for controlling speed and torque. The outer control loop is used for speed control and inner control loop is used for the current control (Torque control).

In the modular design, PMSM phases are fed through H-bridge inverter, so this type of power converter configuration can be considered as the dual two-level inverter. This type of power converter configuration can be made to produce the voltage space vector identical to the three level inverter. By selecting appropriate voltage vector through switching combination in the dual two level inverter configuration common mode voltage produced due to PWM in the machine windings is avoided.

After the implementation of the FOC using the microcontroller based observer. To validate the sensorless control in the three phase machine two tests were performed. The first test was no load test, here the reference speed was applied to the controller and the machine rotor speed was measured through tachometer and verified by the frequency of the measured voltage/current. It was observed that measurements were in good agreement. The second test was to check the performance of the controller, here the machine was accelerated from 200 rpm to 800 rpm using the internal ramp function generator in the microcontroller. It was observed that machine was able to reach the 800 rpm almost at the same time as the controller ramp generator.

The sensorless control from the three phase is extended to six phases of the machine using master-slave controller configuration. In this setup, two microcontrollers are used, here master MC will control the three phases of the machine and slave MC will control the remaining three phases of the machine. In this way, modularity is introduced in the control circuitry. Further using Serial Peripheral Interface (SPI) module communication is established between the two controllers. With this architecture, rotor position information available from both the master and slave MC for the implementation of the FOC. Using the SPI communication protocol current reference from the master MC is sent to the slave MC. Current reference obtained in both the master and slave MC are compared with the actual current measured from the current sensor. Further, current controller in both the MCs will produce the reference space vector PWM in both the master controlled three phases and slave controlled three phases in PMSM. No load and acceleration test was also performed for the six phase machine and it was observed that performance of six phase machine remains the same as compared to the three phase machine at no load.

In conclusion, apart from adding the redundancy in to the control circuit with master slave control architecture, six phase machine will behave has two three phase machine.

7-2 Recommendations

The following recommendations are suggested for future research.

1. Sensorless FOC has to be practically validated for the load condition, to check the performance of the motor.
2. Microcontroller board has to be redesigned for the following reasons :
    - Fixing the existing SPI communication module might reduce the delay in the communication of the signal from master to slave MC.
    - Adding the extra communication protocol hardware, if the currently working one fails. It will also help for implementing the fault tolerant operation since in existing setup master MC will control the FOC of six phases.
3. A modulation technique can be employed to avoid the zero sequence current due to dead time as in the [5].
4. A three phase common mode choke can be designed to avoid the zero sequence currents in the system [51].
5. A pulse based dead time compensation can be applied to the dual two level inverter to avoid the common mode voltage due to dead time [51].

Appendix A

Appendix -A

A-1 Variation of the effect of the semiconductor voltage drop.

As it was described in the section 4-8-3 to check the effect of the semiconductor voltage drop on the current waveform, PMSM was accelerated from reference speed of 200 rpm to 800 rpm with the acceleration set in the controller to 1 krps.

Fig. A-1 indicates legends of all the waveforms in the screenshot from CRO, it also shows

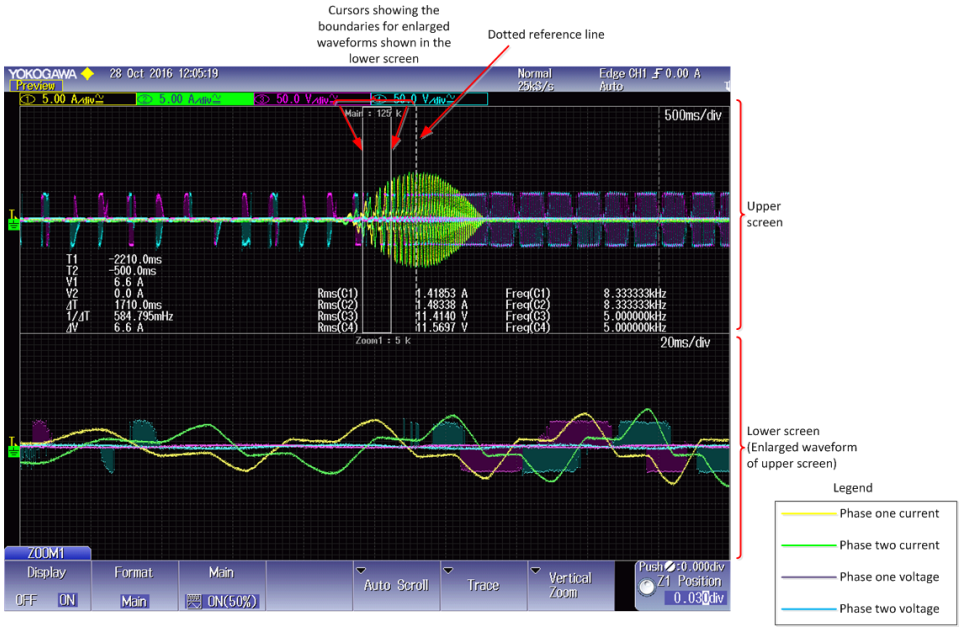

Figure A-1: Reference

the division of the screen into two screens as upper and lower screen. The upper screen indicates the variation of voltage, current during acceleration in two phases of the machine

and lower screen indicates the enlarged view of the upper screen waveform. In the upper screen there two vertical white lines, this is used to enlarge particular section of the waveform, enlarged view can be seen in the lower screen. The dashed vertical line in the upper screen is used as the reference for varying the two vertical lines. Subsequently, subfigures in Fig. A-2 depict the same information in terms of legends and screen indications as in Fig. A-1.

Fig.A-2 shows the variation of the current and voltage in two phases of the machine at each instance during the motor acceleration from 200 rpm to 800 rpm at the set acceleration of 1 krps. In the Fig. A-2, subfigures are numbered in the ascending order starting from speed of 200rpm till machine accelerate 800 rpm.

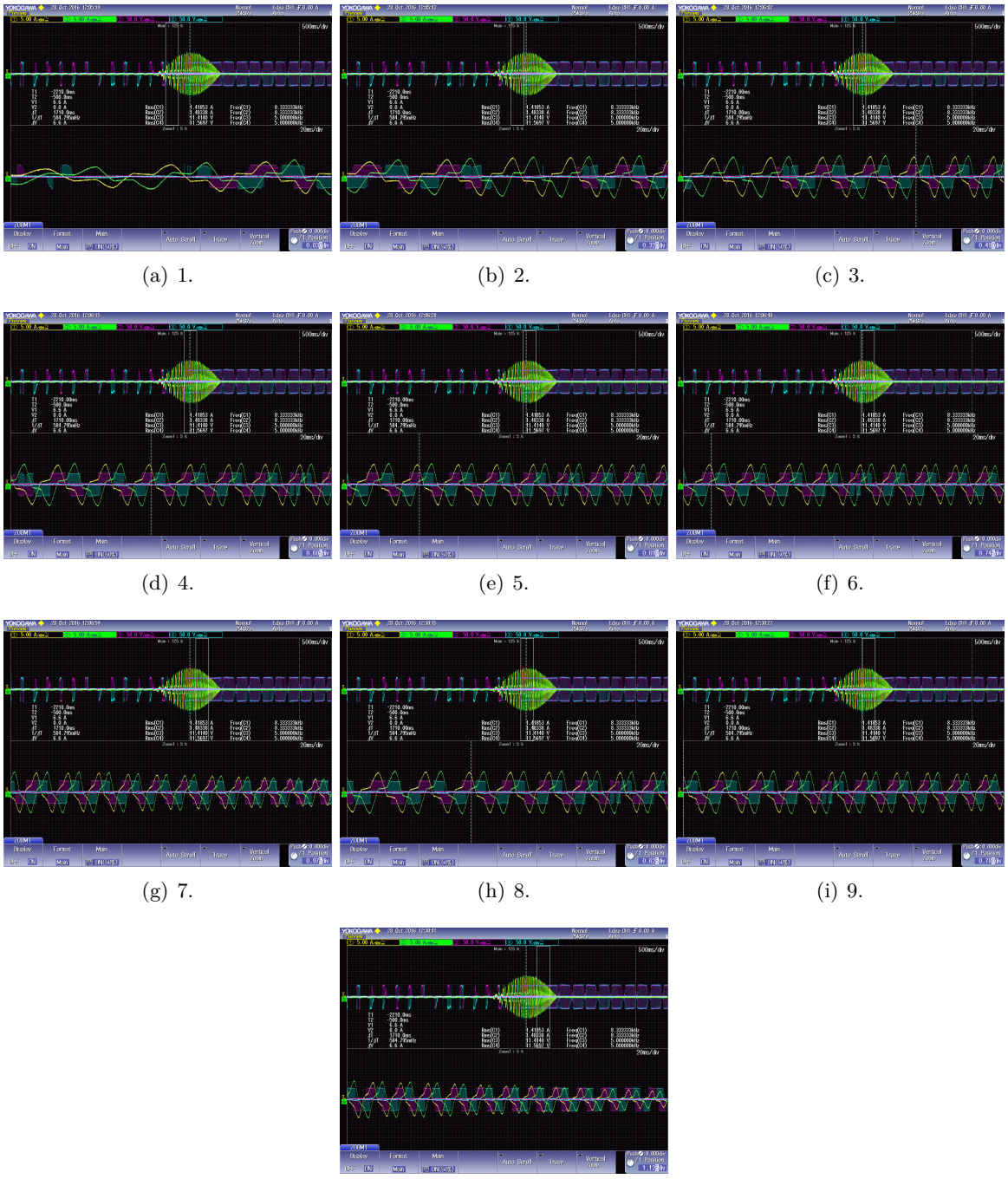

(a) 1. (b) 2. (c) 3.

(d) 4. (e) 5. (f) 6.

(g) 7. (h) 8. (i) 9.

(j) 10.

Figure A-2: Variation of the voltage and current at each instance during the acceleration of the motor from 200 rpm to 800 rpm.

Appendix B

Drive control Design

B-1 Microcontroller Board Design

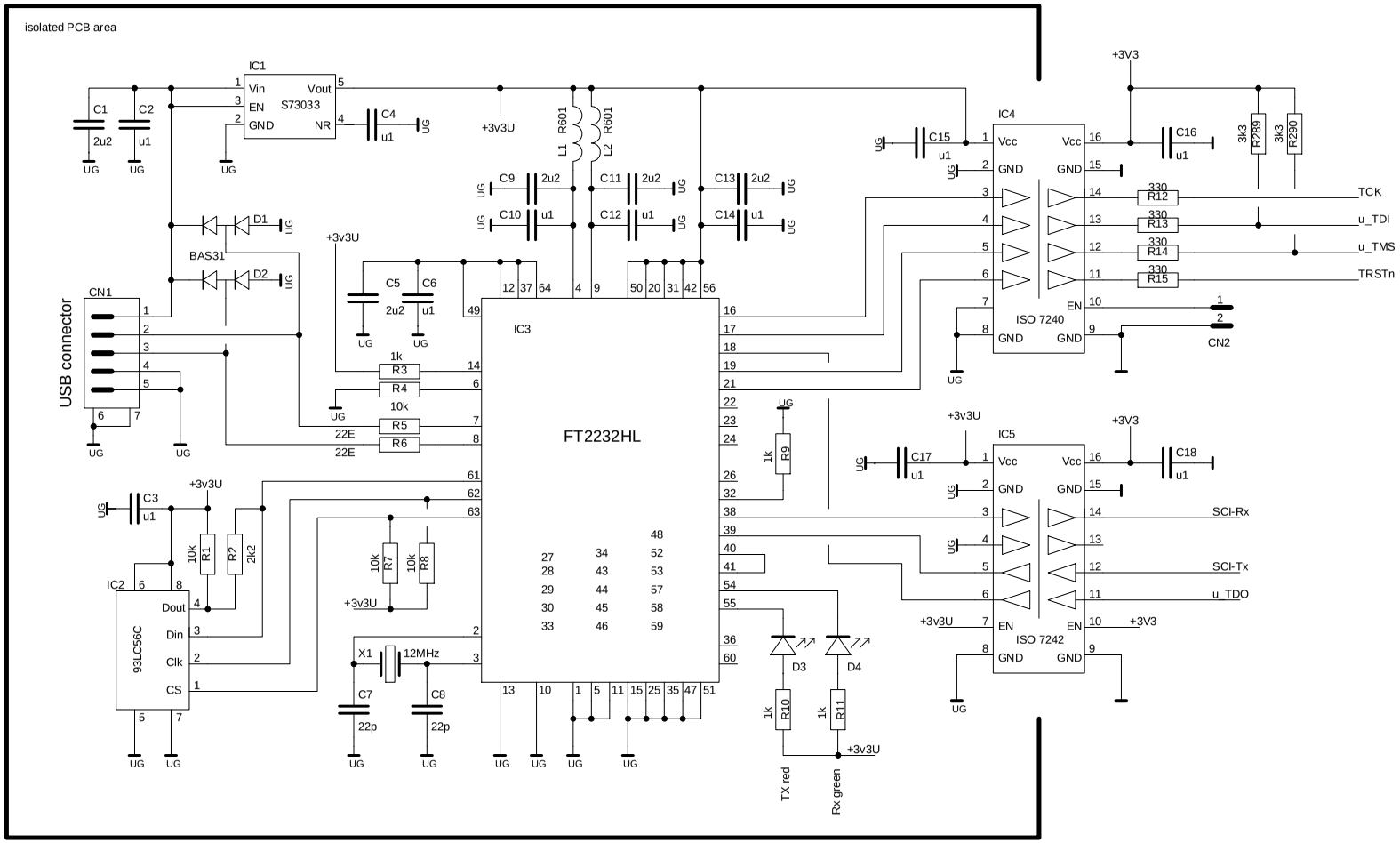

MCU330r2	USB-port
Rev. 10	page 1/6
02-07-2013	GME
albion instruments	

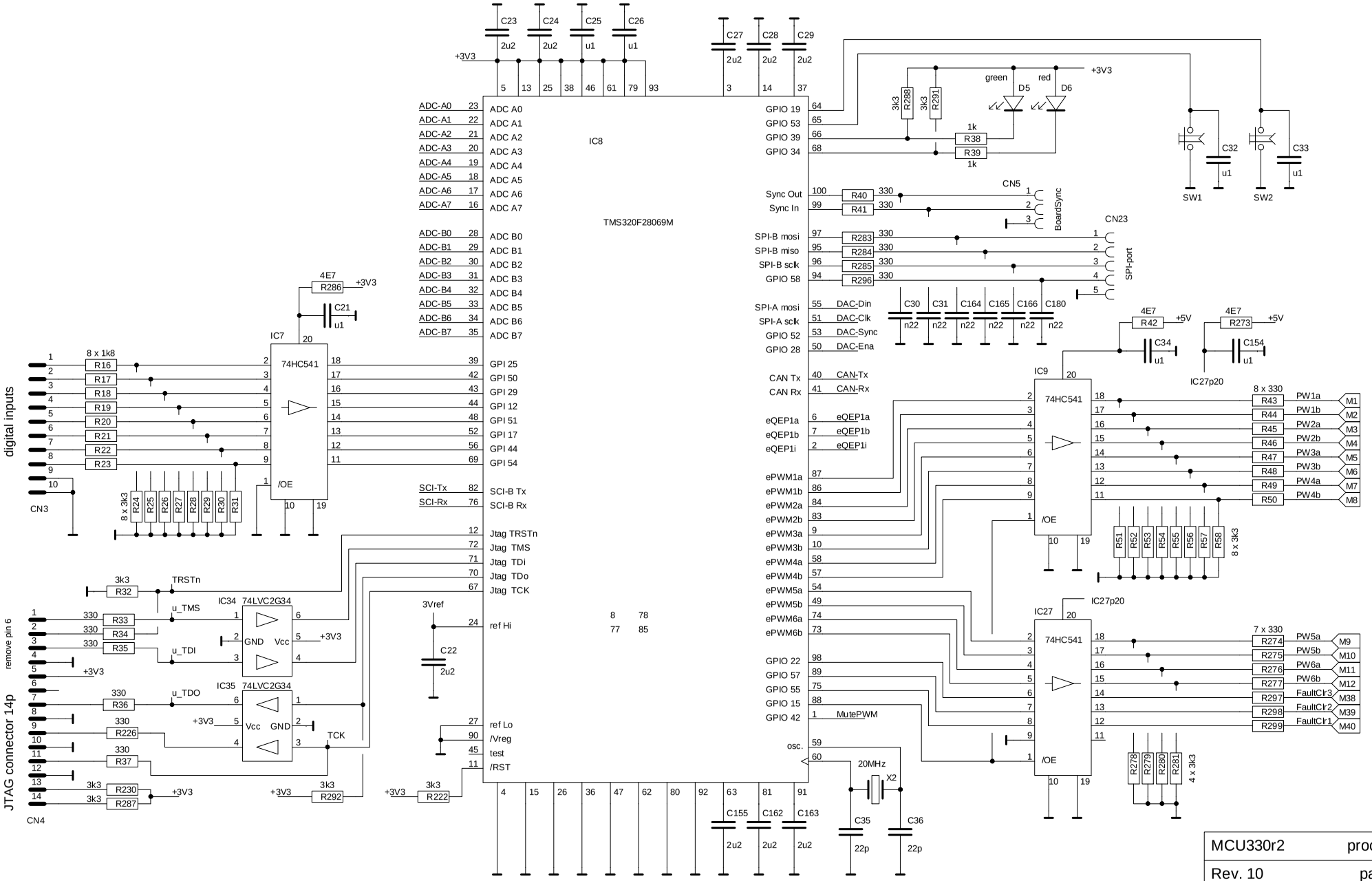
IC8
TMS320F28069M
ADC-A0 ADC-A1 ADC-A2 ADC-A3 ADC-A4 ADC-A5 ADC-A6 ADC-A7
ADC-B0 ADC-B1 ADC-B2 ADC-B3 ADC-B4 ADC-B5 ADC-B6 ADC-B7
GPIO 19 GPIO 53 GPIO 39 GPIO 34
Sync Out Sync In
SPI-B mosi SPI-B miso SPI-B sclk GPIO 58
SPI-A mosi SPI-A sclk GPIO 52 GPIO 28
CAN Tx CAN Rx
eQEP1a eQEP1b eQEP1i
ePWM1a ePWM1b ePWM2a ePWM2b ePWM3a ePWM3b ePWM4a ePWM4b ePWM5a ePWM5b ePWM6a ePWM6b
GPIO 22 GPIO 57 GPIO 55 GPIO 15 GPIO 42
GPI 25 GPI 50 GPI 29 GPI 12 GPI 51 GPI 17 GPI 44 GPI 54
SCI-Tx SCI-Rx
SCI-B Tx SCI-B Rx
Jtag TRSTn Jtag TMS Jtag TDi Jtag TDo Jtag TCK
ref Hi ref Lo /Vreg test /RST
osc.
DAC-Din DAC-Clk DAC-Sync DAC-Ena
CAN-Tx CAN-Rx
MutePWM
20MHz X2
C23 C24 C25 C26 C27 C28 C29 C30 C31 C164 C165 C166 C180 C32 C33 C34 C154 C155 C162 C163 C35 C36 C21 C22
SW1 SW2
green red D5 D6
R38 R39 R40 R41 R42 R273 R283 R284 R285 R296 R286 R288 R291
CN5 BoardSync
CN23 SPI-port
IC7 74HC541
IC9 74HC541
IC27 74HC541
IC27p20
IC34 74LVC2G34
IC35 74LVC2G34
R16 R17 R18 R19 R20 R21 R22 R23 R24 R25 R26 R27 R28 R29 R30 R31
R43 R44 R45 R46 R47 R48 R49 R50 R51 R52 R53 R54 R55 R56 R57 R58
R274 R275 R276 R277 R297 R298 R299 R278 R279 R280 R281
R32 R33 R34 R35 R36 R226 R37 R230 R287 R292 R222
PW1a PW1b PW2a PW2b PW3a PW3b PW4a PW4b PW5a PW5b PW6a PW6b FaultClr3 FaultClr2 FaultClr1
M1 M2 M3 M4 M5 M6 M7 M8 M9 M10 M11 M12 M38 M39 M40
digital inputs
JTAG connector 14p
CN3
CN4
remove pin 6
TRSTn u_TMS u_TDI u_TDO TCK
3Vref
+3V3 +5V
MCU330r2 processor
Rev. 10 page 2/6
02-07-2013 GME
albion instruments

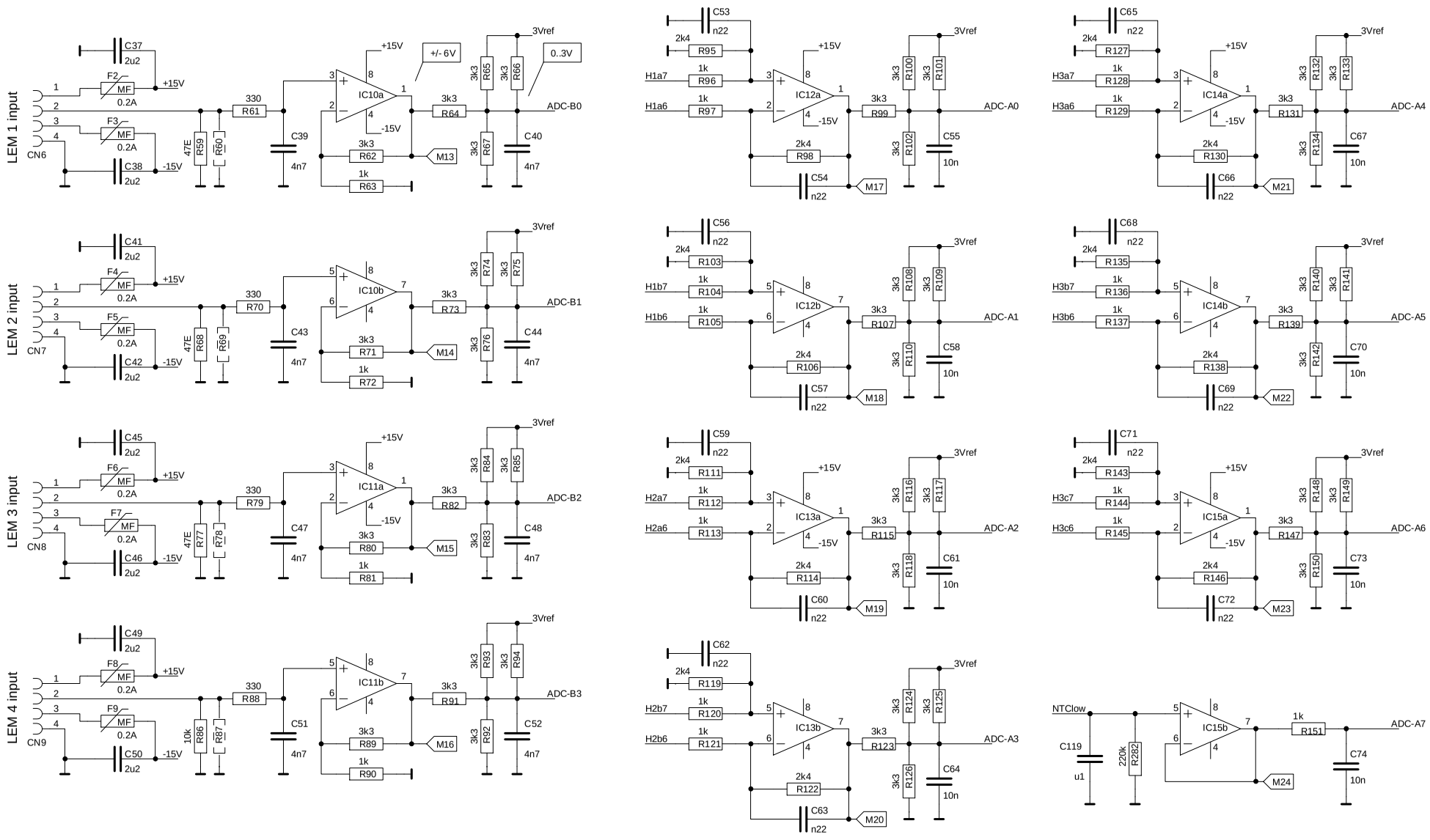

MCU330r2	current inputs
Rev. 10	page 3/6
02-07-2013	GME
albion instruments	

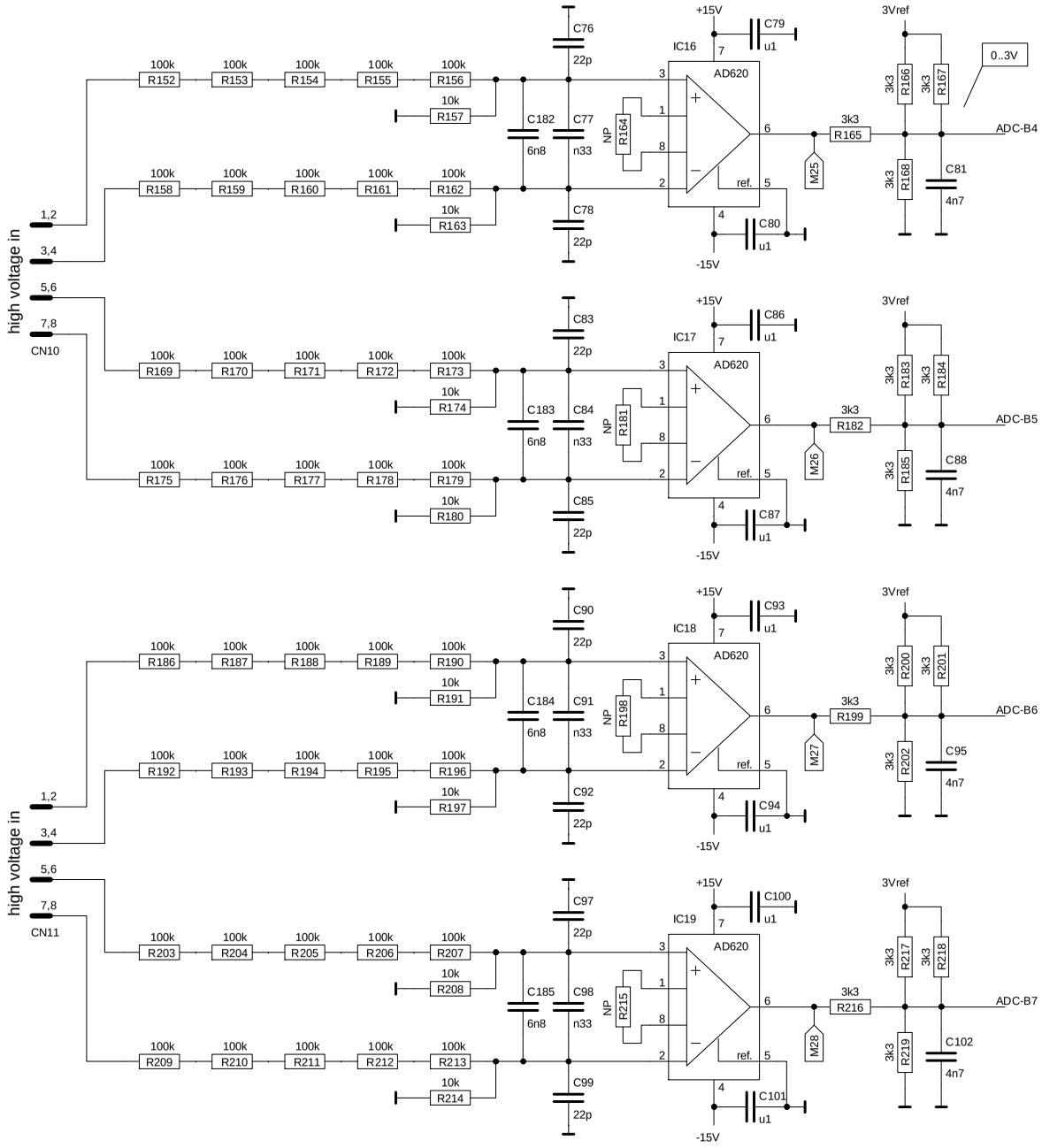

MCU330r2	voltage inputs
Rev. 10	page 4/6
02-07-2013	GME
albion instruments	

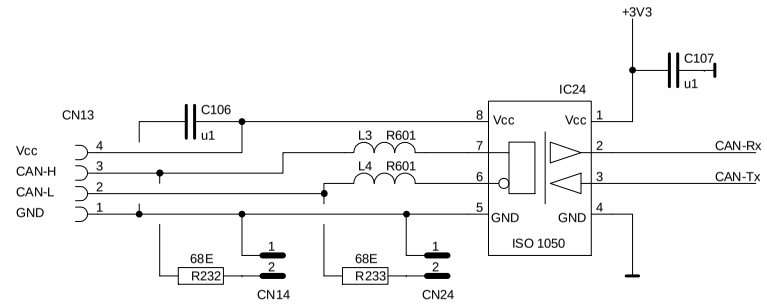

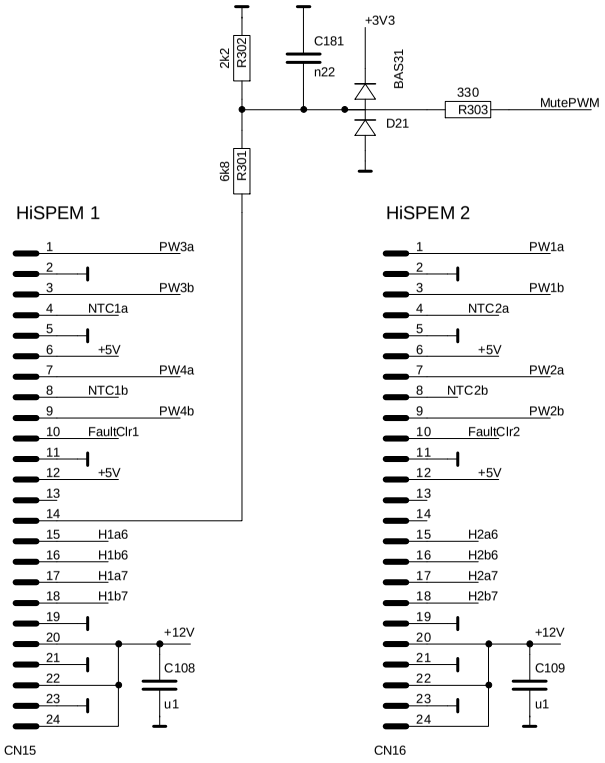

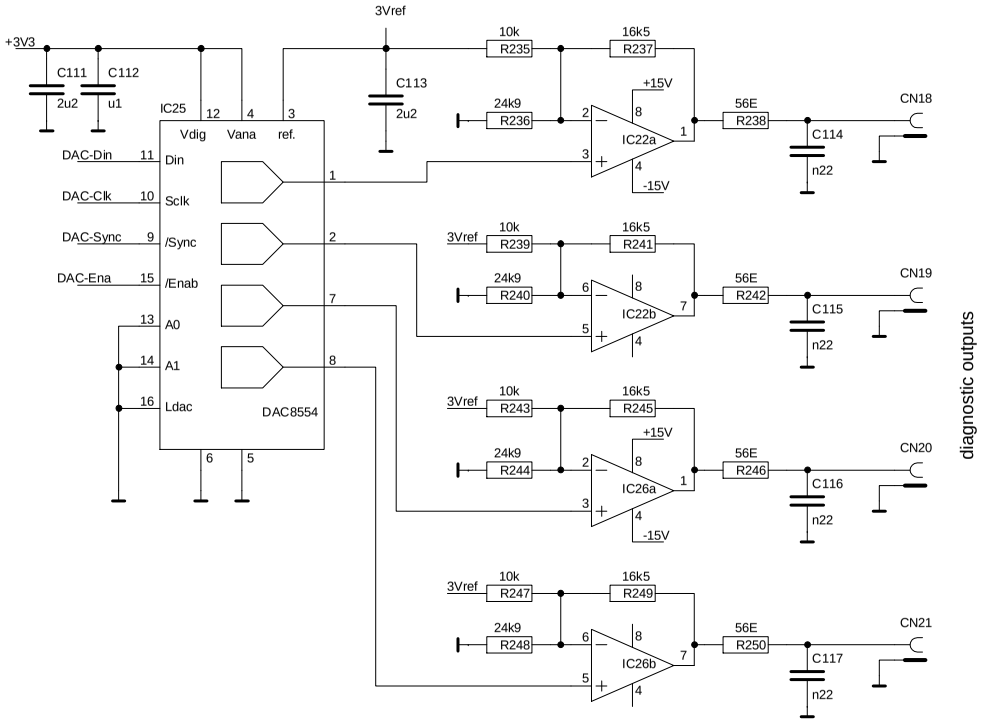

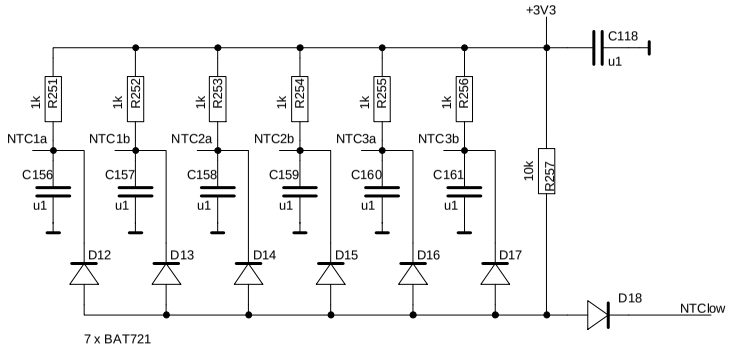

MCU330r2	signal outputs
Rev. 10	page 5/6
02-07-2013	GME
albion instruments	

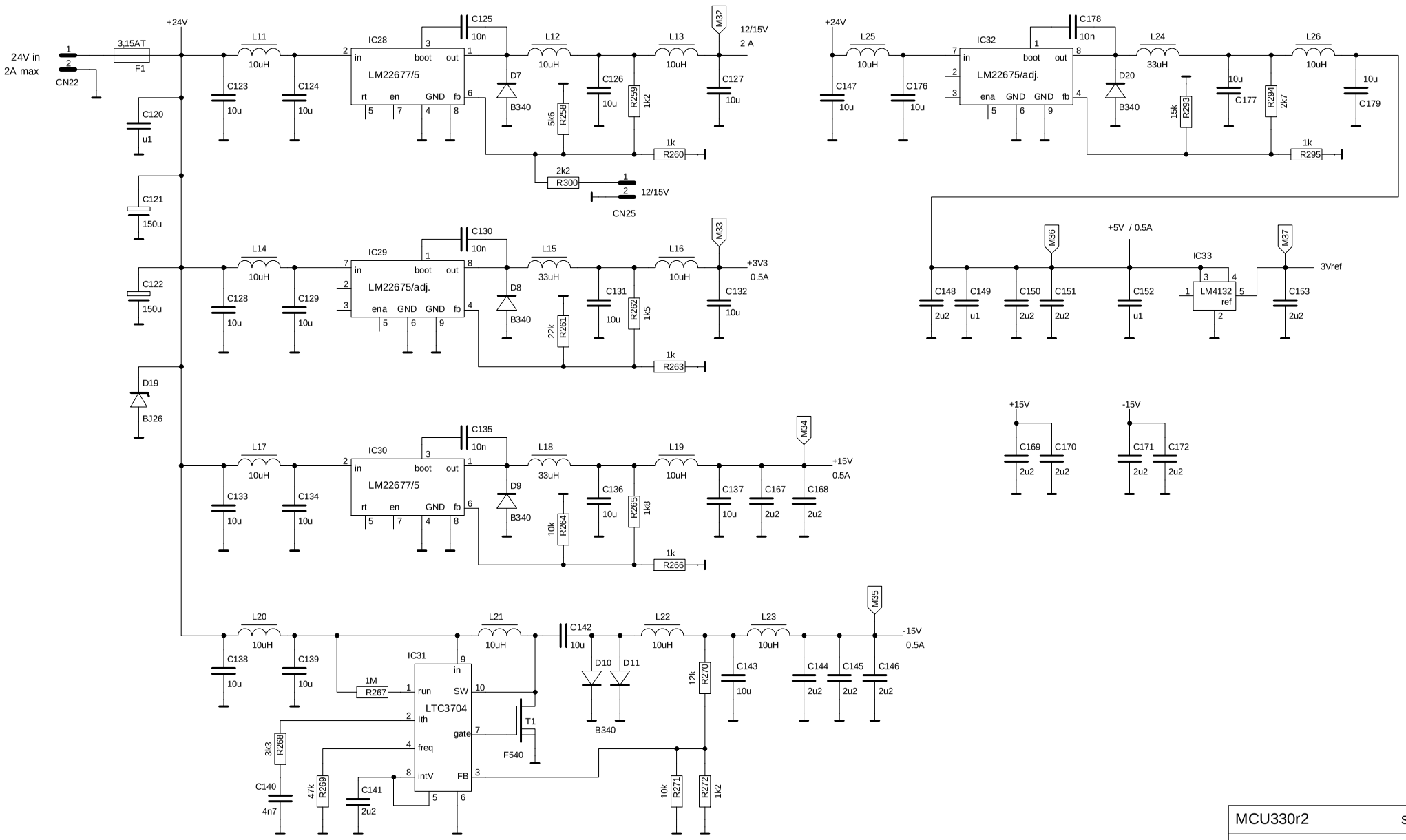

MCU330r2	supply
Rev. 10	page 6/6
02-07-2013	GME
albion instruments	

B-2 Power Converter Design

DC link capacitors (200uF)

DC Link Capacitors

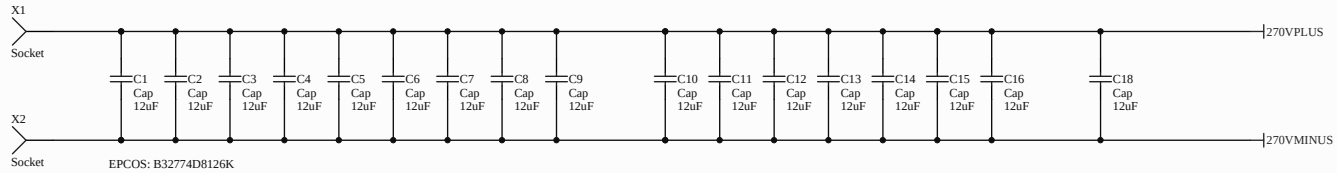

EPCOS: B32774D8126K

Title	HISPEM DC BUS CAPACITANCE		
Size: A4	Number:		Revision: 7.00
Date: 2014/10/06		Sheet of	
File: C:\Users\..\HISPEM3 DC link capacitors.SchDoc		Drawn By:	

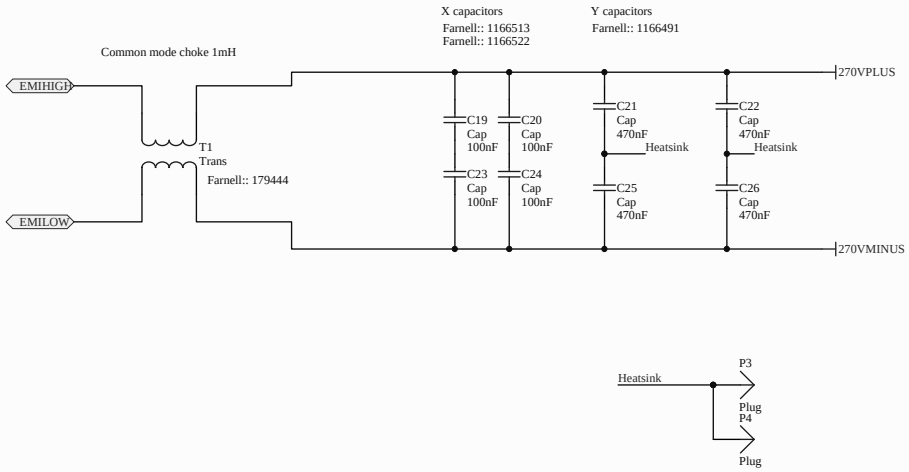

Title	**HISPEM EMI FILTER**		
Size: A4	Number:		Revision: 7.00
Date: 2015/10/17		Sheet of	
File: C:\Users\..\HISPEM3 EMI filter.SCHDOC		Drawn By:	

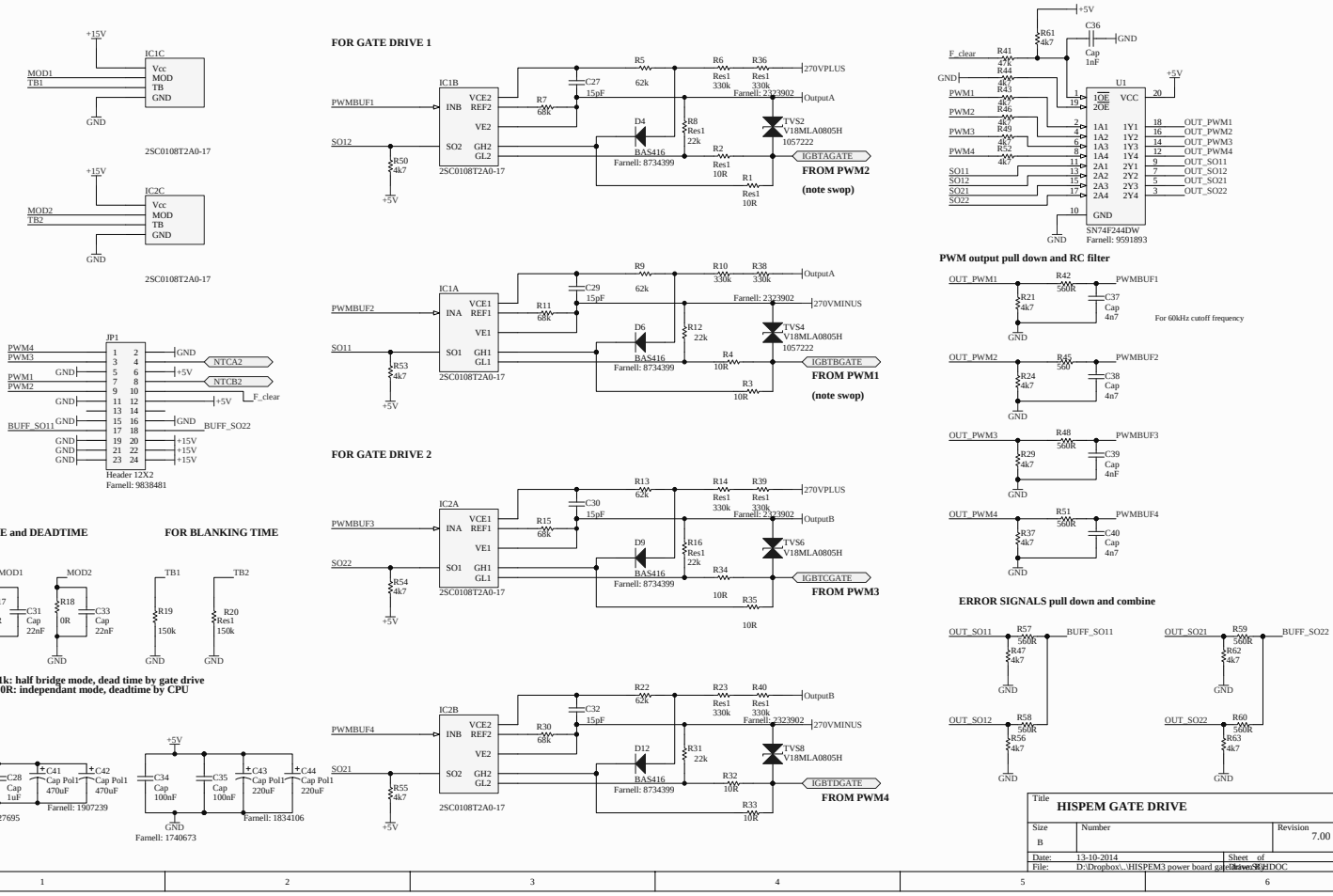
FOR GATE DRIVE 1
INPUT BUFFER (PWM SIGNALS)
IC1C
2SC0108T2A0-17
IC2C
2SC0108T2A0-17
IC1B
IC1A
IC2A
IC2B
2SC0108T2A0-17
FROM PWM2
(note swop)
FROM PWM1
(note swop)
FROM PWM3
FROM PWM4
U1
SN74F244DW
Farnell: 9591893
PWM output pull down and RC filter
For 60kHz cutoff frequency
ERROR SIGNALS pull down and combine
JP1
Header 12X2
Farnell: 9838481
FOR MODE and DEADTIME
FOR BLANKING TIME
R17/18 > 71k: half bridge mode, dead time by gate drive
R17/R18 = 0R: independant mode, deadtime by CPU
Farnell: 1327695
Farnell: 1907239
Farnell: 1740673
Farnell: 1834106
HISPEM GATE DRIVE
Size
B
Number
Revision
7.00
Date: 13-10-2014
Sheet of
File: D:\Dropbox\..\HISPEM3 power board gate drive.SCHDOC
Drawn By:

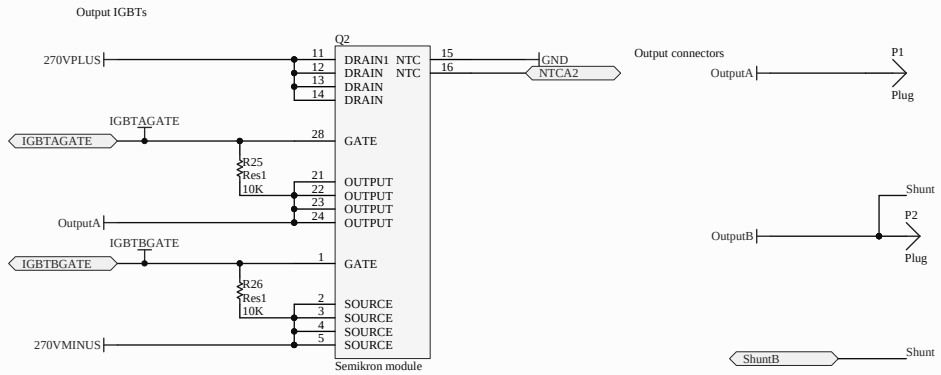

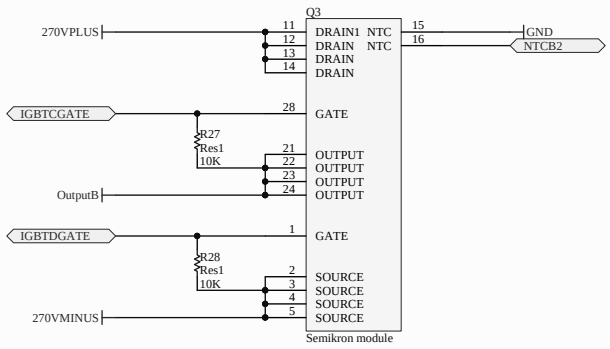

Title: **HISPEM POWER STAGE**		
Size: A4	Number:	Revision: 7.00
Date: 30-9-2014		Sheet of
File: D:\Dropbox\..\HISPEM3 power board.SchDoc		Drawn By:

Bibliography

[1] J. J. Wolmarans, M. B. Gerber, H. Polinder, J. A. Ferreira, and D. Clarenbach, "A 50kW Integrated Fault Tolerant Permanent Magnet Machine and Motor Drive," pp. 345–351, 2008.

[2] R. Krishnan, *Permanent Magnet Synchronous and Brushless DC Motor Drives*. 2010.

[3] J. J. Wolmarans, M. Van Der Geest, H. Polinder, J. A. Ferreira, and D. Zeilstra, "A Low Conductivity Composite Rotor for Fractional Pitch Concentrated Winding Machines,"

[4] Infineon, "How to calculate and minimize the dead time requirement for IGBTs properly," 2007.

[5] Q. An, J. Liu, Z. Peng, L. Sun, L. Sun, and S. Member, "Dual-Space Vector Control of Open-End Winding Permanent Magnet Synchronous Motor Drive Fed by Dual Inverter," vol. 31, no. 12, pp. 8329–8342, 2016.

[6] A. Boglietti, A. Cavagnino, A. Tenconi, and S. Vaschetto, "The safety critical electric machines and drives in the more electric aircraft: A survey," *IECON Proceedings (Industrial Electronics Conference)*, pp. 2587–2594, 2009.

[7] W. Cao, S. Member, B. C. Mecrow, G. J. Atkinson, J. W. Bennett, and D. J. Atkinson, "Overview of Electric Motor Technologies Used for More Electric Aircraft (MEA)," vol. 59, no. 9, pp. 3523–3531, 2012.

[8] E. D. Ganev, "High-performance electric drives for aerospace more electric architectures part I - Electric machines," *2007 IEEE Power Engineering Society General Meeting, PES*, pp. 1–8, 2007.

[9] Dinyu Qin, Xiaogang Luo, and T. Lipo, "Reluctance motor control for fault-tolerant capability," *1997 IEEE International Electric Machines and Drives Conference Record*, pp. WA1/1.1–WA1/1.6, 1997.

[10] C. Cossar, L. Kelly, T. J. E. Miller, C. Whitley, C. Maxwell, and D. Moorhouse, "The design of a switched reluctance drive for aircraft flight control surface actuation," *Electrical Machines and Systems for the More Electric Aircraft (Ref. No. 1999/180), IEE Colloquium on*, no. fig 3, pp. 2/1–2/8, 1999.

[11] C. B. Jacobina, I. S. Freitas, T. M. Oliveira, E. R. C. da Silva, and A. M. N. Lima, "Fault tolerant control of five-phase AC motor drive," *Power Electronics Specialists Conference, 2004. PESC 04. 2004 IEEE 35th Annual*, vol. 5, pp. 3486–3492 Vol.5, 2004.

[12] Y. Lee and T. G. Habetler, "A stator turn fault tolerant strategy for induction motor drives in safety critical applications," *PESC Record - IEEE Annual Power Electronics Specialists Conference*, 2006.

[13] J. Bennett, B. Mecrow, D. Atkinson, and G. Atkinson, "Safety-critical design of electromechanical actuation systems in commercial aircraft," *IET Electric Power Applications*, vol. 5, no. 1, p. 37, 2011.

[14] B. C. Mecrow, A. G. Jack, D. J. Atkinson, S. R. Green, G. J. Atkinson, A. King, and B. Green, "Design and Testing of a Four-Phase Fault-Tolerant Permanent-Magnet Machine for an Engine Fuel Pump," vol. 19, no. 4, pp. 671–678, 2004.

[15] A. G. Jack, B. C. Mecrow, and J. Haylock, "A Comparative Study of Permanent Magnet and Switched Reluctance Motors for High Performance Fault Tolerant Applications.," 1995.

[16] M. D. K. Malik E. Elbuluk, "Motor Drive Technologies for the Power-by-wire (PBW) Program: Options, Trends AND Tradeoffs," 1999.

[17] J. J. Wolmarans, H. Polinder, J. A. Ferreira, and D. Clarenbach, "Selecting an optimum number of system phases for an integrated , fault tolerant permanent magnet machine and drive," 2009.

[18] E. Levi, "Multiphase Electric Machines for Variable-Speed Applications," vol. 55, no. 5, pp. 1893–1909, 2008.

[19] U. Shipurkar, H. Polinder, and J. A. Ferreira, "Modularity in Wind Turbine Generator Systems - Opportunities and Challenges," 2016.

[20] H. A. Toliyat, S. Member, S. P. Waikar, S. Member, and T. A. Lipo, "Analysis and Simulation of Five-Phase Synchronous Reluctance Machines Including Third Harmonic of Airgap MMF," vol. 34, no. 2, pp. 332–339, 1998.

[21] F. Blaschke, "The principle of field orientation as applied to the new transvector closed loop control system for rotating field machines," *Journal of Chemical Information and Modeling*, vol. 34, no. 9, pp. 217–220, 1972.

[22] R. D. Doncker, D. W.J.Pulle, and A. Veltman, *Advanced Electrical Drives Analysis, Modelling, Control*, vol. 53. 2011.

[23] P. Pillay and P. Freere, "Literature survey of permanent magnet ac motors and drives," 1989.

[24] B. Mecrow, A. Jack, J. A. Haylock, and J. Coles, "Fault-tolerant permanent magnet machine drives," vol. 143, 1996.

[25] D. Atkinson, S.Green, B. Mecrow, and A. Jack, "Fault Tolerant Fuel Pump Drives for the All Electric Aircrafts," pp. 1–6, 1998.

[26] O. Of, A. F. Tolerant, P. M. Drive, A. Fuel, P. Application, A. Haylock, A. G. Jack, D. J. Atkinson, F. Toleirant, and D. Requirements, "Operation of a Fault Tolerant PM Drive For An Aerospace Fuel Pump Application.," no. 444, pp. 6–10, 1997.

[27] J. J. Wolmarans, H. Polinder, J. A. Ferreria, and D. Clarenbach, "Modular Sensorless Control of High Speed , Fault Tolerant Machines," pp. 2533–2539, 2010.

[28] W. L. Soong, "Inductance Measurements for Synchronous Machines," *Power Engineering Briefing Note Series*, vol. 2, no. May, pp. 7–8, 2008.

[29] G. J. Li, Z. Q. Zhu, W. Q. Chu, M. P. Foster, and D. A. Stone, "Influence of flux gaps on electromagnetic performance of novel modular pm machines," *IEEE Transactions on Energy Conversion*, vol. 29, no. 3, pp. 716–726, 2014.

[30] D. C. White and H. H. Woodson, *Electromechanical Energy Conversion.* No. 9, 1959.

[31] Texas Instruments, "TMS320x2806x Technical Reference Manual," *Architecture*, no. November, p. 1191, 2016.

[32] NEPTEL and K. IIT, "Power Semiconductor Devices - Insulated Gate Bipolar Transistor(IGBT)," *University of Kharagpur*, pp. 1–23.

[33] P. Integrations, "SCALE -2 and SCALE-2+ 2SC0108T Preliminary Description & Application Manual, Power Integration.," tech. rep., 2015.

[34] Semikron, "Semikron SK100GB12T4T IGBT Datasheet," tech. rep., 2009.

[35] M. Hornkamp, "Latest Generation IGBT Gate Drivers , CT-Concept Technologie AG, Switzerland," Tech. Rep. October, 2009.

[36] L. Bang-sup, K. Kyung-seo, and P. Min-ho, "The Analysis and Compensation of Dead Time Effects in Pwm Inverters," *Proceedings.14 Annual Conference of Industrial Electronics Society*, vol. 3, no. 2, pp. 667–671, 1988.

[37] D. Novotny and T. Lipo, "Vector control and dynamics of AC drives," 1996.

[38] S.-K. Sul, "Control of Electric Machine Drive Systems," *IEEE Press Series on Power Engineering*, p. 415, 2011.

[39] P. Löhdefink, M. Grillenberger, A. Dietz, A. Gröger, A. Hoffmann, and T. Hubert, "Sensorless Vector Control of a Permanent Magnet Synchornous Generator for Micro Hydro Power," pp. 252–256, 2012.

[40] F. Meier and J. Soulard, "dq Theory Applied to a Permanent Magnet Synchronous Machine with Concentrated Windings," no. 6, pp. 194–198.

[41] Texas Instruments, *InstaSPIN-FOC and InstaSPIN-MOTION - User's Guide*. No. January 2013, 2014.

[42] D. W. J. Pulle, P. Darnell, and A. Veltman, *Applied Control of Electrical Drives*. 2015.

[43] K. lund Astrom and T. Hagglund, "PID Controllers Theory, Design-and Tuning - 2nd edition."

[44] J. Albanus, "Coding Schemes Used With Data Converters - Texas Instruments," *Analog Applications Journal, ti*, no. 602, pp. 1–11, 1991.

[45] C. Hall, "It's in the math: how to convert an ADC code to a voltage - Texas Instruments." https://e2e.ti.com/blogs_/b/precisionhub/archive/2016/04/01/it-s-in-the-math-how-to-convert-adc-code-to-a-voltage-part-1/, 2016.

[46] F. Semiconductor, "Sensorless PMSM Field Oriented Control - Design Reference Manual," no. 1, p. 16, 2016.

[47] ABB, "ABB technical catalogue for current sensor and voltage sensor," pp. 1–117, 2006.

[48] ABB, "ABB Control Sensor - ES100C," tech. rep., 2002.

[49] M. R. Baiju, K. K. Mohapatra, R. S. Kanchan, and K. Gopakumar, "A Dual Two-Level Inverter Scheme With Common Mode Voltage Elimination for an Induction Motor Drive," vol. 19, no. 3, pp. 794–805, 2004.

[50] Y. Zhou and H. Nian, "Zero-Sequence Current Suppression Strategy of Open-Winding PMSG System With Common DC Bus Based on Zero Vector Redistribution," vol. 62, no. 6, pp. 3399–3408, 2015.

[51] A. Somani, S. Member, R. K. Gupta, K. K. Mohapatra, and N. Mohan, "On the Causes of Circulating Currents in PWM Drives With Open-End Winding AC Machines," vol. 60, no. 9, pp. 3670–3678, 2013.

[52] R. Kanchan, M. Baiju, K. Mohapatra, P. Ouseph, and K. Gopakumar, "Space vector PWM signal generation for multilevel inverters using only the sampled amplitudes of reference phase voltages," *IEE Proceedings-Electric Power Applications*, vol. 150, no. 2, pp. 139–145, 2003.

[53] Texas Instruments, "TMS320F2806x Piccolo Microcontrollers," tech. rep., 2016.

[54] J.-C. Huang, "EMI Shielding Plastics : A Review," vol. 14, no. 2, 1995.